FACULTY OF SCIENCE
UNIVERSITY OF COPENHAGEN

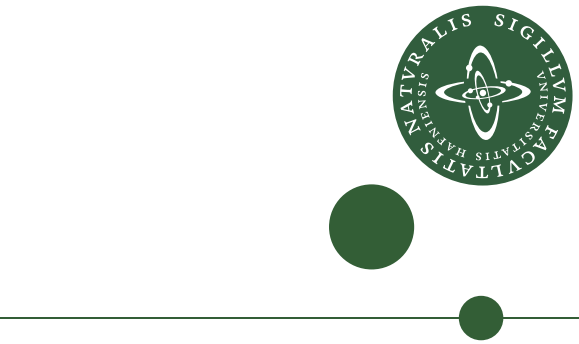

Master's thesis

Johannes Borregaard

Long-Distance Entanglement Distribution Using Coherent States

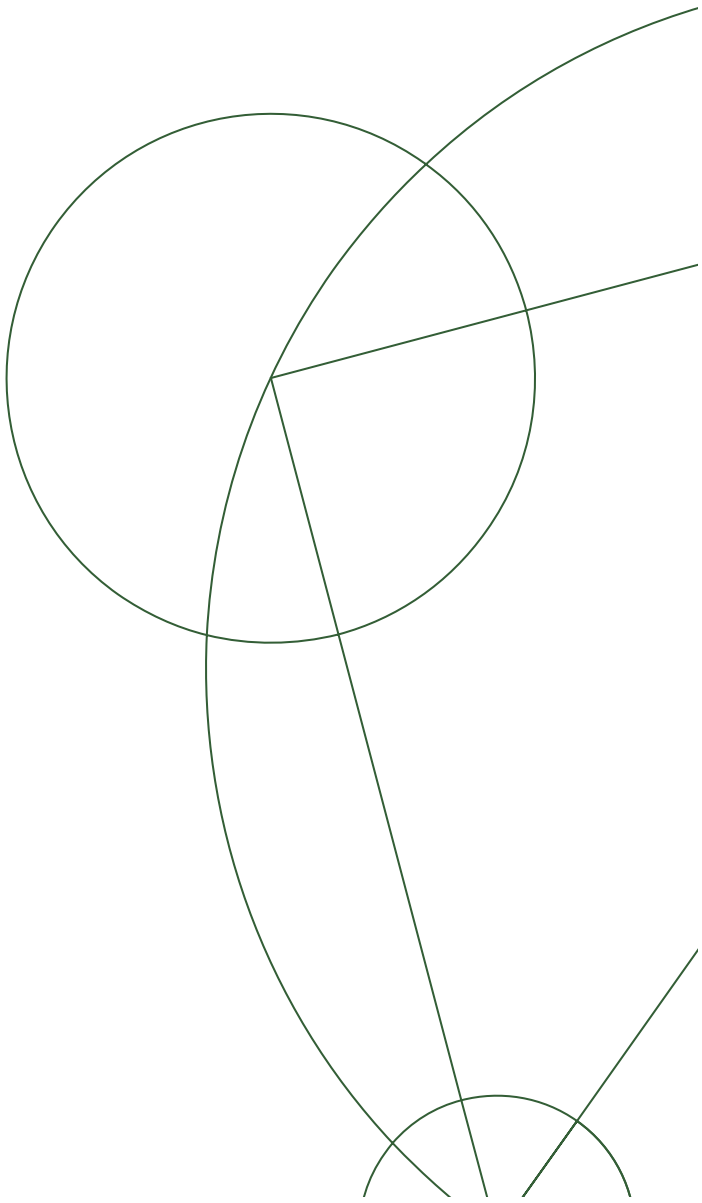

Academic advisor: Anders S. Sørensen

Submitted: 31/08/11

Preface

This master's thesis presents the main results of the project concerning long-distance entanglement distribution that I have worked on at the Theoretical Quantum Optics Group at the Niels Bohr Institute. The project was carried out during the period September 2010 to August 2011.

The main objective of the project was to improve the performance of the hybrid repeater in Ref. [13]. Two ways of how to do this was studied through analytical calculations and numerical simulations.

The thesis is intended for master students of physics or readers with an equivalent background in science. Most of the concepts used are introduced in the thesis but the reader is assumed to have a background of quantum mechanics. Experience with quantum optics and quantum information theory would also be helpful.

Through my work with the project my theoretical knowledge of both quantum optics and quantum information theory has been increased significantly. Furthermore I have learned to perform numerical simulations in the program *Matlab* that I had little knowledge of before. Working at the Theoretical Quantum Optics Group has also given me a chance to follow some of the contemporary research in quantum optics and quantum information theory, which has been very interesting.

First of all I would like to thank my supervisor Anders S. Sørensen for his substantial and comprehensive help with the project. He has guided me in the correct directions during the project and has helped me interpret the results obtained. The main ideas of the project also belong to him. Furthermore I would like to thank Jonathan B. Brask for sharing his work on the hybrid repeater with me and for helping me understand his results. All the group members of the Theoretical Quantum Optics Group at NBI have also helped me with fruitful discussions and technical details about Matlab.

English summary

This thesis is concerned with the distribution of entanglement over large distances. Protocols for long-distance entanglement distribution are called *quantum repeaters*. Quantum repeaters are often divided into two groups: Repeaters in the discrete variable regime and repeaters in the continuous variable regime. This thesis discusses a proposal of a *hybrid* repeater, which combines the elements of the discrete and continuous variable regimes. Jonathan B. Brask et al. suggested the hybrid repeater in Ref [13]

The first part of the thesis describes the fundamental elements of quantum optics and quantum information theory needed to describe the hybrid repeater. The next part describes the hybrid repeater in detail and outlines the results of the performance of the repeater. The results were taken from Ref. [13].
It is shown that changing two of the steps in the protocol might increase the rate of the hybrid repeater. These changes are made in the final part of the thesis and result in an *altered* hybrid repeater. A method for connecting single-mode cat states suggested by N. Sanguard et al. is implemented in the altered hybrid repeater. The performance of the altered hybrid repeater is simulated numerically in the program *"Matlab"* and the optimal rate of entanglement distribution is found.
The rate of the original hybrid repeater and the altered hybrid repeater is finally compared. It is shown that the altered repeater do not perform significantly better than the original repeater except at small distances (<500 km) since the entanglement swapping is not as effective in the altered protocol as in the original protocol.
The effect of two-photon errors in the altered repeater is studied in a perturbative way. It is shown by assuming sources of two-mode squeezed vacuum states to produce the repeater's initial states that a source repetition rate of GHz is necessary in order to have an acceptable rate of entanglement distribution.

Dansk resumé

Dette speciale omhandler, hvordan entanglement distribueres over store afstande. Protokoller for distribution af entanglement kaldes for *kvanterepeatere*. Kvanterepeatere er ofte inddelt i to grupper: Diskret variabel protokoller og kontinuert variabel protokoller. I dette speciale diskuteres et forslag til en *hybridrepeater*, der kombinerer elementerne fra de diskrete og kontinuerte variabel protokoller. Hybridrepeateren er foreslået af Jonathan B. Brask m.fl. i Ref. [13]

Den første del af specialet beskriver de fundamentale elementer i kvanteoptik og kvanteinformationsteori, der er nødvendige for at kunne beskrive hybridrepeateren. I den næste del af specialet gives en detaljeret beskrivelse af hybridrepeateren, og de resultater, der præsenteres i artiklen omkring repeaterens ydeevne, gennemgås. Den sidste del af specialet omhandler, hvordan der kan ændres på opbygningen af hybridrepeateren for at forbedre dens ydeevne. Der foreslås to ændringer som begge behandles og implementeres i en *ændret* hybridrepeater. Det er nødvendigt at inddrage en metode til at skabe entanglement mellem specielle kvantetilstande kaldet *kat*-tilstande. Denne metode er udviklet af N. Sanguard m. fl. Den ændrede repeaterprotokol bliver simuleret numerisk i programmet *"Matlab"* for at bestemme dens optimale ydeevne.
Afslutningsvis sammenlignes den originale og den ændrede hybridrepeaters ydevner. Det konkluderes, at den ændrede repeater ikke er væsentlig bedre end den originale undtagen ved små afstande (<500 km), da metoden til at lave entanglement swapping ikke er lige så effektiv i den ændrede protokol som i den originale.
To-foton fejl i den ændrede repeater behandles pertubativt under antagelse af, at starttilstandene i repeateren er såkaldte *squeezed* vakuum-tilstande. Det vises, at det er nødvendigt at kunne levere disse tilstande med en frekvens omkring GHz for, at den ændrede repeater har en acceptabel ydeevne.

Contents

Chapter 1

Introduction

Quantum information theory is a rather new area of physics in which it is studied how quantum mechanics can form a basis of communication and information processing. So far this has shown impressing results such as teleportation [1, 2], quantum key distribution [3, 4] and quantum computation [5]. Common to many of the techniques used in these fields is that they are based on a peculiar phenomenon described by quantum mechanics called *entanglement*. Entanglement can be illustrated by looking at a system consisting of two particles, which are separated by a very large distance so that no signal can travel between them during measurements. The particles are in other words completely isolated from each other. The behavior of each particle is measured by two sets of scientists who afterwards compare their results. If the particles are fully entangled the scientists will find that their measurements were completely correlated - when one particle moved up the other moved down or vice versa. This phenomenon seems counter intuitive since the particle's behaviors are fully correlated even though the particles cannot communicate during measurements.
Entanglement is an important part of teleportation and key distribution schemes where information is sent between distant locations i.e. where two spatially separated parties need to be correlated [1, 2, 4]. This has fostered the development of schemes of how to distribute entanglement over a large distance, called *quantum repeaters*.

Entanglement is often created locally between two physical systems and the challenge is to send one of the systems to a far away location. When the transmitted signal is a quantum system which is not described within classical physics, the term *quantum signal* is used. A *classical signal* is on the other hand a signal fully described within classical physics. All communication channels add a certain amount of noise to the signal, which in the case of a quantum signal alters the received state and destroys the entanglement it contained. The quality of the signal will drop exponentially with the distance if nothing is done to correct the noise.

Dealing with a classical signal, the problem is solved by inserting repeater stations along the distance to remove noise and amplify the signal. However this is not possible with a quantum signal since the no-cloning theorem of quantum mechanics states that noiseless amplification of a quantum signal is impossible [6, 7]. Instead the distance is divided into smaller segments where entanglement can be created by direct transmission of a quantum signal without significant noise being added to the signal. Afterwards the entanglement is distributed using the process known as *entanglement swapping* to combine pairs of small, entangled segments into larger entangled segments. This is possible by only sending a classical signal between the segments, which can be amplified and purified. The process is iterated until entanglement is created over the whole distance [8].

A quantum signal often consists of photons since this enables the use of optical communication fibers, which are very efficient. So far the suggested quantum repeaters basically work within two regimes of quantum optics. Protocols like the DLCZ - protocol work in the discrete variable regime in which information is encoded in the number of photons contained in the signal [9]. Such protocols require very efficient photodetectors, which has not been realized yet. Nevertheless there is extended research going on to improve the methods of photodetection [10, 11, 12].
The other type of repeaters work in the continuous variable regime in which information is encoded in the amplitude of the electromagnetic field associated with photons. These repeaters use homodyne detection, which is already very efficient ($\sim$99%). However noise is not as easily discovered in this regime as in the discrete variable regime.
Recently Jonathan B. Brask et al. have suggested a hybrid quantum repeater protocol, which combines the advantages of both the discrete and continuous variable regime. This repeater is as efficient as the discrete variable regime protocols but it do not rely on very efficient photodetectors. [13]

The main subject of this master's thesis is the hybrid quantum repeater protocol. I have studied some immediate steps to improve the performance of the originally proposed protocol. The original protocol consists of three steps:

1. Creation of entanglement
2. Growing of cat states
3. Entanglement swapping

Chapter 4 describes the details of the protocol and shows that the first step of the protocol is in the discrete variable regime while the last two are in the continuous variable regime. I have interchanged step one and two of the original protocol. The motivation is that the creation of entanglement is the time consuming part of the repeater since this is

a non-local process. This means that a quantum signal has to be sent between two spatially separated locations, which is time consuming due to the noise added in the channel. In the original repeater scheme it is necessary to restore the entanglement each time the subsequent growing of a cat state fails. First growing the cat states and afterwards create entanglement is therefore expected to be faster since the growing of cat states is a local and thereby fast process. I have implemented a method to create entanglement between cat states suggested by N. Sangouard et al. in Ref. [14] in order to interchange step one and two of the original protocol. Furthermore I have optimized the method used to grow cat states in Ref. [13]

The new method of creating entanglement produces different states than in the original protocol. A substantial part of my work has been to investigate the properties of these new states and especially their behavior during entanglement swapping. I have implemented the mathematical description of the physical operations in the program Matlab in order to make numerical simulations of the behavior of the new states and the overall performance of the altered repeater protocol. The goal has been to find the maximal rate at which the altered repeater could distribute entanglement over a given distance and compare this to the original repeater. It has been necessary to make a numerical optimization of the repeater in order to find the maximal rate. To make the simulation as realistic as possible the optimization included errors and imperfections of the repeater.

Thus the work presented in this thesis consists of:

- Optimizing the method used to grow cat states in Ref. [13]
- Interchanging step one and two of the original hybrid repeater protocol by implementing the method of entanglement creation suggested by N. Sanguard et al. in Ref. [14]
- Implementing the mathematical model of the altered hybrid repeater in Matlab to make numerical simulations of the performance of the repeater
- Investigating the properties of the new states generated in the altered protocol through numerical simulation and analytical calculations
- An overall optimization of the altered repeater protocol including errors and imperfections in order to find the maximal rate of entanglement distribution over a given distance.

The thesis outline is:

Chapter 1: (this chapter) Presents the main objectives and outlines the thesis.

Chapter 2: Provides the reader with the necessary background knowledge of quantum optics and quantum mechanics.

Chapter 3: Outlines the basic elements of quantum information theory focussing on the elements used in quantum repeaters

Chapter 4: Describes the details of the hybrid repeater protocol suggested by Jonathan B. Brask et al.

Chapter 5: Presents the changes made to the hybrid repeater protocol by Jonathan B. Brask et al. and the resulting altered repeater protocol.

Chapter 6: Describes the optimization of the altered repeater protocol and presents the results.

Chapter 7: Concludes on the work presented in chapter 5 and 6 and discusses further improvements to the protocol as well as future work in the field.

Chapter 2

Fundamentals

2.1 The quantized electromagnetic field

[1]The quantized description of the electromagnetic field is of great importance in most quantum repeaters since the quantum signal often consists of photons. Light is often thought of as electromagnetic waves propagating through space but in some cases, like the photoelectric effect, light is considered to be small wave packets of energy called photons. Mathematically these wave packets are described as energy eigenstates of a harmonic oscillator of unit mass. Following this approach, the Hamiltonian for the single mode electric field in the case of no sources of radiation is

$$\hat{H} = \frac{1}{2}\left(\hat{p}^2 + \omega^2 \hat{q}^2\right). \tag{2.1}$$

$\hat{q}$ is the canonical position operator and $\hat{p}$ is the canonical momentum operator. The single mode electromagnetic field can be thought of as a radiation field confined to a one-dimensional cavity. The single mode field is considered for simplicity but the results can be generalized to a multimode field such as a radiation field in free space[2]. $\hat{p}$ and $\hat{q}$ are hermitian operators and therefore correspond to observable quantities (position and momentum) but it is convenient to define two non-hermitian operators called the annihilation ($\hat{a}$) and the creation ($\hat{a}^\dagger$) operators:

$$\hat{a} = (2\hbar\omega)^{-1/2}\left(\omega\hat{q} + i\hat{p}\right) \tag{2.2}$$

$$\hat{a}^\dagger = (2\hbar\omega)^{-1/2}\left(\omega\hat{q} - i\hat{p}\right). \tag{2.3}$$

In terms of these operators the Hamiltonian is

$$\hat{H} = \hbar\omega\left(\hat{a}^\dagger\hat{a} + \frac{1}{2}\right). \tag{2.4}$$

[1]The literature for this chapter is found in [15, 16, 17]

[2]For a radiation field in free space the field is imagined to be confined to a cubic cavity.

The eigenstates of the Hamiltonian are called *Fock states* and are denoted $|n\rangle$. They have energy E_n such that

$$\hat{H}\,|n\rangle = E_n\,|n\rangle \tag{2.5}$$

where

$$E_n = \hbar\omega\left(n + \frac{1}{2}\right), \qquad n = 0, 1, 2, \ldots \tag{2.6}$$

Eq. (2.6) shows that n is the number of energy quanta ($\hbar\omega$) contained in the state $|n\rangle$, which is equivalent to the number of photons. The set of all Fock states ($\{|n\rangle\}$) is an orthonormall basis of the Hilbert space[3] of the Hamiltonian (2.4). It is a *complete set*, which means that any state of the single mode electromagnetic field can be written as a superposition of Fock states. Note that the vacuum ($n = 0$) has energy $\frac{1}{2}\hbar\omega$.
The action of the annihilation operator on a state $|n\rangle$ is

$$\hat{a}\,|n\rangle = \sqrt{n}\,|n-1\rangle \tag{2.7}$$

Thus this operator removes one photon from the state. The effect of the creation operator is

$$\hat{a}^\dagger\,|n\rangle = \sqrt{n+1}\,|n+1\rangle\,, \tag{2.8}$$

which is the creation of one photon.
Another important operator is the number operator $\hat{n} = \hat{a}^\dagger\hat{a}$. The expectation value of the number operator is the average number of photons contained in the state e.g.

$$\langle n|\,\hat{n}\,|n\rangle = n \tag{2.9}$$

2.2 Quadratures

The single mode electromagnetic field can also be expressed in terms of the *quadrature operators*

$$\hat{X}_1 = \frac{1}{2}\left(\hat{a} + \hat{a}^\dagger\right) \tag{2.10}$$

$$\hat{X}_2 = \frac{1}{2i}\left(\hat{a} - \hat{a}^\dagger\right) \tag{2.11}$$

These operators are the analogues of the cosine and sine part of the classical electromagnetic field and are associated with field amplitudes oscillating out of phase with each other by 90°. They can be viewed as the dimensionless analogues of the position and momentum operators of a harmonic oscillator[4]. The quadrature operators satisfy the commutation relation

$$\left[\hat{X}_1, \hat{X}_2\right] = \frac{i}{2} \tag{2.12}$$

[3]The vectors space in which the state vectors live are called the Hilbert space of the system

[4]The quadratures are also denoted the $\hat{X}$ and $\hat{P}$ quadratures where $\hat{X} = \hat{X}_1$ and $\hat{P} = \hat{X}_2$. In this thesis both expressions are used interchangeable

From Heisenberg's uncertainty relation the uncertainty product of the operators, which corresponds to the uncertainty product of the position and momentum, is

$$\left\langle (\Delta \hat{X}_1)^2 \right\rangle \left\langle (\Delta \hat{X}_2)^2 \right\rangle \geq \frac{1}{16} \tag{2.13}$$

This result yields one of differences between classical physics and quantum mechanics. In classical physics it is possible to know both the precise position and the precise momentum, which is not possible in quantum mechanics.
The vacuum ($|0\rangle$) minimizes the uncertainty of the quadratures since

$$\left\langle (\Delta \hat{X}_1)^2 \right\rangle_{vac} = \frac{1}{4} = \left\langle (\Delta \hat{X}_2)^2 \right\rangle_{vac} \tag{2.14}$$

Another state with the same fluctuations is the coherent state, which is also known as the displaced vacuum state.

2.3 Coherent states

Like the Fock states the set of coherent states $\{|\alpha\rangle\}$ spans the entire Hilbert space of the Hamiltonian (2.4) but it is not an orthogonal set since $|\langle \alpha' |\, \alpha\rangle|^2 = e^{-|\alpha' - \alpha|^2} \neq 0$. The coherent states are eigenstates of the annihilation operator i.e.

$$\hat{a}\,|\alpha\rangle = \alpha\,|\alpha\rangle \tag{2.15}$$

where α is a complex number. They can be written in terms of Fock states as

$$|\alpha\rangle = \exp\left(-\frac{1}{2}|\alpha|^2\right) \sum_{n=0}^{\infty} \frac{\alpha^n}{\sqrt{n!}}\,|n\rangle\,. \tag{2.16}$$

Another way of picturing the coherent states is as displaced vacuum states:

$$|\alpha\rangle = \hat{D}(\alpha)\,|0\rangle \tag{2.17}$$

where $\hat{D}(\alpha)$ is the displacement operator defined as

$$\hat{D}(\alpha) = \exp(\alpha \hat{a}^\dagger - \alpha^* \hat{a}). \tag{2.18}$$

It is illuminating to consider the action of the displacement operator on the vacuum state in phase space. The phase space represents all possible states of a system. In classical mechanics it often consists of all possible values for the momentum and position variables and each possible state of the system corresponds to a unique point. However, a quantum state is not a well-localized point in phase space since the momentum and position operators

do not commute (see eq. 2.12). Nevertheless the phase space of the coherent states can be defined from the expectation values of the quadrature operators:

$$\left\langle \hat{X}_1 \right\rangle_\alpha = \mathrm{Re}(\alpha), \qquad \left\langle \hat{X}_2 \right\rangle_\alpha = \mathrm{Im}(\alpha). \tag{2.19}$$

Thus the phase space of the coherent states is the complex α plane and the real and imaginary part of α accounts for the position and momentum variables respectively. The uncertainty in the quadratures is the same as for the vacuum:

$$\left\langle (\Delta \hat{X}_1)^2 \right\rangle_\alpha = \frac{1}{4} = \left\langle (\Delta \hat{X}_2)^2 \right\rangle_\alpha . \tag{2.20}$$

The phase space picture of the vacuum state and a coherent state α is seen in figure 2.1.

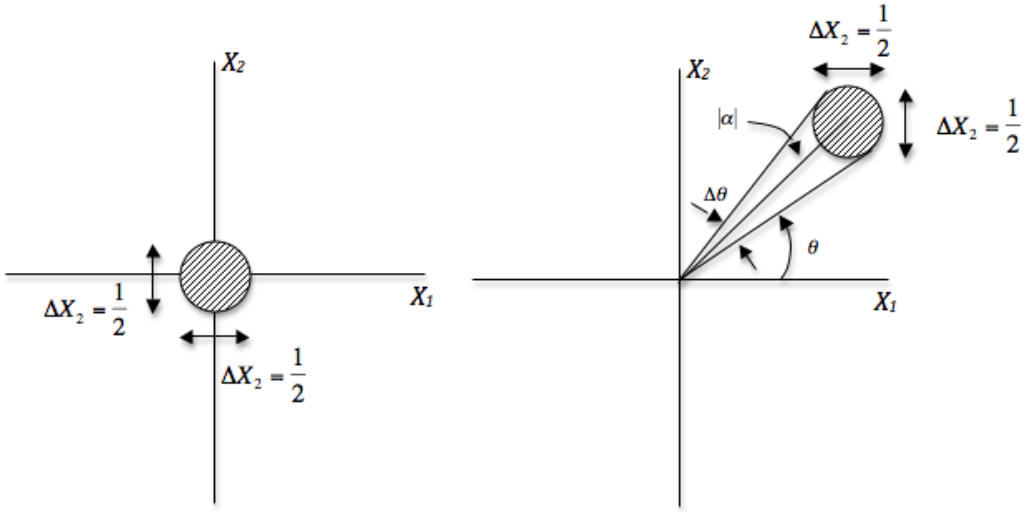

(a) Vacuum state (b) Coherent state

Figure 2.1: Phase space pictures of the vacuum state (a) and a coherent state α (b)

Figure 2.1 shows that a coherent state $|\alpha\rangle$ is simply the vacuum state displaced by α in phase space.
The average photon number contained in a coherent state can be found by taking the expectation value of the number operator:

$$\langle \alpha | \, \hat{n} \, | \alpha \rangle = |\alpha|^2 . \tag{2.21}$$

Thus the average photon number in the state $|\alpha\rangle$ is $|\alpha|^2$.

Eq. (2.20) shows that the coherent states minimizes the uncertainty product of the field quadratures and furthermore the uncertainty in both field quadratures are equal. Nevertheless states exist in which the uncertainty in one of the quadratures is less that $\frac{1}{4}$. These are called *squeezed* states.

2.4 Squeezed states

For any two operators $\hat{A}, \hat{B}$ satisfying the commutation relation $[\hat{A}, \hat{B}] = i\hat{C}$ it is true that

$$\left\langle (\Delta\hat{A})^2 \right\rangle \left\langle (\Delta\hat{B})^2 \right\rangle \geq \frac{1}{4} \left| \left\langle \hat{C} \right\rangle \right|^2 . \tag{2.22}$$

A state is squeezed if either

$$\left\langle (\Delta\hat{A})^2 \right\rangle < \frac{1}{2} \left| \left\langle \hat{C} \right\rangle \right| \quad \text{or} \quad \left\langle (\Delta\hat{B})^2 \right\rangle < \frac{1}{2} \left| \left\langle \hat{C} \right\rangle \right| . \tag{2.23}$$

Many types of squeezing exist dependent on which operators the squeezing exists in. When a state is quadrature squeezed either

$$\left\langle (\Delta\hat{X}_1)^2 \right\rangle < \frac{1}{4} \quad \text{or} \quad \left\langle (\Delta\hat{X}_2)^2 \right\rangle < \frac{1}{4}. \tag{2.24}$$

An important type of squeezed states is the squeezed vacuum state, $|\xi\rangle$. Physically this state can be generated by e.g. parametric down conversion using nonlinear processes in a medium pumped by a strong coherent field [27]. Mathematically the state can be generated by letting the *squeeze operator*, $\hat{S}(\xi)$ act on vacuum

$$|\xi\rangle = \hat{S}(\xi) |0\rangle . \tag{2.25}$$

The squeeze operator is defined as

$$\hat{S}(\xi) = \exp(\frac{1}{2}(\xi^* \hat{a}^2 - \xi \hat{a}^{\dagger 2})) \tag{2.26}$$

where $\xi = re^{i\theta}$. r is the squeeze parameter, which is a real, non-negative number and θ is a phase between 0 and 2π. The annihilation and creation operators appear in pairs in the squeeze operator, which means that photons are created and destroyed in pairs. In that sense the squeezed vacuum state is a sort of coherent state of photon pairs. For the squeezed vacuum state the uncertainties in the field quadratures are

$$\left\langle (\Delta\hat{X}_1)^2 \right\rangle_\xi = \frac{1}{4}[\cosh^2(r) + \sinh^2(r) - 2\sinh(r)\cosh r(r)\cos(\theta)] \tag{2.27}$$

$$\left\langle (\Delta\hat{X}_2)^2 \right\rangle_\xi = \frac{1}{4}[\cosh^2(r) + \sinh^2(r) + 2\sinh(r)\cosh r(r)\cos(\theta)]. \tag{2.28}$$

For $\theta = 0$ squeezing is obtained in $\hat{X}_1$:

$$\left\langle (\Delta \hat{X}_1)^2 \right\rangle = \frac{1}{4} e^{-2r} \tag{2.29}$$

$$\left\langle (\Delta \hat{X}_2)^2 \right\rangle = \frac{1}{4} e^{2r}. \tag{2.30}$$

Note that the uncertainty product still is $\frac{1}{16}$. For $\theta = \pi$ the squeezing is in the $\hat{X}_2$ quadrature. The phase space picture of the squeezed vacuum state with $\theta = 0$ is shown in figure 2.2.

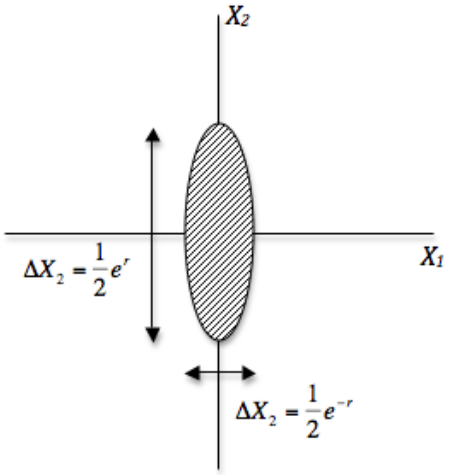

Figure 2.2: Phase space picture of a squeezed coherent state. The squeezing is in the $\hat{X}_1$ quadrature

Squeezed states exhibit less noise in some parts of the light wave than others. This can be used in technological applications such as detection of weak signals [19].

2.5 Wave functions

Another way to express a quantum state is with the wave function, which is a representation of the state in the position space. The position space is spanned by the position eigenkets $|x'\rangle$ satisfying the relation

$$\hat{x} \left| x' \right\rangle = x' \left| x' \right\rangle . \tag{2.31}$$

Since space is not considered to be discrete the position operator $\hat{x}$ has a continuous spectrum and a corresponding continuum of eigenkets. The set of position eigenkets is a

complete set and any arbitrary state $|\phi\rangle$ can be expanded as

$$|\phi\rangle = \int_{-\infty}^{\infty} \mathrm{d}x \, |x\rangle \langle x| \, \phi\rangle \, . \tag{2.32}$$

The expansion coefficient $\langle x| \, \phi\rangle$ is called the wave function of the state $|\phi\rangle$ and is usually denoted $\psi_\phi(x)$. From the wave function it is possible to find the probability distribution of the position of the arbitrary particle described by the state. The probability distribution as a function of x' is

$$P_\psi(x) = |\psi_\phi(x)|^2 = |\langle x| \, \phi\rangle|^2 \, . \tag{2.33}$$

The wave function is a nice way of visualizing a quantum state. As an example the wave function of a Fock state $|n\rangle$ is

$$\psi_n(x) = \left(\frac{1}{\pi\lambda^2}\right)^{1/4} \frac{1}{\sqrt{2^n n!}} H_n\left(\frac{x}{\lambda}\right) e^{-x^2/2\lambda^2} \tag{2.34}$$

where $\lambda = \sqrt{\hbar/\omega}$ and $H_n(\zeta)$ are the Hermite polynomials. The wave functions for $n = 1, 2$ and 3 are seen in figure 2.3.

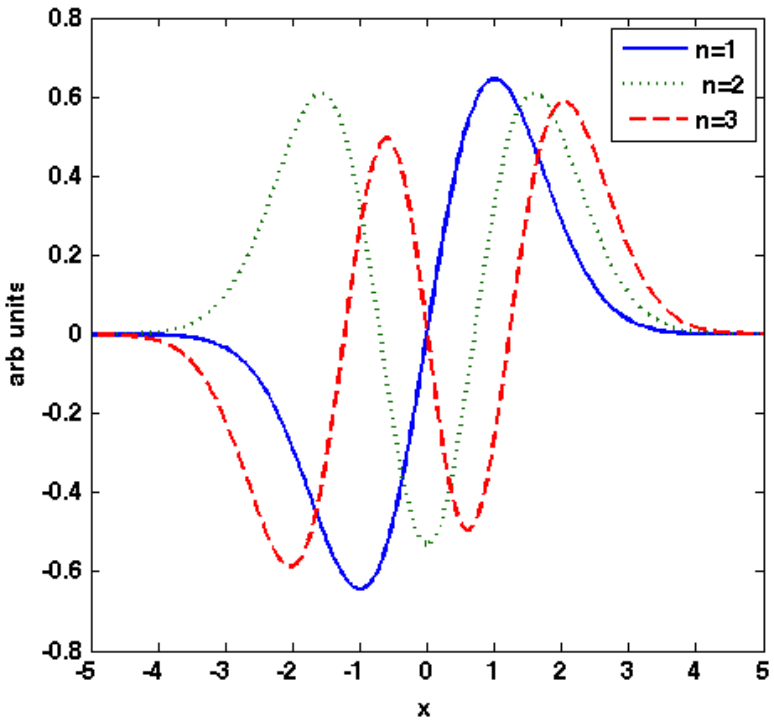

Figure 2.3: The wave functions of the first three Fock states above vacuum

A state can also be represented in momentum space instead of position space. The wave function in momentum space, $\varphi_\phi(p)$ is obtained from the wave function in position space by a Fourier transformation:

$$\varphi_\phi(p) = \frac{1}{\sqrt{2\pi\hbar}} \int_{-\infty}^{\infty} \mathrm{d}x \exp\left(-ipx/\hbar\right) \psi_\phi(x). \tag{2.35}$$

2.6 Wigner functions

Section 2.5 showed that a state's probability distribution could be obtained from its wave function and with a Fourier transformation the corresponding probability distribution in momentum space could be obtained. The Wigner function is a quasi-probability distribution over phase space from which the probability distribution for both the position and the momentum can be obtained. The Wigner function is defined for an arbitrary *density operator*. The general expression of the density operator is

$$\hat{\rho} = \sum_i p_i \left|\psi_i\right\rangle \left\langle\psi_i\right|. \tag{2.36}$$

The density operator describes both *pure* and *mixed* states. A pure state is described by a single vector $|\psi\rangle$ with corresponding wave function $\psi(x)$. In this case the density operator is

$$\hat{\rho} = \left|\psi\right\rangle \left\langle\psi\right|. \tag{2.37}$$

A single vector cannot describe a mixed state. Instead the mixed state has a certain probability, p_i to be in state $|\psi_i\rangle$. Thus the density operator of a mixed state is of the from (2.36). It follows that

$$0 \leq p_i \leq 1, \qquad \sum_i p_i = 1. \tag{2.38}$$

The Wigner function of a state with density operator $\hat{\rho}$ is

$$W(x,p) \equiv \frac{1}{2\pi\hbar} \int_{-\infty}^{\infty} \mathrm{d}x \left\langle x + \frac{1}{2}q \right| \hat{\rho} \left| x - \frac{1}{2}q \right\rangle e^{-ipq/\hbar}. \tag{2.39}$$

The vectors $\left|x \pm \frac{1}{2}q\right\rangle$ are eigenkets of the position operator. In the special case of a pure state the Wigner function takes the form

$$W(x,p) \equiv \frac{1}{2\pi\hbar} \int_{-\infty}^{\infty} \mathrm{d}x\, \psi^*\left(x + \frac{1}{2}q\right) \psi\left(x - \frac{1}{2}q\right) e^{-ipq/\hbar}. \tag{2.40}$$

The position probability distribution is obtained from the Wigner function by integrating over momentum

$$P_\psi(x) = \int_{-\infty}^{\infty} \mathrm{d}p\, W(x,p) \tag{2.41}$$

and in the same manner the momentum probability distribution is obtained by integrating over position. It follows that

$$\int_{-\infty}^{\infty} \mathrm{d}p \int_{-\infty}^{\infty} \mathrm{d}x\, W(x,p) = 1 \tag{2.42}$$

The Wigner function is called a *quasi*-probability distribution because it can take negative values. This is a property that a real probability distribution cannot have. The negativity of the Wigner function is a fingerprint of the state being a quantum state since classical states all have positive phase space probability distributions. The Wigner function of the Fock state with n=1 and for a coherent state $|\alpha\rangle$ is shown in figure 2.4a and 2.4b. Note that the Wigner function of the coherent state is positive and consequently the coherent state is referred to as a "classical" quantum state.

2.7 Fidelity

The fidelity of two states or "the state overlap" is a measure of how similar the states are. This is useful when investigating the properties of an "unknown" state since the fidelity with states of known properties gives information about the "unknown" state. The definition of the fidelity, F between an arbitrary state with density operator $\hat{\rho}_1$ and a pure state, $|\psi\rangle$ is

$$F(\hat{\rho}, \psi) = \mathrm{Tr}\left[\hat{\rho}_1 |\psi\rangle \langle\psi|\right] = \langle\psi| \hat{\rho}_1 |\psi\rangle . \tag{2.43}$$

where Tr is the trace. The fidelity can be understood as the probability that a measurement will have the same outcome for both states and it follows that $0 \leq F \leq 1$. if $F = 0$ the two states are orthogonal and if $F = 1$ the two states are equal.
The fidelity can be calculated from the Wigner functions of the states:

$$F = 2\pi \int_{-\infty}^{\infty} \mathrm{d}x \int_{-\infty}^{\infty} \mathrm{d}p\, W_1(x,p) W_\psi(x,p) \tag{2.44}$$

where W_1 is the Wigner function of the arbitrary state and W_ψ is the Wigner function of the pure state.
The concept of fidelity is very useful in quantum information theory to determine the entanglement contained in an arbitrary state described by density matrix, $\hat{\rho}$. For this purpose the fidelity with a *maximally entangled state* is calculated (see section 3.2).

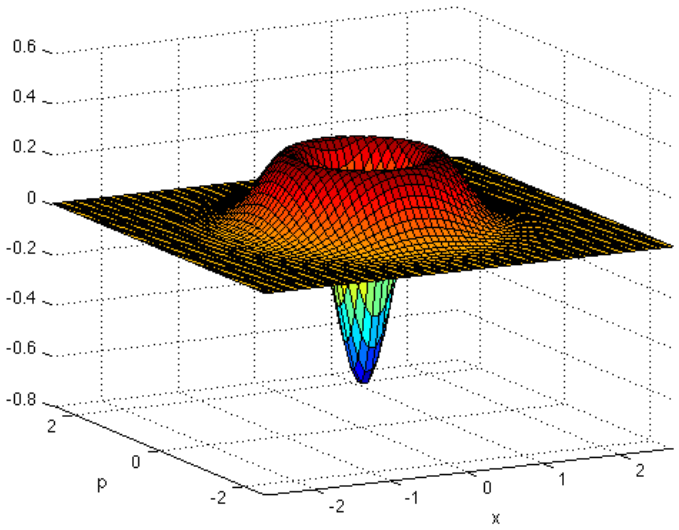

(a) The Wigner function of the Fock state with n=1. Note that the Wigner function have negative values and consequently is not a real probability distribution

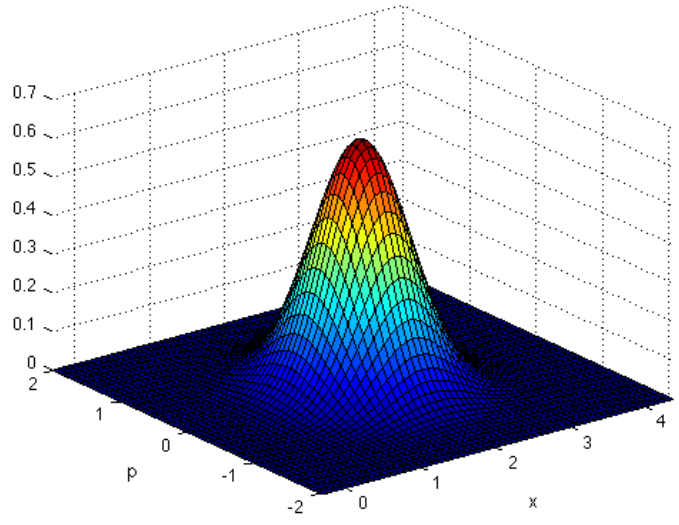

(b) The Wigner function of a coherent state with $\alpha = 2$. The function is everywhere positive like a real probability distribution.

Figure 2.4: Wigner functions of the Fock state with n=1 and a coherent state with $\alpha = 2$.

Chapter 3

Quantum Information Theory

3.1 Qubits and computational basis

[1]An important element in classical information theory is *bits*. Bits are binary information carriers that can take the values 1 or 0. The quantum mechanical analogue of the bit is the *qubit* and is the corner stone of quantum information theory. A qubit is a quantum system with only two possible states called a two level quantum system. There are many examples of such quantum systems such as the spin states of spin-$\frac{1}{2}$ particles, two electronic states of an atom or polarization states of photons. The notion of the qubit is independent of which system is used for the implementation of it as long as the state vectors live in a two dimensional Hilbert space. The basis of the Hilbert space is called the *computational basis* and consists of the elements $|1\rangle$ and $|0\rangle$ [2]. A great strength of the qubit is that it can be a superposition of $|1\rangle$ and $|0\rangle$ while the classical bit is either 0 or 1. Thus an arbitrary qubit state, $|\psi\rangle$ can be written as

$$|\psi\rangle = a\,|0\rangle + b\,|1\rangle \tag{3.1}$$

where $|a|^2 + |b|^2 = 1$. This among other things enables faster computation algorithms than in classical information theory.

One of the main fields in quantum information theory is quantum computation, where the construction of gates enables computational algorithms. In classical information theory the gates are logic operations such as the AND/OR gate, which works on bits. In quantum computation the gates are linear, unitary transformations working on qubits. Details about the construction of quantum gates will not be reviewed in this thesis but it is important to know the difference between *local* and *non-local* qubit operations. Non-local operations act on two or more qubits and cannot be factored into local operations

[1]The literature for this chapter is found in [18, 20]. The chapter is also build on course material from the course *"Quantum Information Theory"* at NBI, Copenhagen

[2]The computational basis should not be confused with the Fock states $|1\rangle$ and $|0\rangle$.

while local operations only works on single qubits.

A very important phenomenon in quantum information theory is *entanglement*. When a person sends a message to another person the sender and receiver get correlated in the sense that information has been shared between them. In quantum mechanics this correlation can be of a stronger kind than in classical physics. This is called *entanglement*.

3.2 Entanglement

Entanglement is a property of multipartite systems. A multipartite system consists of two or more subsystems, which can be thought of as different modes or degrees of freedom of the multipartite system. A system of two atoms would e.g. be a multipartite system with two subsystems, each describing one atom. Another example is a multipartite system consisting of the electronic states and the vibrational modes of a single atom.
Each subsystem is described in its own Hilbert space. The Hilbert space of the multipartite system is the tensor product of the Hilbert spaces of the subsystems. The Hilbert space, $\mathcal{H}$ of a multipartite system with n subsystems is

$$\mathcal{H} = \mathcal{H}_1 \otimes \mathcal{H}_2 \otimes \ldots \otimes \mathcal{H}_n \tag{3.2}$$

where $\mathcal{H}_1 \ldots \mathcal{H}_n$ are the Hilbert spaces of the subsystems. This means that

$$dim\,(\mathcal{H}) = dim\,(\mathcal{H}_1) \cdot dim\,(\mathcal{H}_2) \cdot \ldots \cdot dim\,(\mathcal{H}_n) \tag{3.3}$$

i.e. the dimension of $\mathcal{H}$ is the product of the dimensions of the subsystems. Entanglement is easiest described in a joint system of two subsystems called a bipartite system. The subsystems are denoted $\mathcal{A}$ and $\mathcal{B}$ and the state $|\psi\rangle_{AB}$ is a state of the joint system. Entanglement is defined as:

Entanglement 1 *The state $|\psi\rangle_{AB}$ is entangled if it cannot be written as a product of states of the subsystems i.e.*

$$|\psi_{AB}\rangle \neq |\psi_A\rangle \otimes |\psi_B\rangle \tag{3.4}$$

An entangled state is called a *non-separable* state. A state that can be written as $|\psi_{AB}\rangle = |\psi_A\rangle \otimes |\psi_B\rangle$ is a separable state[3].

Only entanglement of bipartite systems are considered in this thesis but entanglement is, as mentioned, a general property of multipartite systems. The general definition of entanglement is

[3]The definition of entanglement in (3.4) refers to a pure state $|\psi\rangle_{AB}$. For a mixed state the state vectors are replaced with density operators.

Entanglement 2 *A multipartite state with density operator, ρ is entangled or non-separable if*

$$\rho \neq \sum_i p_i \rho_1^i \otimes \ldots \otimes \rho_n^i \tag{3.5}$$

where $\rho_1 \ldots \rho_n$ are states of the subsystems 1 to n

Examples of entangled states in a bipartite system with two-dimensional subsystems $\mathcal{A}$ and $\mathcal{B}$ are the *Bell states*. The orthonormal basis of the subsystems is denoted $\{|0\rangle, |1\rangle\}$. The *Bell states* are

$$\begin{aligned} \left|\Psi^+\right\rangle &= \frac{1}{\sqrt{2}}\left(|01\rangle_{AB} + |10\rangle_{AB}\right) \quad \left|\Psi^-\right\rangle = \frac{1}{\sqrt{2}}\left(|10\rangle_{AB} - |01\rangle_{AB}\right) \\ \left|\Phi^+\right\rangle &= \frac{1}{\sqrt{2}}\left(|11\rangle_{AB} + |00\rangle_{AB}\right) \quad \left|\Phi^+\right\rangle = \frac{1}{\sqrt{2}}\left(|00\rangle_{AB} - |11\rangle_{AB}\right). \end{aligned} \tag{3.6}$$

The system could be the spin states of two atoms where the spin either points up $|1\rangle$ or down $|0\rangle$. Now the spin orientation of system A is measured. Mathematically this is described by acting with the operator

$$\hat{S} = \lambda_0 |0\rangle_{AA} \langle 0| \otimes \mathbb{I}_B + \lambda_1 |1\rangle_{AA} \langle 1| \otimes \mathbb{I}_B, \qquad \{\lambda_0, \lambda_1\} \in \mathbb{R} \tag{3.7}$$

on the state. λ_0 and λ_1 are eigenvalues of $\hat{S}$ and are the possible measurement outcomes.[4] If the system is in state $|\Psi^+\rangle$ a measurement with outcome λ_0 will leave the system in the state

$$\lambda_0 |0\rangle_{AA} \left\langle 0\right| \Psi^+\rangle = \frac{\lambda_0}{\sqrt{2}} |01\rangle_{AB} \tag{3.8}$$

while a measurement yielding λ_1 will leave the system in the state

$$\lambda_1 |1\rangle_{AA} \left\langle 1\right| \Psi^+\rangle = \frac{\lambda_1}{\sqrt{2}} |10\rangle_{AB}. \tag{3.9}$$

Thus the measurement outcome of system A determines any subsequent measurement outcome of system B. If two groups of scientists measured each their system the measurement outcomes would be completely correlated. Every time group A measured spin down, group B measured spin up and vice versa. From this example it is not clear that entanglement can be a stronger correlation than classical correlations. The real test of this is the CHSH inequality, which is an inequality that holds for classical correlations. This inequality can be broken with quantum variables, which then are thought to contain stronger correlations than classical variables. [23]

The states in eq. (3.6) are called *maximally entangled* states. A maximally entangled

[4] The identity operator $\mathbb{I}_B$ means that system B is not changed

state has complete correlation between the subsystems. It is not easy to tell how entangled an arbitrary state is without making a correlation experiment since it is hard to find a unique measure of entanglement. Nonetheless a unique measure of entanglement exists in a bipartite pure system. To define this it is necessary to look at the reduced density operators of the bipartite system.
Suppose that the bipartite system is in state $|\Psi\rangle_{AB}$ with the corresponding density matrix $\hat{\rho}_{AB} = |\Psi\rangle\langle\Psi|_{AB}$. System A and B are described by their reduced density matrices

$$\hat{\rho}_A = \mathrm{Tr}_B[\hat{\rho}_{AB}] = \sum_i {}_B\langle i|\,\hat{\rho}_{AB}\,|i\rangle_B\,, \qquad \hat{\rho}_B = \mathrm{Tr}_A[\hat{\rho}_{AB}] = \sum_i {}_A\langle i|\,\hat{\rho}_{AB}\,|i\rangle_A\,. \tag{3.10}$$

$\mathrm{Tr}_{A,B}$ is the partial trace over A,B. The measure of entanglement is the entropy of one of the reduced density matrices. The entropy is the von Neumann entropy

$$S(\hat{\rho}) = -\mathrm{Tr}[\hat{\rho}\log(\hat{\rho})] = -\sum_i \lambda_i \log(\lambda_i) \tag{3.11}$$

where $\{\lambda_i\}$ are the eigenvalues of $\hat{\rho}$. It is the quantum pendant to the classical entropy and describes how much information the state $\hat{\rho}$ contains. The bigger the entropy, the less information is contained in the state. For a pure bipartite system this is a measure of entanglement since the *bigger the entropy of the reduced density matrix is, the more entangled the state is.* This can be understood as if the entropy of the reduced density is large the subsystems cannot be described individually but need to be described collectively - they are entangled. Schrödinger described this as:

> *"Thus one disposes provisionally (until the entanglement is resolved by actual observation) of only a* **common** *description of the two in that space of higher dimension. This is the reason that knowledge of the individual systems can decline to the scantiest, even to zero, while that of the combined system remains continually maximal. Best possible knowledge of a whole does* **not** *include best possible knowledge of its parts"*[5]

For a bipartite system with two-dimensional subsystems the base number for the logarithm in the definition of the entropy is two. A maximally entangled state $\hat{\rho}_{AB}$ has $S(\hat{\rho}_A) = 1 = S(\hat{\rho}_B)$, while a product state has $S(\hat{\rho}_A) = 0 = S(\hat{\rho}_B)$.

The entropy of the reduced density matrix cannot be used as a measure of entanglement when the bipartite system is in a mixed state. Therefore the fidelity with a maximally entangled state has been used as a measure of entanglement in this thesis when dealing with a mixed state. The bigger the fidelity is, the bigger the entanglement is. It is of course necessary to have an idea about which maximally entangled state to calculate the fidelity with.

[5]Original text in german is found in [21]. The english translation appears in [22, p. 167]

3.3 Teleportation

Entanglement assisted teleportation is an important element of quantum information theory and one of the corner stones in quantum repeaters (see section 3.5). Charles H. Benett et al. showed that a quantum state could be teleportet through an entangled state by means of local operations and classical communication. The general teleportation scheme can be seen in Appendix A but it is more instructive to look at the original scheme proposed by Charles H. Bennett et al. in Ref. [2].
Consider two persons named "Alice" and "Bob" who shares the Bell state

$$\left|\Psi^{-}\right\rangle_{AB} = \frac{1}{\sqrt{2}}(\left|1\right\rangle_{A}\left|0\right\rangle_{B} - \left|0\right\rangle_{A}\left|1\right\rangle_{B}) \tag{3.12}$$

Alice also has a unknown state $\left|\phi\right\rangle_{C} = a\left|1\right\rangle_{C} + b\left|0\right\rangle_{C}$ that she wants to teleport to Bob (note that $a^2 + b^2 = 1$). Thus the complete state of the system is

$$\begin{aligned}\left|\Psi\right\rangle_{ABC} &= \left|\phi\right\rangle_{C}\left|\Psi^{-}\right\rangle_{AB} = \frac{a}{\sqrt{2}}(\left|1\right\rangle_{A}\left|0\right\rangle_{B}\left|1\right\rangle_{C} - \left|0\right\rangle_{A}\left|1\right\rangle_{B}\left|1\right\rangle_{C}) + \\ &\quad \frac{b}{\sqrt{2}}(\left|1\right\rangle_{A}\left|0\right\rangle_{B}\left|0\right\rangle_{C} - \left|0\right\rangle_{A}\left|1\right\rangle_{B}\left|0\right\rangle_{C}).\end{aligned} \tag{3.13}$$

Now Alice performs a joint measurement of the von Neumann type on her two systems A and C.[6] She can do this in the Bell operator basis consisting of the states $\{\left|\Psi^{\pm}\right\rangle_{AC}, \left|\Phi^{\pm}\right\rangle_{AC}\}$ (see eq. (3.6) in section 3.2). To find the possible outcomes of such a measurement the state $\left|\Psi\right\rangle_{ABC}$ is written in the Bell basis as

$$\begin{aligned}\left|\Psi\right\rangle_{ABC} &= \frac{1}{2}\left[\left|\Psi^{-}\right\rangle_{AC}(-a\left|1\right\rangle_{B} - b\left|0\right\rangle_{B}) + \left|\Psi^{+}\right\rangle_{AC}(-a\left|1\right\rangle_{B} + b\left|0\right\rangle_{B})\right] + \\ &\quad \frac{1}{2}\left[\left|\Phi^{-}\right\rangle_{AC}(a\left|0\right\rangle_{B} + b\left|1\right\rangle_{B}) + \left|\Phi^{+}\right\rangle_{AC}(a\left|0\right\rangle_{B} - b\left|1\right\rangle_{B})\right].\end{aligned} \tag{3.14}$$

Eq.(3.14) shows that the probability of each measurement outcome is $\frac{1}{4}$. After the measurement the state in Bobs system will be one of the four states

$$-\left|\phi\right\rangle_{B}, -\sigma_z\left|\phi\right\rangle_{B}, \sigma_x\left|\phi\right\rangle_{B}, -i\sigma_y\left|\phi\right\rangle_{B} \tag{3.15}$$

corresponding to Alice's four possible measurement outcomes. $\sigma_{x,y,z}$ are the Pauli matrices defined as:

$$\sigma_x = \begin{pmatrix} 0 & 1 \\ 1 & 0 \end{pmatrix}, \sigma_y = \begin{pmatrix} 0 & -i \\ i & 0 \end{pmatrix}, \sigma_z = \begin{pmatrix} 1 & 0 \\ 0 & -1 \end{pmatrix} \tag{3.16}$$

The Pauli matrices satisfy that $\sigma_x^2 = \sigma_y^2 = \sigma_z^2 = 1$, which means that Bob can get the original state $\left|\phi\right\rangle$ if he can implement the Pauli matrices on his system. All he needs to

[6] A measurement of the von Neumann type means that Alice acts with a projection operator that project onto a basis of the joint system

know is the measurement outcome of Alice's measurement so that he knows, which Pauli matrix he should apply.
The only information that has to travel between Alice and Bob is the measurement outcome of Alice's measurement, which is classical information. This is why it is called teleportation.

3.4 Entanglement swapping

Entanglement swapping is a generalized form of teleportation using entangled input states. The idea is to teleport one of the subsystems of an entangled state. Imagine that Alice shares an maximally entangled state $|\Psi^-\rangle$ with Clare and that David shares the same state with Bob:

$$|\Psi^-\rangle_{AC} \otimes |\Psi^-\rangle_{DB} \tag{3.17}$$

Now the teleportation protocol is applied and David and Clare perform a joint measurement on their systems. Afterwards having been told the measurement outcome of the joint measurement Bob and Alice can obtain the state $|\Psi^-\rangle_{AB}$ by local operations. It is quite remarkably that it is possible to create entanglement between Alice and Bob's systems though they may never have seen each other. Furthermore it is possible without sending any quantum signal between Alice and Bob.
This procedure is iterated to distribute entanglement over larger distances. A schematic view of this is seen in figure 3.1.

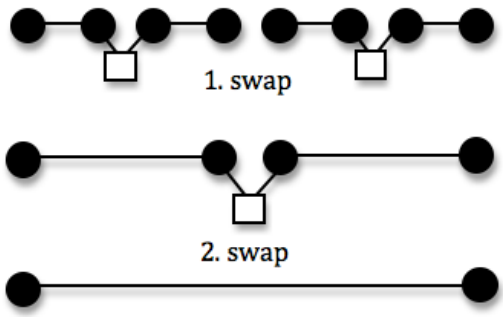

Figure 3.1: Schematic overview of entanglement swapping. In the first swap level the four entangled pairs are connected pairwise and swapped. The subsequent entangled pairs are then connected and swapped in the second swap level to distribute entanglement over the whole distance

Entanglement swapping is the basic idea in quantum repeaters. The purpose of a quantum repeater is to distribute entanglement, which is hard using direct quantum signaling if

the distance is large[7]. Entanglement swapping makes it possible to distribute entanglement using classical signals.

3.5 Quantum repeater

A drawback of using quantum systems is that they are vulnerable to noise because it is hard to remove noise in a quantum signal. Classical signals are also subject to noise but there exist various methods of removing noise in a classical signal because it is possible to copy a classical signal in order to amplify it or do error correction.

Most of our daily communication is transmitted in optical fibers or sent as free space propagation. Both of these channels contain noise, which leads to decoherence and loss of the signal. In classical signaling stations are created along the communication channel where the signal is amplified and the noise removed. These stations are called repeater stations.
The same procedure is not applicable in quantum signaling because the no-cloning theorem states that noiseless amplification of a quantum signal is impossible. This has a drastic impact on the communication rate of quantum signaling. A typical telecommunication optical fiber has losses of about 0.2 dB/km for optical wavelengths around 1.5 μm. This means that after 150 km only 0.1% of the signal is transmitted if there is no amplification. After 1000 km only 10^{-18}% is transmitted.
The time needed to transmit a quantum signal can be illustrated by considering the task of transmitting a quantum signal consisting of one photon over a distance of 1000 km. For a source repetition rate of 10 GHz meaning that 10^{10} photons are produced every second it would take about 300 years to transmit just one photon! It is clear that direct transmission of a quantum signal is not the best way to sent information over a large distance. Instead quantum repeaters can be used.
The general quantum repeater consists of two steps:

1. Divide the total distance L over which entanglement should be created into smaller segments of length $L_0 = \frac{L}{2^n}$ where it is possible to create entanglement by direct transmission of a quantum signal between two neighboring stations [8]. The segments of length L_0 between neighboring stations are called the elementary links of the repeater. It is important that the entanglement in these is created in a heralded way!

2. Connect the elementary links pairwise and perform entanglement swapping. This procedure is repeated n times until entanglement is created over the total distance L

The creation of entanglement in the elementary links should to be done in a heralded way because it is necessary to know if a link contains entanglement before it is swapped with

[7] This is due to the noise problem (see section 3.5)
[8] There will be 2^{n+1} stations covering the distance L (see figure 3.1)

another link. This brings forward the need of *quantum memories* in quantum repeaters.

Quantum memories are basically any type of system where a quantum signal can be stored for an amount of time. A lot of research is put into finding efficient quantum memories and various systems have been proposed such as crystals, atomic ensembles and quantum dots [24, 33, 25]. The reason for this is that the performance of quantum repeaters drop drastically without quantum memories. Without quantum memories the entanglement has to be created simultaneously in all elementary links and all later swaps would also have to work simultaneously in each level. In most repeater schemes the swapping is probabilistic meaning that it has some probability to work. Consequently the condition that all swaps work simultaneously in every level dramatically decreases the performance of the repeater. With quantum memories the signal can be kept until entanglement is created the neighboring segment and a swap can be made. A quantum memory is in a sense a system that convert *flying* qubits into *stationary* qubits and vice versa. A *flying* qubit can move (e.g. photons) while the *stationary* qubit is spatially fixed. Investigating the performance of a given quantum repeater scheme it is common to assume that efficient quantum memories exist. This is also an assumption of this thesis.

3.5.1 Rate of repeaters

Quantum repeaters are compared at the rate of which entanglement is distributed over a given distance. This rate depends on the probabilities for successful generation of the initial states, entanglement creation and entanglement swapping. It is common to assume that all local operations in a quantum repeater take negligible time compared to the time it takes to send a signal between to neighboring stations, which is denoted $\tau_0 = L_0/c$ where c is the speed of light and L_0 is the distance between the stations. Then $1/\tau_0$ is the *source repetition rate* of the repeater meaning that τ_0 is the waiting time at the elementary level of the repeater. Let P_0 denote the probability of a successful entanglement creation. The time it takes to create entanglement in one elementary link is

$$\tau = \tau_0 \frac{1}{P_0} \tag{3.18}$$

The time it takes to establish entanglement in two neighboring elementary links is

$$\tau = \tau_0 \frac{3 - 2P_0}{(2 - P_0)P_0} = \tau_0 \nu_0 \tag{3.19}$$

where ν_0 is the average number of tries needed for two independent binomial events each with probability P_0 to both succeed [26][9]. If $P_0 \ll 1$ it is seen that $\nu_0 \approx \frac{3}{2P_0}$.

[9] This formula assumes that the signal can be kept e.g. in a quantum memory.

Let P_n denote the probability of a successful swap at the n'th level ($n \geq 1$). The time it takes to perform n levels of swapping will be

$$\tau = \tau_0 \frac{3 f_2 f_3 \dots f_n}{2 P_0 P_1 \dots P_n} \tag{3.20}$$

where the factors $f_2 \dots f_n$ take into account that entanglement has to be created in two neighboring links at level $i-1$ in order to swap at the i'th level. These factors obey that $1 \leq f_i \leq 2$ [29]. It is shown in Ref. [26, p. 24] that all $f_i \approx \frac{3}{2}$ if $P_i < \frac{1}{2}$. Within these assumptions the rate of a repeater with quantum memories is

$$r_n = \left(\frac{2}{3}\right)^{n+1} P_0 P_1 \dots P_n \tag{3.21}$$

where n is the number of swap levels. Note that this rate is far higher than in the case of no quantum memories. In that case the time needed to establish entanglement in two neighboring links would be proportional to P_i^{-2} instead of $\frac{3}{2P_i}$.

Chapter 4

A Hybrid Repeater

[1]The main part of this thesis is based on the hybrid repeater protocol suggested by Jonathan B. Brask et al. in Ref. [13]. Many of the elements in the altered hybrid repeater protocol presented in chapter 5 are found in the original protocol and therefore the hybrid repeater by Jonathan B. Brask et al. is treated in some detail.

4.1 Creation of entanglement

The first step of the hybrid repeater protocol is to create entanglement in the elementary links of the repeater. This is obtained in a heralded way using two sources of two-mode squeezed vacuum states and relies on SPD (Single Photon Detection), which is in the discrete variable regime. The setup is seen in figure 4.1.

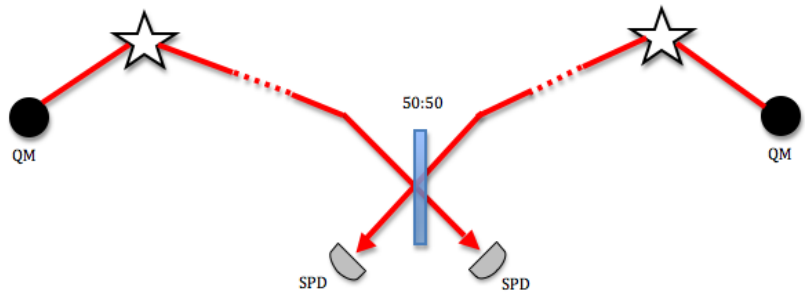

Figure 4.1: The setup for generation of entanglement in the elementary links. The stars are the sources of two-mode squeezed vacuum states and the black circles are quantum memories.

[1]The literature for this chapter is found in [13] and [26, p. 77-92]

The two sources of two-mode squeezed vacuum states can be realized using *parametric down conversion* where a strong coherent signal is sent through a nonlinear medium that creates or destroys photons in pairs [27]. The output from one of the sources is

$$|out\rangle = \hat{S}(\xi)\,|00\rangle\,. \tag{4.1}$$

$\hat{S}(\xi)$ is the two-mode squeeze operator

$$\hat{S}(\xi) = \exp\left(\xi^*\hat{a}\hat{b} - \xi\hat{a}^\dagger\hat{b}^\dagger\right) \tag{4.2}$$

where $\xi = re^{i\theta}$ and $\hat{a}, \hat{b}$ are operators of the two modes.
Like the one-mode squeeze operator the two-mode squeeze operator creates and destroys photons in pairs, but with the difference that the photons are created in different modes. The state (4.1) can be written in the form

$$|out\rangle = \frac{1}{\mathrm{cosh}r}\sum_{n=0}^{\infty}\frac{(\mathrm{tanh}r)^n}{n!}(\hat{a}^\dagger\hat{b}^\dagger)\,|00\rangle \tag{4.3}$$

assuming $\theta = 0$. For weak squeezing the state essentially is

$$|00\rangle + \sqrt{p}\,|11\rangle + O(p) \tag{4.4}$$

where p is the probability to create a pair of excitations and $O(p)$ denotes contributions from multiple excitations. From each source one of the output modes is read into a quantum memory and the other is sent to a balanced beam splitter positioned between the two sources. The output from the beam splitter is measured and following a single SPD click the two modes in the quantum memories are projected to a Bell state of the form

$$\frac{1}{\sqrt{2}}\left(|01\rangle \pm |10\rangle\right). \tag{4.5}$$

where the sign depends on which detector clicked. However, the probability of a single SPD click even though more than two photons were generated by the sources exists. A single SPD click would occur if one of the photons were lost in the fiber on its way to the beam splitter. Therefore the type of state generated is not a perfect Bell state but

$$\frac{1}{\sqrt{2}}\left(|01\rangle \pm |10\rangle\right) + O(\sqrt{p}). \tag{4.6}$$

The extra term $O(p)$ accounts for contributions from multiple excitations, which is small when the pair production probability p is small. This means that better Bell states are produced for small values of p but the rate at which these states are produced will also be small.
The rate at which entanglement is created in the elementary links depends on the pair production probability p and the efficiency of the detectors. In Ref. [13] detector efficiencies of 50% are assumed, which means that there is a 50% chance that the detectors detect a photon hitting them.

4.2 Growing of cat states

The goal of the hybrid repeater is to distribute entanglement in the form of states resembling

$$|\gamma(\theta,\alpha)\rangle = \frac{1}{\sqrt{M_\alpha^+(\theta)}}\left(e^{i\theta}|\alpha\rangle|\alpha\rangle + e^{-i\theta}|-\alpha\rangle|-\alpha\rangle\right) \tag{4.7}$$

where $M_\alpha^+(\theta) = 2(1+\cos(2\theta)e^{-4|\alpha|^2})$. Such states are called *Schrödinger cat states* named after the cat paradox by Schrödinger. The entanglement is stored in the field operators, which is in the continuous variable regime[2].
The next step of the repeater is to grow the Bell-like states from the first step into states resembling (4.7). This is realized by means of balanced beam splitters and homodyne detection (see figure 4.2[3]).

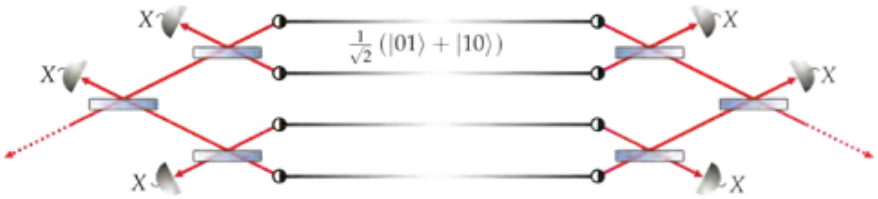

Figure 4.2: The growing of cat states. This is performed locally on each of the input modes in the bell state. The figure shows two iterations of the procedure.

The process is performed on each mode of the Bell-like states but can be explained with one-mode inputs. In the one-mode case the input state of the first beam splitter is two one-photon states, $|1\rangle|1\rangle$, which has the wave function

$$\psi_0(x,y) = \psi_0'(x)\psi_0'(y) = \sqrt{2}\pi^{-\frac{1}{4}}xe^{-\frac{1}{2}x^2}\cdot\sqrt{2}\pi^{-\frac{1}{4}}ye^{-\frac{1}{2}y^2} \tag{4.8}$$

The balanced beam splitter reflects and transmits the input signal in a 50:50 ratio. This transforms the state (4.8) into

$$\psi_1(x,y) = \psi_0'\left(\frac{1}{\sqrt{2}}(x+y)\right)\psi_0'\left(\frac{1}{\sqrt{2}}(x-y)\right). \tag{4.9}$$

The $\hat{X}$ quadrature of one of the output modes e.g. mode y is measured and the measurement outcome is y_0. Provided that y_0 lies in a interval $[-\Delta,\Delta]$ around zero the other

[2]The entanglement of the state in eq. 4.7 depends on both θ and α but for $\alpha > 2$ the state is a maximally entangled state more or less independent of the phase θ

[3]This figure was taken from [26, p. 83]

output mode is kept. Ideally $y_0 = 0$ but conditioning on this would result in a probability of success of zero. In the ideal case where $y_0 = 0$ the other output mode is

$$\psi_1(x) = \Gamma \left(\frac{5}{2}\right)^{-\frac{1}{2}} x^2 e^{-\frac{1}{2}x^2}. \tag{4.10}$$

The state (4.10) resembles that of a squeezed one-mode cat state

$$\hat{S}(2) \left|\xi^+(\alpha)\right\rangle = \hat{S}(2) \frac{1}{\sqrt{N_\alpha^+}} (|\alpha\rangle + |-\alpha\rangle) \tag{4.11}$$

where $\hat{S}(p)$ denotes squeezing in the $\hat{X}$ quadrature by a factor of p and $N_\alpha^+ = 2(1+e^{-2|\alpha|^2})$. For $\alpha = \sqrt{5/2}$ the fidelity of (4.10) and the squeezed one-mode cat state is 98%. The process can be iterated to grow better cat states. After m iterations the output is

$$\psi_m = \Gamma \left(2 + \frac{1}{2}\right)^{-\frac{1}{2}} x^{2^m} e^{-\frac{1}{2}x^2} \tag{4.12}$$

For $m = 2$ the fidelity with a squeezed one-mode cat state

$$\hat{S}(2) \left|\xi^+(\mu_m)\right\rangle = \hat{S}(2) \frac{1}{\sqrt{N_{\mu_m}^+}} (|\mu_m\rangle + |-\mu_m\rangle) \tag{4.13}$$

where $\mu_m = \sqrt{2^m + 1/2}$, exceeds 99%.

The procedure works with an arbitrary number of modes in the input states. In the repeater the relevant number of modes in the input is two and then the squeezing is a non-local effect. Using the Bell-like states as input states the output state after m iterations resembles the state

$$\hat{S}_+(2) \left|\gamma(0, \mu_m/\sqrt{2})\right\rangle_{ab}. \tag{4.14}$$

where a and b are the two spatially separated modes and $\hat{S}_+(2)$ is non-local squeezing by a factor of two in the quadrature $\hat{X}_+ = (\hat{X}_a + \hat{X}_b)/\sqrt{2}$ [26, p. 82]

The rate at which the squeezed cat states are grown depends on the choice of the acceptance interval $[-\Delta, \Delta]$. When increasing Δ the probability of a successful growing procedure is increased. However, the fidelity of the output state and a squeezed cat state decreases when Δ is increased. This behavior is seen in figure 4.3.

The rate is calculated within the same approximations leading to eq.(3.21) and is in units of the source repetition rate. Thus the rate, r_i of growing a cat state of i'th iterations is

$$r_i = \left(\frac{3}{2}\right)^{i-1} P_1 P_2 \dots P_i \tag{4.15}$$

where P_i is the probability of a successful growing at iteration i.

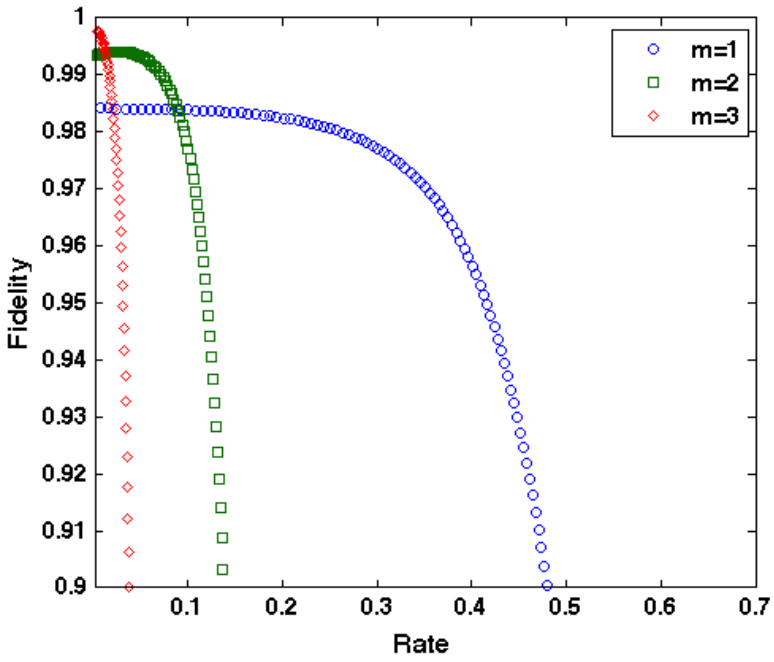

Figure 4.3: The fidelity of the output state and a squeezed one-mode cat state as a function of the rate for $m = 1$, 2 and 3. The rate is measured in units of the source repetition rate. m is the number of iterations

4.3 Entanglement swapping

It is illustrative to start by looking at the swap procedure using ideal two-mode cat states as inputs. This is the limit where the two previous steps in the repeater are done perfectly and squeezing in the cat states is neglected. The swap procedure is illustrated in figure 4.4a[4].

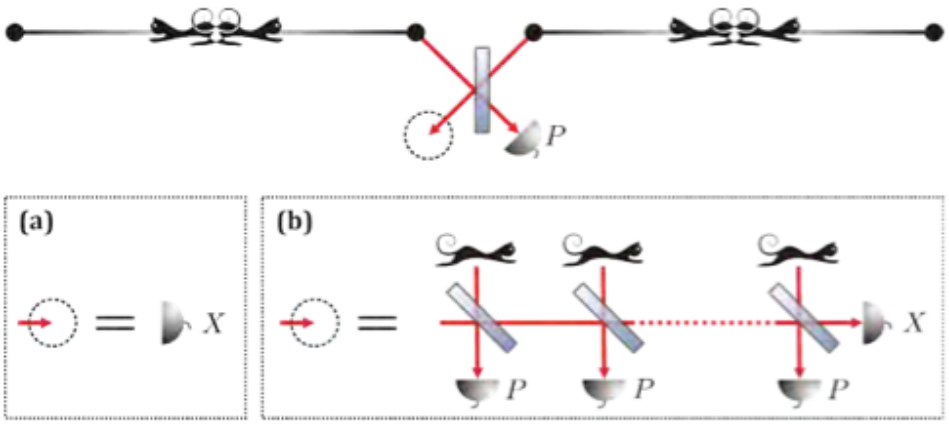

Figure 4.4: a) Simple entanglement swapping using a 50:50 beam splitter and homodyne detection. A success is conditioned on an $\hat{X}$ measurement close to zero. b) Swapping using auxiliary cat states, which are inserted before the $\hat{X}$ measurement to obtain near-deterministic swapping

Two modes - one from each two-mode cat state - are connected on a 50:50 beam splitter. Afterwards the $\hat{X}$ quadrature of one of the output modes and the $\hat{P}$ quadrature of the other output mode are measured. The input state of the beam splitter is

$$|\gamma(0,\alpha)\rangle_{12}\,|\gamma(0,\alpha)\rangle_{34} = \frac{1}{M_\alpha^+(0)}\left(|\alpha,\alpha\rangle_{12} + |-\alpha,-\alpha\rangle_{12}\right)\left(|\alpha,\alpha\rangle_{34} + |-\alpha,-\alpha\rangle_{34}\right). \quad (4.16)$$

It is assumed that $\alpha \in \mathbb{R}$ since this is true for the squeezed cat states generated in the second step of the repeater. A 50:50 beam splitter transforms an arbitrary coherent state input $|\alpha_1\rangle\,|\alpha_2\rangle$ into a product of coherent states with amplitudes of $(\alpha_1 \pm \alpha_2)/\sqrt{2}$. It is assumed that mode 2 and 3 are combined on the beam splitter. The output modes are called p and x, which refers to the measurements performed on these modes. The beam

[4]This figure was taken from [26, p. 83]

splitter brings the input state into the unnormalized state

$$\left[|\alpha,\alpha\rangle_{14}\left|\sqrt{2}\alpha\right\rangle_p + |-\alpha,-\alpha\rangle_{14}\left|-\sqrt{2}\alpha\right\rangle_p\right]|0\rangle_x + \left[|\alpha,-\alpha\rangle_{14}\left|\sqrt{2}\alpha\right\rangle_x + |-\alpha,\alpha\rangle_{14}\left|-\sqrt{2}\alpha\right\rangle_x\right]|0\rangle_p . \tag{4.17}$$

Now the $\hat{P}$ quadrature is measured. The momentum space wave function of an arbitrary coherent state $|\alpha\rangle$ is

$$\langle p|\ \alpha\rangle = \frac{1}{\pi^{1/4}} e^{-\frac{1}{2}p^2 - i\sqrt{2}\alpha p + i\alpha \mathrm{Im}(\alpha)}. \tag{4.18}$$

Thus after a $\hat{P}$ measurement with outcome p_0 the state (4.17) is

$$\left[|\alpha,\alpha\rangle_{14}\, e^{-i2\alpha p_0} + |-\alpha,-\alpha\rangle_{14}\, e^{i2\alpha p_0}\right]|0\rangle_x + \left[|\alpha,-\alpha\rangle_{14}\,|\sqrt{2}\alpha\rangle_x + |-\alpha,\alpha\rangle_{14}\,|-\sqrt{2}\alpha\rangle_x\right]. \tag{4.19}$$

If α is large enough $\langle 0|\ \sqrt{2}\alpha\rangle = \langle 0|\ -\sqrt{2}\alpha\rangle \approx 0$. Thus if the $\hat{X}$ measurement has an outcome close to zero the state (4.19) after the measurement is

$$|\alpha,\alpha\rangle\, e^{-2i\alpha p_0} + |-\alpha,-\alpha\rangle\, e^{2i\alpha p_0} = \left|\gamma'(\theta_0,\alpha)\right\rangle \tag{4.20}$$

where $\theta_0 = -2\alpha p_0$. This state is a two-mode cat state with a phase of θ_0 and therefore the swap has been a success. Given that $|0\rangle$ and $\left|\pm\sqrt{2}\alpha\right\rangle$ are orthogonal, the probability of an $\hat{X}$ measurement that projects the state (4.19) into (4.20) is 1/2 since the norm of the first and last bracket in eq.(4.19) is both 2. Note that an $\hat{X}$ measurement yielding one of the states $\left|\pm\sqrt{2}\alpha\right\rangle$ will bring the output state into a product state since $\left\langle -\sqrt{2}\alpha\right|\ \sqrt{2}\alpha\rangle \approx 0$. The probability of a successful swap is bounded by $\frac{1}{2}$, which is reached for large α values. The requirement that the $\hat{X}$ measurement is close to zero means that it is necessary to choose an acceptance interval $[-\delta,\delta]$ around zero in which the contribution from the states $\left|\pm\sqrt{2}\alpha\right\rangle$ is negligible. The probability of a successful swap is less than $\frac{1}{2}$ for small values of α since a non-negligible part of the $|0\rangle$ state distribution will lie outside the acceptance interval. For small values of α, a large δ will give a high success probability but a low fidelity between the output state and a two-mode cat state. Likewise a small δ will reduce the probability of a successful swap but increase the fidelity.

4.4 Near-deterministic swapping

It is shown in Ref. [13] that near-deterministic swapping can be obtained using auxiliary cat states. To do this, additional beam splitters are inserted between the first beam splitter output and the $\hat{X}$ measurement. A one-mode cat state $\left|\xi^+(2^{j/2}\alpha)\right\rangle = \frac{1}{\sqrt{N^+_{2^{j/2}\alpha}}}\left(\left|2^{j/2}\alpha\right\rangle + \left|2^{j/2}\alpha\right\rangle\right)$ is injected at the j'th beam splitter (see figure 4.4b).

For simplicity the details of inserting a single auxiliary cat state is described to show how this increases the probability of a successful swap. The starting state is (4.19), which is after the first beam splitter and the subsequent $\hat{P}$ measurement. After mixing with a one-mode cat state $\left|\xi^{+}(\sqrt{2}\alpha)\right\rangle$ the state is

$$\left|\gamma'(\theta_0,\alpha)\right\rangle_{14}\left(\left|\alpha\right\rangle_p\left|\alpha\right\rangle_x+\left|-\alpha\right\rangle_p\left|-\alpha\right\rangle_x\right)+\left|\alpha,-\alpha\right\rangle_{14}\left(\left|2\alpha\right\rangle_p\left|0\right\rangle_x+\left|0\right\rangle_p\left|2\alpha\right\rangle_x\right)$$
$$+\left|-\alpha,\alpha\right\rangle_{14}\left(\left|0\right\rangle_p\left|-2\alpha\right\rangle+\left|-2\alpha\right\rangle_p\left|0\right\rangle_x\right). \quad (4.21)$$

After the second $\hat{P}$ measurement the state becomes

$$\left|\gamma'(\theta_0,\alpha)\right\rangle_{14}\left(e^{-i\sqrt{2}\alpha p_1}\left|\alpha\right\rangle_x+e^{i\sqrt{2}\alpha p_1}\left|-\alpha\right\rangle_x\right)+$$
$$\left(e^{-2^{3/2}\alpha p_1}\left|\alpha,-\alpha\right\rangle_{14}+e^{2^{3/2}\alpha p_1}\left|-\alpha,\alpha\right\rangle_{14}\right)\left|0\right\rangle_x+$$
$$\left|\alpha,-\alpha\right\rangle_{14}\left|2\alpha\right\rangle_x+\left|-\alpha,\alpha\right\rangle_{14}\left|-2\alpha\right\rangle_x. \quad (4.22)$$

Up to a local phase shift the state $\left|\tilde{\gamma}'(\theta_1,\alpha)\right\rangle = e^{\theta_1}\left|\alpha,-\alpha\right\rangle_{14}+e^{\theta_1}\left|-\alpha,\alpha\right\rangle_{14}$ is equal to $\left|\gamma'(\theta_1,\alpha)\right\rangle$ and therefore is also a desirable output state of the swap. Letting $\theta_1=-2^{3/2}\alpha p_1$ and $\nu=\sqrt{2}\alpha p_1$ the state (4.22) is

$$\left|\gamma'(\theta_0,\alpha)\right\rangle_{14}\left(e^{i\nu}\left|\alpha\right\rangle_x+e^{-i\nu}\left|-\alpha\right\rangle_x\right)+\left|\tilde{\gamma}'(\theta_1,\alpha)\right\rangle_{14}\left|0\right\rangle_x+$$
$$\left|\alpha,-\alpha\right\rangle_{14}\left|2\alpha\right\rangle_x+\left|-\alpha,\alpha\right\rangle_{14}\left|-2\alpha\right\rangle_x. \quad (4.23)$$

Assuming that α is large enough for $\left|0\right\rangle$ and $\left|\alpha\right\rangle$ to be orthogonal an $\hat{X}$ measurement falling in the distributions of either $\left|0\right\rangle$ or $\left|\pm\alpha\right\rangle$ will be a successful swap[5]. The probability of this to happen is 3/4.
The procedure can be generalized to using k auxiliary cat states. The probability of a successful swap will scale as

$$1-2^{-k-1} \quad (4.24)$$

assuming that all states remain distinguishable [13]. This means that α must scale with k as $\alpha\sim 2^{k/2}$ to keep the fidelity with a perfect two-mode cat state above some arbitrary threshold. Thus to obtain near-deterministic swapping it is necessary to generate very large cat states, which is hard to do. Therefore the overall performance of the repeater is not necessarily improved by the use of auxiliary cat states.

4.5 Swapping with approximate squeezed two-mode cat states

[6] The states generated in the second step of the hybrid repeater protocol are well approximated by the squeezed two-mode cat state in eg. (4.14). The wave function of this state

[5] This implies that also $\left|\alpha\right\rangle$ and $\left|2\alpha\right\rangle$ are orthogonal
[6] The formulas in this section is taken from [26, p. 116-118]

is

$$\psi_{0m}(x_a, x_b) = N_{0,m}^{-1/2} e^{-\frac{1}{4}(x_a - x_b)^2} \left[e^{-\frac{1}{2}(x_a + x_b - \mu_m)^2} + e^{-\frac{1}{2}(x_a + x_b + \mu_m)^2} \right] \tag{4.25}$$

where $N_{0,m} = 2^{-1/2}\pi(1+e^{-\mu_m^2})$ and $\mu_m = \sqrt{2^m + 1/2}$. Assuming that all $\hat{X}$ measurements yield zero and performing n swap levels with this state gives the output state

$$\begin{aligned} \psi_{nm}(x_a, x_b) = N_{nm}^{-1/2} e^{-i(\phi_{a,n} x_a + \phi_{b,n} x_b)} e^{-\frac{k_n}{8}(x_a - x_b)^2} \times \\ \left[e^{-\frac{1}{k_n}(x_a + x_b - \mu_m)^2 - i\phi_n} + e^{-\frac{1}{k_n}(x_a + x_b + \mu_m)^2 + i\phi_n} \right]. \end{aligned} \tag{4.26}$$

where $k_n = 2\sqrt{2}\text{coth}(2^n \text{arccoth}(1/\sqrt{2}))$ and $\{\phi_{a,n}, \phi_{b,n}, \phi_n\}$ depend on the outcome of the $\hat{P}$ measurements in all swap levels. Using that $\phi_{a,0} = \phi_{b,0} = \phi_0 = 0$ they can be found recursively from the relations

$$\phi_{n+1} = \frac{8\mu_m}{k_{n+1}k_n} \left(\frac{p}{\sqrt{2}} + \phi_{b,n} + \phi'_{a,n} \right) + \phi_n + \phi'_n \tag{4.27}$$

$$\phi_{a,n+1} = \frac{1}{k_{n+1}} \left(\frac{k_n}{4} + \frac{2}{k_n} \right) \left(\frac{p}{\sqrt{2}} + \phi_{b,n} + \phi'_{a,n} \right) + \phi_{a,n} \tag{4.28}$$

$$\phi_{b,n+1} = \frac{1}{k_{n+1}} \left(\frac{k_n}{4} + \frac{2}{k_n} \right) \left(\frac{p}{\sqrt{2}} + \phi_{b,n} + \phi'_{a,n} \right) + \phi'_{b,n} \tag{4.29}$$

The parameters $\phi_{a,n}$ and $\phi_{b,n}$ can be cancelled by local operations since they correspond to displacements in phase space along the quadratures $\hat{P}_a$ and $\hat{P}_b$. Neglecting the term containing these parameters in eq. (4.26) and using that k_n converges in a fast way to $2\sqrt{2}$ the output state is

$$|\phi_{target}\rangle_{ab} = \hat{S}_a(\sqrt{2})\hat{S}_b(\sqrt{2}) \left| \gamma(\phi_n, 2^{-5/4}\mu_m) \right\rangle_{ab} \tag{4.30}$$

This state is the target state of the hybrid repeater in Ref. [13]. It is a two-mode cat state with local squeezing.

4.6 Performance

To study the performance of the hybrid repeater all of the three steps described i.e. entanglement generation, growing of cat states and entanglement swapping have to be collected. They are collected in a nested way such that the entanglement swapping lies on top of the growing of cat states, which lies on top of entanglement creation in the elementary links. The parameters that have an influence on the performance are:

- p: A small value of p reduces the contributions from higher excitations in the input states of the entanglement creation but also decreases the rate of the procedure.

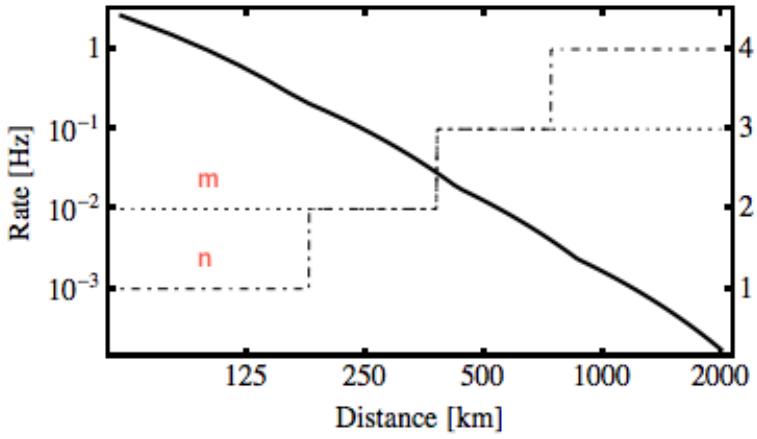

Figure 4.5: The optimal rate of the hybrid repeater resulting from the optimization. The figure also shows the optimal values of m and n on the axis to the right.

- Δ: A large value of Δ increases the rate of the growing procedure but decreases the fidelity of the output state with a squeezed cat state.
- m: The more iterations (m) performed, the higher the fidelity of the output state with a squeezed cat state is. However, the rate of the growing procedure will decrease with m.
- δ: For small values of α the fidelity with the target state after swapping is increased as δ is decreased. Nevertheless the probability of a successful swap is also decreased when δ is decreased.
- n: The number of swap levels n determines the classical communication time in the elementary links and the loss in the fibers connecting the stations.

The optimization of the repeater is made in Ref. [13] by making a grid of values for Δ, m, δ, n and treat p perturbatively. The rate of the total repeater is calculated using the expression in eq. (3.21) where the source repetition rate is c/L_0 and a lower bound of 90% on the output fidelity with the target state (4.30) is assumed i.e.

$$F = |\langle\psi_{target}|\, \hat{\rho_{out}}\, |\psi_{target}\rangle|^2 \geq 0.9 \tag{4.31}$$

The result of the optimization is seen in figure 4.5[7].

Figure 4.5 shows that the hybrid repeater manages to distribute states with a fidelity ≥ 0.9 over a distance of 1000 km at a rate of 0.1 pairs pr. min. This is a quite good result

[7]The plot was provided by Jonathan B. Brask and is also found in Ref. [13]

compared to other repeater schemes that either use highly efficient SPD's or complicated swap procedures [9, 14].
Nonetheless there are some elements in the hybrid repeater scheme suggested by Jonathan B. Brask et al. that could be altered to increase the performance. This has lead to the development of an *altered* hybrid repeater, which is described in the next chapter.

Chapter 5

The Altered Hybrid Repeater

The repeater protocol suggested by Jonathan B. Brask et al. consists of the tree steps described in chapter 4. These steps are

1. Creation of entanglement
2. Growing of cat states
3. Entanglement swapping

The rate of each of the individual steps determines the overall rate of the repeater. If step two or three of the repeater fails, the previous steps are repeated[1]. This means that every time step two or three fails it is necessary to reestablish entanglement in the elementary links. The source repetition rate of step one is L_0/c since the creation of entanglement is a non-local process. The time needed to perform local operations is negligible compared to L_0/c.
Therefore it is desirable to create entanglement later in the repeater protocol so that it does not have to be repeated as many times. This is the main idea of the *altered* hybrid repeater protocol presented in this thesis. The altered hybrid repeater protocol consists of the same three steps as the original but in a different order:

1. Growing of cat states
2. Creation of entanglement
3. Entanglement swapping

The time consuming process of entanglement creation is now step two in the repeater protocol and therefore only has to be repeated when the entanglement swapping fails. The procedure of growing cat states is almost the same as in the original repeater except that

[1]The term "fails" means that you get an $\hat{X}$ measurement outside your acceptance intervals (Δ and δ)

one-mode squeezed cat states are grown and not two-mode squeezed cat states. Furthermore the procedure of choosing the acceptance interval $[-\Delta, \Delta]$ is changed. In the original repeater the acceptance interval is fixed to the same value for every iteration. Nonetheless a higher rate might be obtained by increasing the acceptance interval after each iteration. The creation of entanglement cannot be made in the same way as in the original repeater but the general idea is similar. A method suggested by N. Sanguard et al. in Ref. [14] to connect one-mode cat states into entangled two-mode cat states is used to create entanglement in the elementary links of the altered repeater. Using SPD this method is in the discrete variable regime.
The procedure of entanglement swapping is the same as in the original repeater since the entangled states of the altered repeater are similar to the entangled states of the original scheme.

5.1 Growing of cat states

The procedure of growing cat states in the altered repeater is described in section 4.2 since it is similar to the procedure of the original repeater. Nevertheless it is interesting to consider how the wave function of the output state behaves as a function of the number of iterations. This is shown in figure 5.1.
Figure 5.1 shows how the right and left top becomes more separated as the number of iterations increases. When two of these states are combined on a beam splitter to make the next iteration the subsequent measurement of the $\hat{X}$ quadrature will determine how the states were combined.
Suppose that the $\hat{X}$ measurement is performed in the output in which the tops in the wave functions of the input states are added[2]. If the two tops to the right are combined the outcome of the $\hat{X}$ measurement will have a positive value. If the two tops to the left are combined the measurement outcome will have a negative value. These two possibilities are not desirable since the wave function of the corresponding output state essentially will be a top around zero. However, if a top to the right is combined with a top to the left or vice versa the outcome of the $\hat{X}$ measurement will in both cases be a value in the vicinity of zero and the output state will be the desired approximate cat state. This behavior is illustrated in figure 5.2.

In the original repeater protocol by Jonathan B. Brask et al. the acceptance interval of the $\hat{X}$ measurement was fixed for all iterations. This is not the optimal way of growing the cat states. A small acceptance interval is needed because there is a probability that an $\hat{X}$ measurement close to zero comes from a combination of two right or two left tops, which gives the wrong output state. The closer the tops are to each other in the input states the smaller acceptance interval is needed. When iterating the growing process the

[2] A similar argument exists if the $\hat{X}$ measurement is performed in the other output

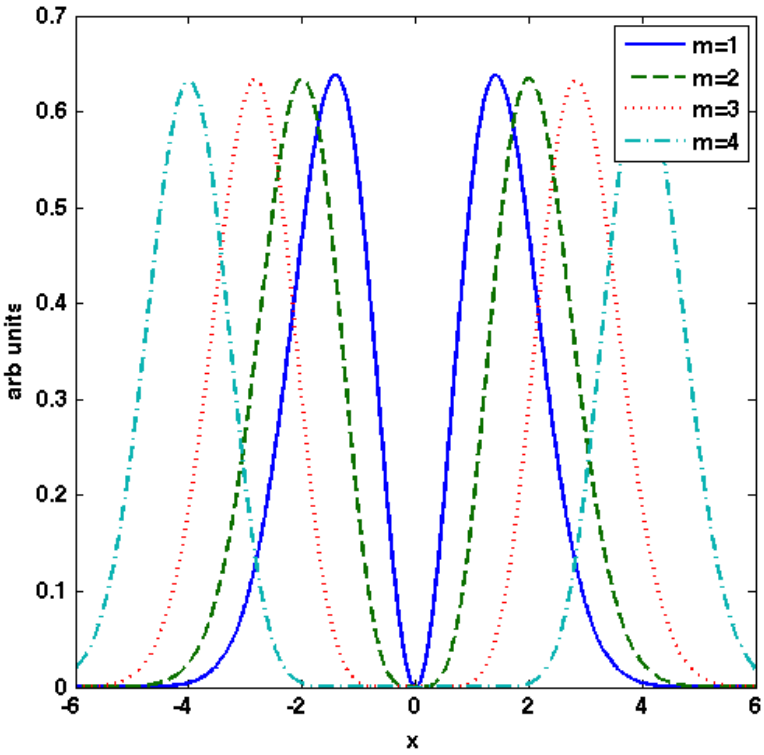

Figure 5.1: Wavefunction of the optimal output state for m=1,2,3 and 4. The expression of the wave function of the states can be seen in eq. (4.12). The tops become more separated as m increases

tops become more separated and a bigger acceptance interval can be chosen, which will result in a higher probability for a successful growing. The possibility of choosing different acceptance intervals for every iteration is included in the altered repeater protocol and an optimization in the choice of Δ has been made.

5.1.1 Optimizing acceptance intervals

In the optimization of the acceptance intervals the physical states are described by their Wigner functions, which makes it possible to calculate an average fidelity of the output states. Sources of perfect one-photon states are assumed to provide the input states. The Wigner function of a one-photon state is

$$W_0(x,p) = \frac{1}{\pi}\left(1 - x^2 - p^2\right) e^{-(x^2+p^2)}. \tag{5.1}$$

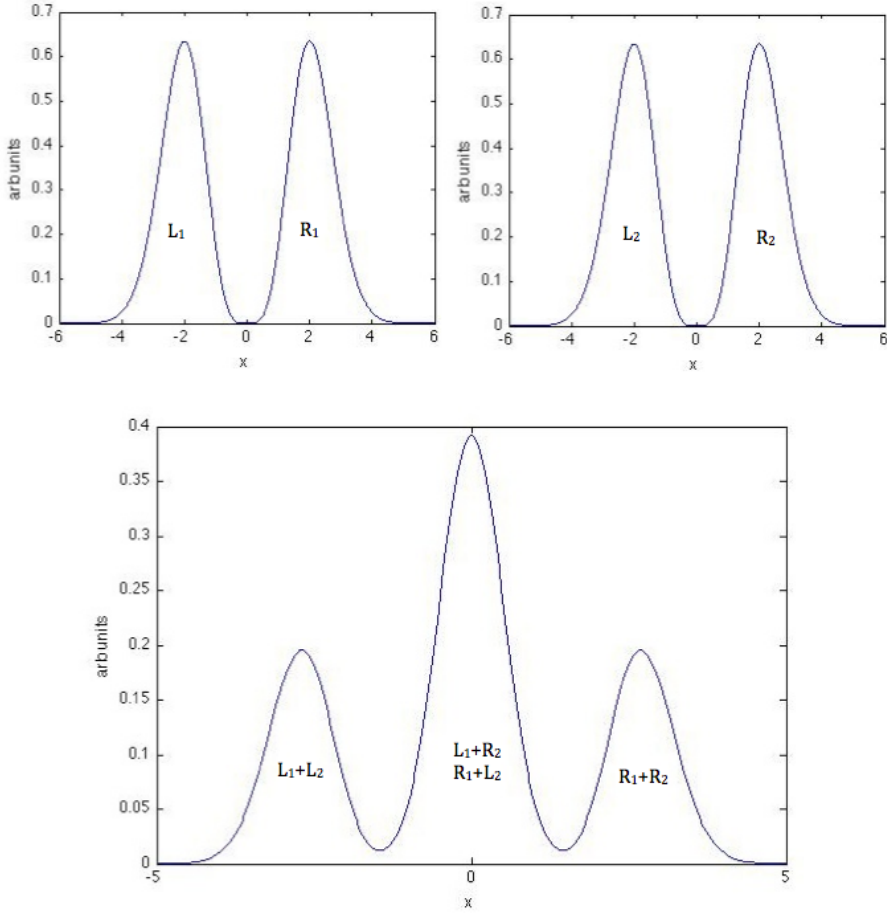

Figure 5.2: The input states have two tops that combine to yield 3 different tops in the probability distribution of the output where the $\hat{X}$ quadrature is measured. An $\hat{X}$ measurement that falls in the top around 0 will produce an approximately squeezed cat state.

When two of such states are combined on a 50:50 beam splitter it gives the state

$$W_0\left(\frac{1}{\sqrt{2}}(x+x'),\frac{1}{\sqrt{2}}(p+p')\right)W_0\left(\frac{1}{\sqrt{2}}(x-x'),\frac{1}{\sqrt{2}}(p-p')\right). \tag{5.2}$$

The unnormalized average output after measuring $x' \in [-\Delta, \Delta]$ is

$$W_1(x,p) = \int_{-\infty}^{\infty} \mathrm{dp}' \int_{-\Delta}^{\Delta} \mathrm{dx}' W_0\left(\frac{1}{\sqrt{2}}(x+x'),\frac{1}{\sqrt{2}}(p+p')\right)W_0\left(\frac{1}{\sqrt{2}}(x-x'),\frac{1}{\sqrt{2}}(p-p')\right). \tag{5.3}$$

The normalization constant of the state (5.3) is the inverse of the probability of measuring $x' \in [-\Delta, \Delta]$. To see how the Wigner function changes after each iteration, it is an advantage to write the input Wigner function as

$$W_m(x,p) = \sum_{i=0}^{2^{m+1}} \sum_{j=0}^{2^{m+1}} w_{ij} x^i p^j e^{-(x^2+p^2)}. \tag{5.4}$$

The one-photon input state can be written is this form with m=0 and

$$\mathbf{w} = \begin{pmatrix} -\frac{1}{\pi} & 0 & \frac{2}{\pi} \\ 0 & 0 & 0 \\ \frac{2}{\pi} & 0 & 0 \end{pmatrix}. \tag{5.5}$$

Two of these states are combined on the 50:50 beam splitter. The combined state is

$$\begin{aligned} W_{m+1}(x,p,x',p') = & \sum_{\{i,i\}=0'}^{2^{m+1}} \sum_{\{j,j'\}=0}^{2^{m+1}} w_{ij} w_{i'j'} \left(\frac{x+x'}{\sqrt{2}}\right)^i \left(\frac{p+p'}{\sqrt{2}}\right)^j \\ & \times \left(\frac{x-x'}{\sqrt{2}}\right)^{i'} \left(\frac{p-p'}{\sqrt{2}}\right)^{j'} e^{-(x^2+x'^2+p^2+p'^2)}. \end{aligned} \tag{5.6}$$

This can be written as

$$\begin{aligned} W_{m+1}(x,p,x',p') = & \sum_{\{i,i'\}=0}^{2^{m+1}} \sum_{\{j,j'\}=0}^{2^{m+1}} \left[\sum_{k=0}^{i+i'} \sum_{s'=s_{\min}}^{s_{\max}} \binom{i}{k-s'} \binom{i'}{s'} (-1)^{i'-s'} x'^{i+i'-k} x^k \right] \\ & \times \left[\sum_{l=0}^{j+j'} \sum_{t'=t_{\min}}^{t_{\max}} \binom{j}{l-t'} \binom{j'}{t'} (-1)^{j'-t'} p'^{j+j'-l} p^l \right] e^{-(x^2+x'^2+p^2+p'^2)} w_{ij} w_{i'j'} \end{aligned} \tag{5.7}$$

where $s_{\min} = \max(0, k-i), s_{\max} = \min(i', k), t_{\min} = \max(0, l-j)$ and $t_{\max} = \min(j', l)$
The unnormalized average output after measuring $x' \in [-\Delta, \Delta]$ is

$$W_{m+1}(x,p) = \sum_{k=0}^{2^{m+2}} \sum_{l=0}^{2^{m+2}} \tilde{w}_{kl} x^k p^l e^{-(x^2+p^2)}. \tag{5.8}$$

The matrix elements $\tilde{w}_{kl}$ is

$$\tilde{w}_{kl} = \sum_{\{i,i'\}=0}^{2^{m+1}} \sum_{\{j,j'\}=0}^{2^{m+1}} w_{ij} w_{i'j'} \mu_k^{ii'}(\Delta) \mu_l^{jj'}(\infty) \tag{5.9}$$

where

$$\mu_k^{ii'}(\varepsilon) = 2^{-(i+i')/2} \sum_{s'=s_{\min}}^{s_{\max}} \binom{i}{k-s'} \binom{i'}{s'} (-1)^{i+i'-k} \Lambda(\varepsilon, i+i'-k), \tag{5.10}$$

$$\Lambda(\varepsilon, \lambda) = \begin{cases} 0 & \text{if} \quad \lambda < 0, \lambda \text{ odd}, \\ \int_{-\varepsilon}^{\varepsilon} x^{\lambda} e^{-x^2} \mathrm{dx} & \text{if} \quad \lambda \text{ even}. \end{cases} \tag{5.11}$$

From eq. (5.8) it is seen that the Wigner function of the output state after m iterations will be of the form (5.4). The matrix elements w_{ij} depend on the choice of acceptance interval in each iteration.

The fidelity of the output Wigner function and a squeezed one-mode cat state of the form (4.13) is calculated on a grid of different acceptance intervals in order to find the optimal rate of the growing procedure. The grid is subject to the constraint that $\Delta_{m+1} \geq \Delta_m$. The program Matlab is used for the calculation and the code is described in Appendix D. The calculation is restricted to $m \leq 3$ iterations due to runtime reasons[3]. The result of the calculation is seen in figure 5.3.

Figure 5.3 shows that a higher rate is obtained by choosing a larger acceptance interval after each iteration. However the rate is not significantly increased, which is evident from table 5.1 where an output fidelity of 0.9 was assumed.

m	rate for diff. Δ	rate for fixed Δ
2	0.1423	0.1378
3	0.04104	0.03791

Table 5.1: Gain by choosing different acceptance intervals. The rate is in units of the source repetition rate. An output fidelity of 0.9 with a squeezed one-mode cat state was assumed.

From the optimization it is difficult to conclude anything about the general behavior for $m \geq 4$ iterations. Nevertheless it seems likely that the fractional difference in the rate for fixed and different Δ will grow for larger values of m because for every iteration the two tops in the input states become more separated. For very large m the two tops will be so far from each other that neither the fidelity nor the rate will be affected by choosing a larger acceptance interval.

In the optimization the fidelity was calculated with a squeezed cat state of the form (4.13). In the next step of the altered repeater protocol the one-mode states are connected to form

[3]The runtime refers to the runtime of the calculation.

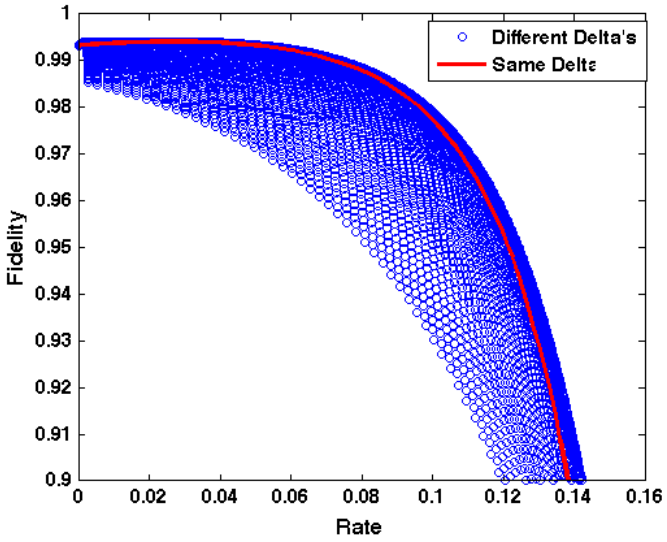

(a) Optimization for m=2

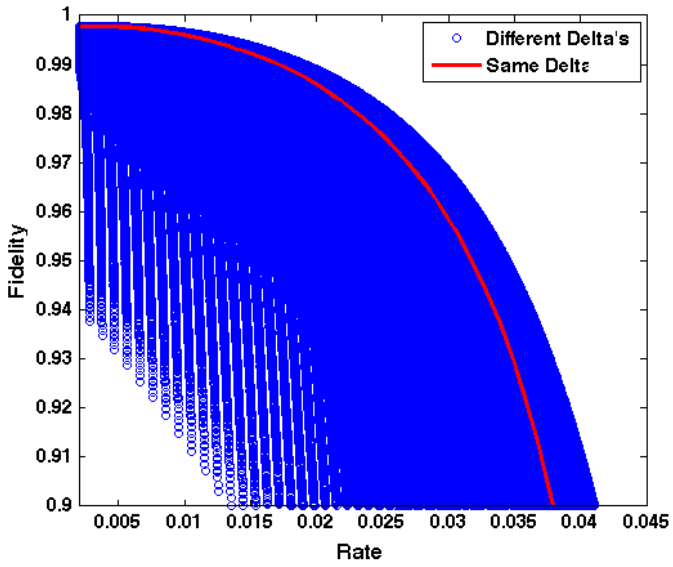

(b) Optimization for m=3

Figure 5.3: Result of the optimization for m=2 and m=3. The fidelity is with a squeezed cat state of the form (4.13) and the rate in units of the source repetition rate was calculated using the approximation in eq.(4.15). The optimal curve for different acceptance intervals is the edge of the blue grid and the red curve is the result for fixed Δ in every iteration. The rate at which the input states to the growing procedure can be provided is the source repetition rate.

entangled two-mode states. The two-mode states generated do not look like two-mode cat states unless m is relatively high (see section 5.2). Therefore it is interesting to also calculate the fidelity with a state of the form (4.12) in the optimization. The optimal curves of the output fidelity as a function of the rate are seen in figure 5.4.

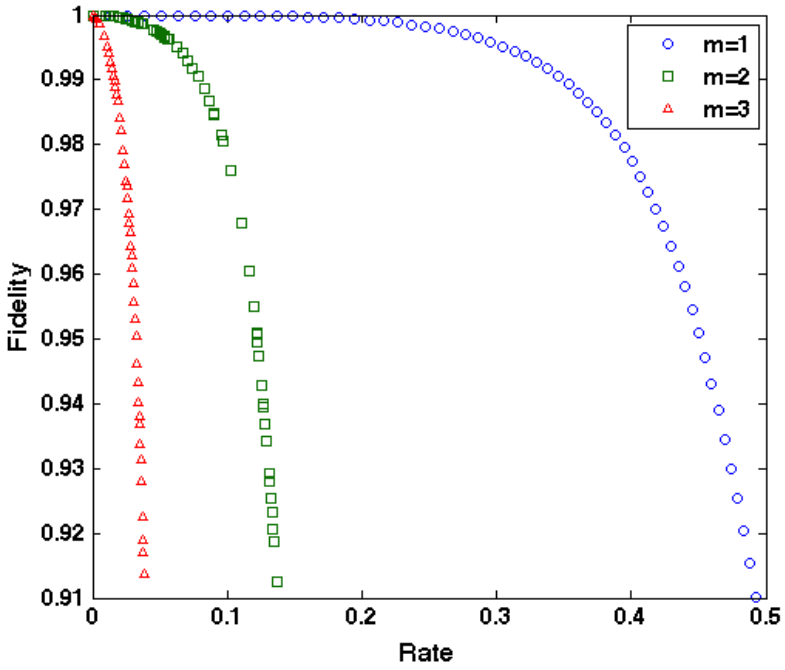

Figure 5.4: The fidelity with state (4.12) vs. the rate in units of the source repetition rate for m=1,2 and 3 iterations. The curves result from a optimization in the choice of acceptance intervals.

Note that the fidelity with state (4.12) is not increased by performing more iterations. However, the number of iterations has an effect on the subsequent steps of the repeater.

5.1.2 Two-photon components

So far sources of perfect one-photon states were assumed to produce the initial states. This is not a realistic assumption since all systems used as one-photon sources today have a non-vanishing probability of emitting two photons. Accordingly the input states provided for the growing of cat states will contain some two-photon component. This component can be made small at the cost of the rate at which the states are produced.
A two-photon component will lower the fidelity of the output state with the desired target state - this being an approximately squeezed cat state or the state in eq.(4.12). To simulate

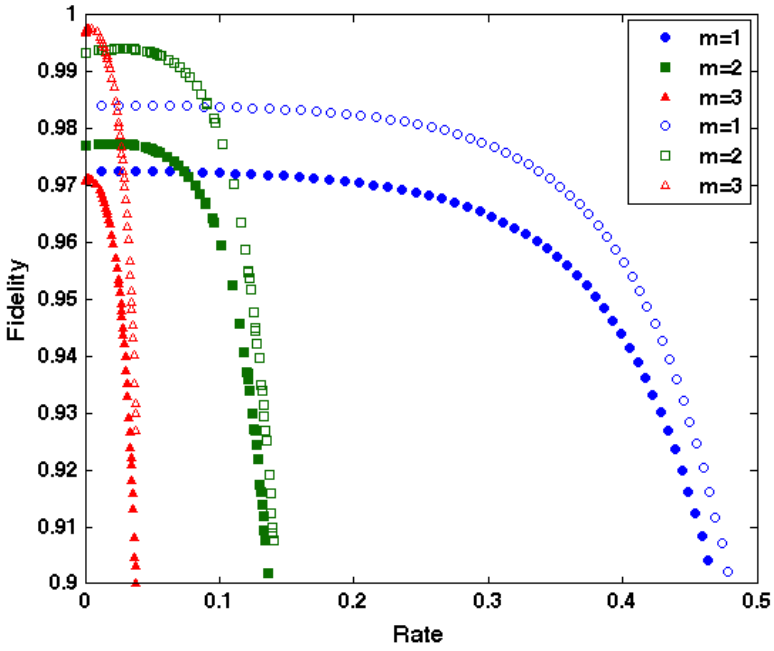

Figure 5.5: The effect of having a two-photon contribution of 1% in the input states. The fidelity is with a squeezed one-mode cat state of the form (4.13). The empty markers are calculated with a pure one-photon input and the filled markers are calculated with a 1% two-photon contribution.

the effect of two-photon contributions the input Wigner function is

$$W(x,p) = (1-p)W_1(x,p) + pW_2 \tag{5.12}$$

where $W_{1,2}$ are the Wigner functions of a one-photon state and a two-photon state respectively. p is the percentage contribution from the two-photon state. The effect of having a 1% two-photon contribution is shown in figure 5.5.

The next steps of the altered repeater protocol are treated without two-photon errors i.e. for $p \to 0$. This will give an idea about how well the altered repeater performs in the ideal limit where all input states are perfect single-photon states. The effect of two-photon errors is further discussed in section 6.2 where the full repeater is simulated.

5.2 Connection of one-mode states

The second step of the altered hybrid repeater protocol is to create entanglement in the elementary links. This is obtained by connecting the one-mode states generated in step one

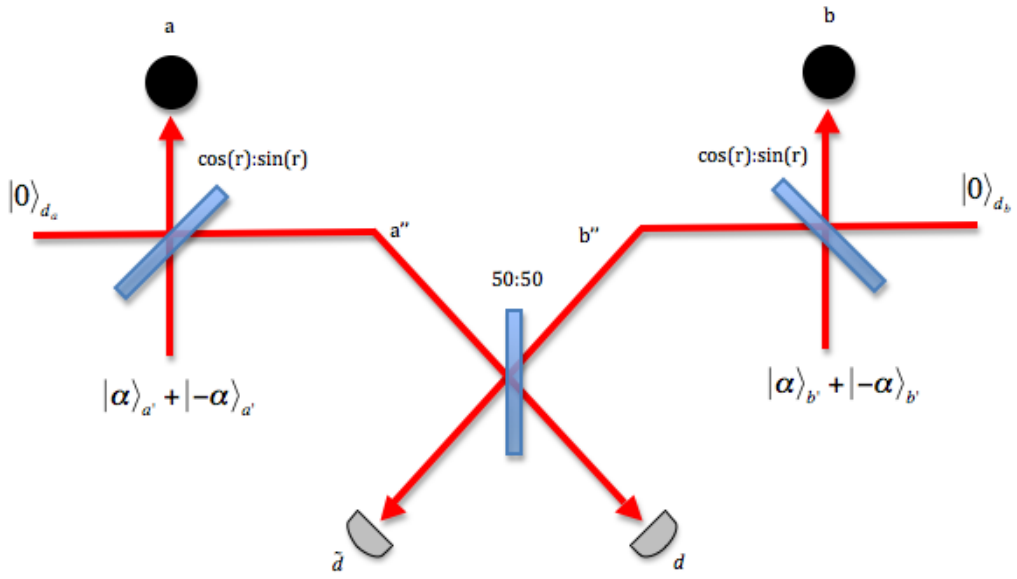

Figure 5.6: Setup for connecting one-mode cat states. The black dots are quantum memories where the modes a, b are stored. The modes a'' and b'' are combined on a 50:50 beam splitter halfway between location A and B. The reflection and transmission of the first two beam splitters are described by the parameter r.

of the protocol using a method suggested by N. Sanguard et al. in Ref. [14]. Instead of the approximately squeezed one-mode cat states generated in the repeater perfect one-mode cat states are assumed in Ref. [14].

The method is first described where perfect one-mode cat states are assumed as input states. The setup is shown in figure 5.6. The input state at location A (and B) is a one-mode cat state

$$\left|\xi^{-}(\alpha)\right\rangle = \frac{1}{\sqrt{N_\alpha^-}}\left(|\alpha\rangle - |-\alpha\rangle\right) \tag{5.13}$$

where $N_\alpha^- = 2(1 - e^{-2|\alpha|^2})$.
The state is sent to an asymmetric beam splitter with low reflection[4]. The transmitted part of the state is stored in a quantum memory and the reflected part is sent to a 50:50 beam splitter halfway between location A and B. The two signals - one coming from location A and one from location B - are combined on a balanced beam splitter and the two output states are measured with photodetectors. Ideally only one of the detectors 'clicks'

[4]In the article this is a beam splitter with low transmission but outcome is the same

corresponding to the measurement of one photon. This will project the modes in the quantum memories into an entangled two-mode cat state. The method operates in the discrete variable regime since it relies on single photon detection. Nonetheless the entanglement is stored in the field quadratures of the two-mode cat state, which is in the continuous variable regime.

The two-mode input state of the connection procedure is the product state

$$\left|\xi^{-}(\alpha)\right\rangle_{a'}\left|\xi^{-}(\alpha)\right\rangle_{b'}=\frac{1}{N_{\alpha}^{-}}(|\alpha\rangle-|-\alpha\rangle)_{a'}(|\alpha\rangle-|-\alpha\rangle)_{b'}. \tag{5.14}$$

The action of the asymmetric beam splitters is described by the unitaries

$$U_{d_a a'}=e^{r(\hat{a}'^{\dagger}\hat{d}_a-\hat{a}'\hat{d}_a^{\dagger})} \tag{5.15}$$

$$U_{d_b b'}=e^{r(\hat{b}'^{\dagger}\hat{d}_b-\hat{b}'\hat{b}_a^{\dagger})}. \tag{5.16}$$

These unitaries transforms the modes a', b' and d_a, d_b into the modes a,b and a'',b'':

$$\hat{a}=\cos(r)\hat{a}'+\sin(r)\hat{d}_a, \qquad \hat{b}=\cos(r)\hat{b}'+\sin(r)\hat{d}_b \tag{5.17}$$

$$\hat{a}''=\cos(r)\hat{d}_a-\sin(r)\hat{a}', \qquad \hat{b}''=\cos(r)\hat{d}_b-\sin(r)\hat{b}'. \tag{5.18}$$

Consequently low reflection of the beam splitters corresponds to a small value of the parameter r. The modes a'' and b'' are sent to the 50:50 beam splitter. The action of the balanced beam splitter is described by the unitary

$$U_{a''b''}=e^{\frac{\pi}{4}(\hat{a}''\hat{b}''^{\dagger}-\hat{a}''^{\dagger}\hat{b}'')} \tag{5.19}$$

which transformes the modes a'', b'' into the modes d, d'':

$$\hat{d}=\frac{1}{\sqrt{2}}(\hat{a}''+\hat{b}''), \qquad \hat{\tilde{d}}=\frac{1}{\sqrt{2}}(\hat{b}''-\hat{a}''). \tag{5.20}$$

A successful connection is conditioned on the measurement of the two photodetectors. Assuming that only detector d clicks, corresponding to a single photon in mode d and no photon in mode $\tilde{d}$, the state in the quantum memories will be projected into the state

$$|\Psi\rangle_{ab}={}_{\tilde{d}}\langle 0|\,{}_{d}\langle 1|\,BS\left(U_{a''b''}\right)BS\left(U_{d_a a'}\right)BS\left(U_{d_b b'}\right)\left|\xi^{-}(\alpha)\right\rangle_{a'}\left|\xi^{-}(\alpha)\right\rangle_{b'}|0\rangle_{d_a}|0\rangle_{d_b}. \tag{5.21}$$

where $BS\left(U_{a''b''}\right)$ denotes the beam splitter described by the unitary $U_{a''b''}$. Taking the states through the beam splitters gives the normalized state

$$\left|\Psi^{-}(r)\right\rangle_{ab}=\frac{1}{\sqrt{M_{\alpha,r}^{-}}}\left(|\alpha\cos(r)\rangle_a|\alpha\cos(r)\rangle_b-|-\alpha\cos(r)\rangle_a|-\alpha\cos(r)\rangle_b\right) \tag{5.22}$$

where $M^{-}_{\alpha,r} = 2\left(1 - e^{-4|\alpha|^2\cos^2(r)}\right)$.[5] This state is created with probability

$$P(\alpha, r) = \frac{2}{N_\alpha^{-2}} e^{-2\sin^2(r)|\alpha|^2} \sin^2(r)\,|\alpha|^2\, M^{-}_{\alpha,r}. \tag{5.23}$$

There is a probability that two photons are extracted from the first two beam splitters and afterwards one of these is lost on the way to the detectors. In that case the connection would be mistaken as a success even though two photons were extracted. The state in the quantum memories would be

$$\left|\Psi^{+}(r)\right\rangle = \frac{1}{\sqrt{M^{+}_{\alpha,r}}} \left(\left|\alpha\cos(r)\right\rangle_a \left|\alpha\cos(r)\right\rangle_b + \left|-\alpha\cos(r)\right\rangle_a \left|-\alpha\cos(r)\right\rangle_b\right), \tag{5.24}$$

which is orthogonal to (5.22). Consequently to obtain a high fidelity with state (5.22) the parameter r should be so small that the probability of two photons being extracted is negligible. Accordingly low reflectivity of the first two beam splitters will mean a small probability of a successful connection.

The method suggested by N. Sanguard et al. works provided perfect one-mode cat states as input states. However, the states generated in step one of the altered hybrid repeater look like *squeezed* one-mode cat states. The method still work in the sense that entanglement is created if only one photon is detected since the photon could originate from both location A or B but the resulting entangled state in the quantum memories is not state (5.22).

The method is now considered with input states of the form (4.12). The resulting entangled state will be the target state when connecting the approximately squeezed one-mode cat states from step one of the repeater.
Assuming that detector d clicks corresponding to a single photon in mode d and no photon in mode $\tilde{d}$ the two-mode state in the quantum memories is projected into

$$\left|\Psi_m\right\rangle_{ab} = {}_{\tilde{d}}\left\langle 0\right|{}_d\left\langle 1\right| BS\left(U_{a''b''}\right) BS\left(U_{d_a a'}\right) BS\left(U_{d_b b'}\right) \left|\psi_m\right\rangle_{a'} \left|\psi_m\right\rangle_{b'} \left|0\right\rangle_{d_a} \left|0\right\rangle_{d_b} \tag{5.25}$$

Taking the state ${}_{\tilde{d}}\left\langle 0\right|{}_d\left\langle 1\right|$ through $BS\left(U_{a''b''}\right)$ gives the state

$$\left|\Psi_m\right\rangle_{ab} = \frac{1}{\sqrt{2}} \left({}_{a''}\left\langle 1\right|{}_{b''}\left\langle 0\right| + {}_{a''}\left\langle 0\right|{}_{b''}\left\langle 1\right|\right) BS\left(U_{d_a a'}\right) BS\left(U_{d_b b'}\right) \left|\psi_m\right\rangle_{a'} \left|\psi_m\right\rangle_{b'} \left|0\right\rangle_{d_a} \left|0\right\rangle_{d_b} \tag{5.26}$$

[5] If detector $\tilde{d}$ fired instead of detector d the state in the quantum memories would be $\left|\Phi^{-}(r)\right\rangle_{ab} = \frac{1}{\sqrt{M^{-}_{\alpha,r}}}\left(\left|\alpha\cos(r)\right\rangle_a \left|-\alpha\cos(r)\right\rangle_b - \left|-\alpha\cos(r)\right\rangle_a \left|\alpha\cos(r)\right\rangle_b\right)$. This state is equal to (5.22) up to a single qubit rotation.

The unitaries $U_{da,a'}, U_{db,b'}$ can be expanded as

$$U_{da,a'} = 1 + r(\hat{a}'^{\dagger}\hat{d}_a - \hat{a}'\hat{d}_a^{\dagger}) + \frac{r^2}{2!}(\hat{a}'^{\dagger}\hat{d}_a - \hat{a}'\hat{d}_a^{\dagger})^2 + \frac{r^3}{3!}(\hat{a}'^{\dagger}\hat{d}_a - \hat{a}'\hat{d}_a^{\dagger})^3 + \dots \tag{5.27}$$

$$U_{db,b'} = 1 + r(\hat{b}'^{\dagger}\hat{d}_b - \hat{b}'\hat{b}_a^{\dagger}) + \frac{r^2}{2!}(\hat{b}'^{\dagger}\hat{d}_b - \hat{b}'\hat{b}_a^{\dagger})^2 + \frac{r^3}{3!}(\hat{b}'^{\dagger}\hat{d}_b - \hat{b}'\hat{b}_a^{\dagger})^3 + \dots \tag{5.28}$$

In the ideal limit where only one photon is extracted the parameter r is very small. Consequently terms with $r^{n>1}$ are neglected and the unnormalized state in the quantum memories is

$$\left|\Psi'_m\right\rangle_{ab} = (\hat{a} + \hat{b})\left|\psi_m\right\rangle_a \left|\psi_m\right\rangle_b . \tag{5.29}$$

The normalized wave function of this state is

$$\Psi_m(x,y) = [2\Gamma(2^m + 1/2)\Gamma(2^m - 1/2)]^{-1/2}\left(x^{2^m-1}y^{2^m} + x^{2^m}y^{2^m-1}\right)e^{-\frac{1}{2}(x^2+y^2)} \tag{5.30}$$

where x denotes mode a and y denotes mode b. This is a maximally entangled state. Defining a orthonormal two-dimensional basis of $\{|0_m\rangle, |1_m\rangle\}$ where

$$\langle x|\, 0_m\rangle = \Gamma(2^m - 1/2)^{-1/2}x^{2^m-1}e^{-\frac{1}{2}x^2}, \qquad \langle x|\, 1_m\rangle = \Gamma(2^m + 1/2)^{-1/2}x^{2^m}e^{-\frac{1}{2}x^2}, \tag{5.31}$$

the state (5.30) can be written as

$$|\Psi_m\rangle_{ab} = \frac{1}{\sqrt{2}}(|0_m\rangle_a |1_m\rangle_b + |1_m\rangle_a |0_m\rangle_b), \tag{5.32}$$

which clearly is a maximally entangled state. Physically this state corresponds to a superposition of odd and even photon states. The state $|0_m\rangle$ is a superposition of odd photon states with a maximum of $2^m - 1$ photons and $|1_m\rangle$ is a superposition of even photon states with a maximum of 2^m photons.
The state $|1_m\rangle$ is well approximated by the squeezed one-mode cat in eq. (4.13) and the state $|0_m\rangle$ is equally well approximated by an odd squeezed one-mode cat of the form

$$\hat{S}(2)|\xi^-(\tilde{\mu}_m)\rangle = \hat{S}(2)\frac{1}{\sqrt{N^-_{\tilde{\mu}_m}}}(|\tilde{\mu}_m\rangle - |-\tilde{\mu}_m\rangle) \tag{5.33}$$

where $\tilde{\mu}_m = \sqrt{2^m - 1/2}$. The fidelity with $|0_m\rangle$ exceeds 99% for $m \geq 2$. Hence the connected state (5.30) is approximated by the state

$$|\Xi(\mu_m, \tilde{\mu}_m)\rangle = \frac{1}{\sqrt{2}}\hat{S}_a(2)\hat{S}_b(2)(|\xi^-(\tilde{\mu}_m)\rangle_a \left|\xi^+(\mu_m)\right\rangle_b + \left|\xi^+(\mu_m)\right\rangle_a |\xi^-(\tilde{\mu}_m)\rangle_b). \tag{5.34}$$

In the limit of large m, $\tilde{\mu}_m \approx \mu_m \approx 2^{m/2}$ and the connected state will look like

$$\hat{S}(2)_a\hat{S}(2)_b\frac{1}{\sqrt{M^+_{\alpha,0}}}(|\alpha\rangle_a |\alpha\rangle_b - |-\alpha\rangle_a |-\alpha\rangle_b) \tag{5.35}$$

i.e. a locally squeezed two-mode cat state. The fidelity between this state and the state (5.32) exceeds 99% for $m \geq 5$.
If the photon was detected in mode $\tilde{d}$ instead of mode d the state in the quantum memories would be

$$|\Psi_m\rangle_{ab} = \frac{1}{\sqrt{2}}(|0_m\rangle_a |1_m\rangle_b - |1_m\rangle_a |0_m\rangle_b) \tag{5.36}$$

Up to a local phase shift this is equal to (5.32) and is created with the same probability. Therefore, when only one photon is detected - no matter in what detector - a successful connection is obtained.

5.2.1 Connection of Wigner functions

The ideal limit of the connection step is the state in eq. (5.32), which is maximally entangled and for large m looks like a locally squeezed two-mode cat state. This state is used as a target state when connecting the Wigner functions generated in step one of the repeater protocol meaning that the fidelity with this state is used as a measure of the entanglement of the Wigner functions.

The connection setup is changed slightly to incorporate it in the repeater protocol. Losses in the fibers are included and number resolving photodetectors are not assumed. The losses are simulated by inserting two beam splitters before the central station that mixes the reflected signal from the first two beam splitters with vacuum. This is seen in figure 5.7.
The probability that a photon is lost on the way to the central station is $\sin^2(\theta)$. θ is determined by the distance L between the first beam splitter and the central station and the attenuation length L_{att} of the transmission fiber used:

$$\cos^2(\theta) = e^{-\frac{L}{L_{att}}} \tag{5.37}$$

The state before the first two beam splitters is the product of the Wigner functions generated in step one in the repeater and two vacuum states:

$$W_m(x,y)W_m(q,p)W_{vac}(x',y')W_{vac}(q',p') \tag{5.38}$$

$W_m(-,-)$ has the form in eq. (5.4) and $W_{vac}(x,y) = \frac{1}{\pi}e^{-\frac{1}{2}(x^2+y^2)}$.
The modes described by (x,x',y,y') are to the left of the central station and the modes described by (q,q',p,p') are to the right. Before the central station it is only necessary to focus on the modes described by (x,x',y,y'). The action of the first beam splitter is

$$\begin{aligned} x &\to \cos(r)x + \sin(r)x', x' \to \cos(r)x' - \sin(r)x \\ y &\to \cos(r)y + \sin(r)y', y' \to \cos(r)y' - \sin(r)y \end{aligned} \tag{5.39}$$

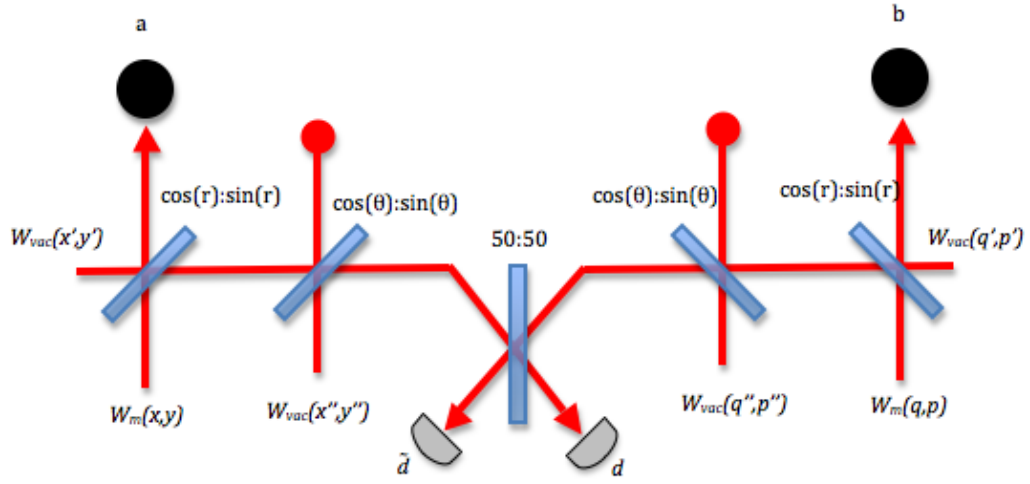

Figure 5.7: Setup for connecting the one-mode Wigner functions. The black dots are quantum memories that store the modes described by x, y and q, p. The losses in the fibers are described by inserting two beam splitters between the first beam splitters and the central station. At the central station the modes described by x', y' and q', p' are combined on a balanced beam splitter and the outputs are measured with detector d and $\tilde{d}$.

which results in the state

$$W_{a1}(x,x',y,y') = W_m(\cos(r)x + \sin(r)x', \cos(r)y + \sin(r)y') \\ \times W_{vac}(\cos(r)x' - \sin(r)x, \cos(r)y' - \sin(r)y). \tag{5.40}$$

The next beam splitter mixes x' and y' with vacuum (x'', y''):

$$x' \to \cos(\theta)x' + \sin(\theta)x'', x'' \to \cos(\theta)x'' - \sin(\theta)x' \\ y' \to \cos(\theta)y' + \sin(\theta)y'', y'' \to \cos(\theta)y'' - \sin(\theta)y' \tag{5.41}$$

The number of photons that are lost is not known and consequently a trace over x'' and y'' is made. This produces the state:

$$W_{a2}(x,x',y,y') = \int_{-\infty}^{\infty} \mathrm{d}x'' \int_{-\infty}^{\infty} \mathrm{d}y'' W_{a1}(x, \cos(\theta)x' + \sin(\theta)x'', y, \cos(\theta)x' + \sin(\theta)x'') \\ \times W_{vac}(\cos(\theta)x'' - \sin(\theta)x', \cos(\theta)y'' - \sin(\theta)y'). \tag{5.42}$$

The modes described by (q, q', y, y') is brought to the central beam splitter in the same manner producing the state $W_{b2}(q, q', p, p')$.The action of the central beam splitter is:

$$\begin{aligned} x' &\to \frac{x'+q'}{\sqrt{2}}, \quad q' \to \frac{x'-q'}{\sqrt{2}} \\ y' &\to \frac{y'+p'}{\sqrt{2}}, \quad p' \to \frac{y'-p'}{\sqrt{2}} \end{aligned} \tag{5.43}$$

Assuming that mode $\tilde{d}$ only contains vacuum and mode d contains anything but vacuum the subsequent state is projected onto

$$W_{vac}(q', p')(1 - W_{vac}(x', y')) = \underbrace{W_{vac}(q', p')}_{\text{a}} - \underbrace{W_{vac}(q', p')W_{vac}(x', y')}_{\text{b}} \tag{5.44}$$

Term a describes the situation when there is no click in detector $\tilde{d}$ while anything could happen at detector d and term b describes the situation when no detector clicks. Accordingly the combination $a - b$ is when detector d clicks and detector $\tilde{d}$ do not.
Consequently the state in the quantum memories is:

$$\begin{aligned} W_{ab}(x, y, q, p) = &\int_{-\infty}^{\infty} \mathrm{d}x' \int_{-\infty}^{\infty} \mathrm{d}y' \int_{-\infty}^{\infty} \mathrm{d}q' \int_{-\infty}^{\infty} \mathrm{d}p' W_{vac}(q', p')(1 - W_{vac}(x', y')) \\ &\times W_{a2}(x, (x'+q')/\sqrt{2}, y, (y'+p')/\sqrt{2}) \\ &\times W_{b2}(q, (x'-q')/\sqrt{2}, p, (y'-p')/\sqrt{2}) \end{aligned} \tag{5.45}$$

This Wigner function can be written in the form (5.4) as

$$W_{ab}(x, y, q, p) = \sum_{\{s,t,k,l\}=0}^{2^{m+1}} w_{stkl} x^k p^l y^s q^t e^{-x^2-p^2-y^2-q^2}, \tag{5.46}$$

which is seen by performing the integrals in eq.(5.45). The expressions for the matrix elements w_{stkl} can be seen in Appendix B.1

The probability of obtaining the state in eq. (5.45) is found by tracing over x, y, q, p:

$$P_{W_{ab}}(r, \theta) = \int_{-\infty}^{\infty} \mathrm{d}x \int_{-\infty}^{\infty} \mathrm{d}y \int_{-\infty}^{\infty} \mathrm{d}q \int_{-\infty}^{\infty} \mathrm{d}p W_{ab}(x, y, q, p) \tag{5.47}$$

Note that $W_{ab}(x, y, q, p)$ is the average state obtained when connecting the one-mode Wigner functions from step one in the repeater.
The expression in eq.(5.47) assumes that the efficiencies of the detectors are 100%. A more

realistic efficiency would be 50%. In what follows the probability of obtaining the state (5.45) is set to $\eta_d P_{W_{ab}}$ where $\eta_d = 50\%$ is the detector efficiency. This is a lower limit since it assumes that there is a 50% chance that the detector clicks independently of the number of photons hitting it. However, in the limit of high fidelity with the state (5.32) essentially only one photon hits the detector. Note that the probability of a successful connection is $P_{connect} = 2\eta_d P_{W_{ab}}$ since a successful connection is also obtained when detector $\tilde{d}$ fires and detector d does not.

For a fixed value of m the fidelity of the state (5.45) and the maximally entangled state in eq. (5.32) depends on the parameters $\vec{\Delta}$,r and θ.
$\vec{\Delta} = (\Delta_1, \Delta_2, \ldots)$[6] determines the initial fidelity of the one-mode Wigner functions and the state (4.12). Hence $\vec{\Delta}$ gives an upper limit to the fidelity of the connected state and the state (5.32).
r determines the number of photons extracted from the two one-mode states and consequently the fidelity decreases when r is increased.
The probability of loosing a photon on the way to the central station is determined by θ, which also influences the fidelity of the connected state and state (5.32). The probability of a connected state when two photons or more are extracted from the one-mode states increases as a function of theta compared to the same probability when only one photon is extracted. Therefore the fidelity decreases as a function of θ given a fixed r. However this effect will be small for $r \ll 1$. The dependence on the parameters described above is seen in figure 5.8b,5.8a and 5.8c.

The performance of the connection step can be compared to Ref. [14]. A number resolving detector with an efficiency of 90%, an attenuation length of 22 km and a connection distance of 100 km are assumed in Ref. [14]. Within these assumptions it is shown that the average time needed to create an entangled pair with a fidelity of 90% with the state (5.22) is $T_0 \sim 54$ ms.
Assuming perfect one-mode states of the form (4.12), an attenuation length of 22 km and a detector efficiency of 90% (not number resolving) an entangled pair with a fidelity of 90% with a maximally entangled state is created over a distance of 100 km in an average time of $T_0 \sim 29$ ms in the altered repeater protocol. Hence the rates are comparable but number resolving detectors were not assumed in the repeater.

[6] $\vec{\Delta}$ is the vector of acceptance intervals for the different iterations in the growing step.

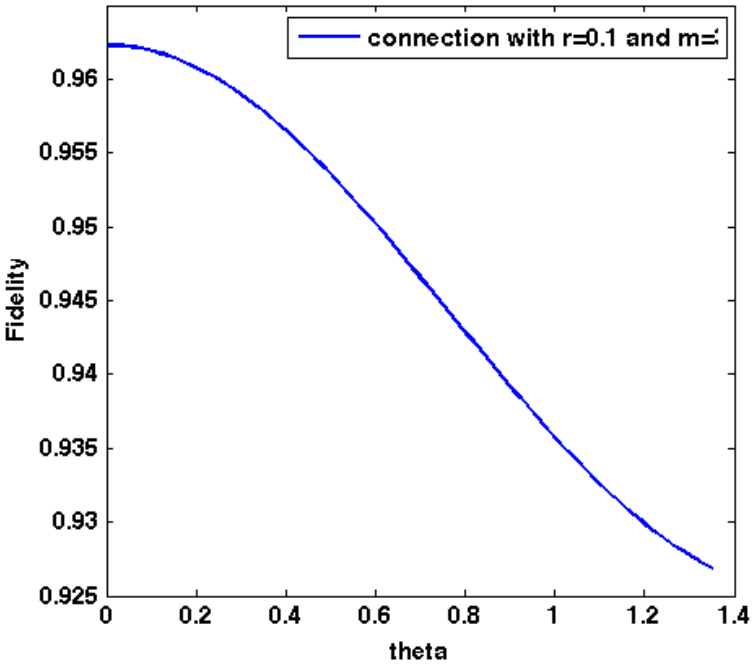

(a) θ dependence of the fidelity

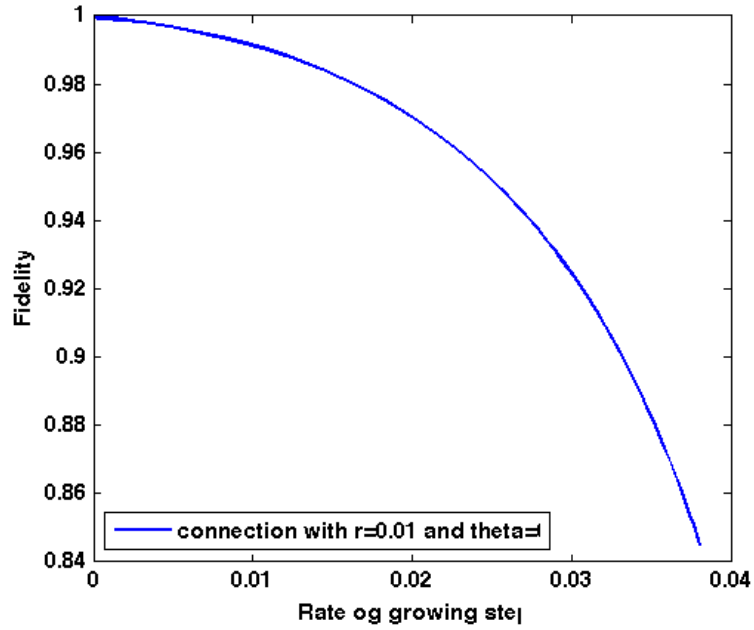

(b) $\vec{\Delta}$ dependence of the fidelity

Figure 5.8

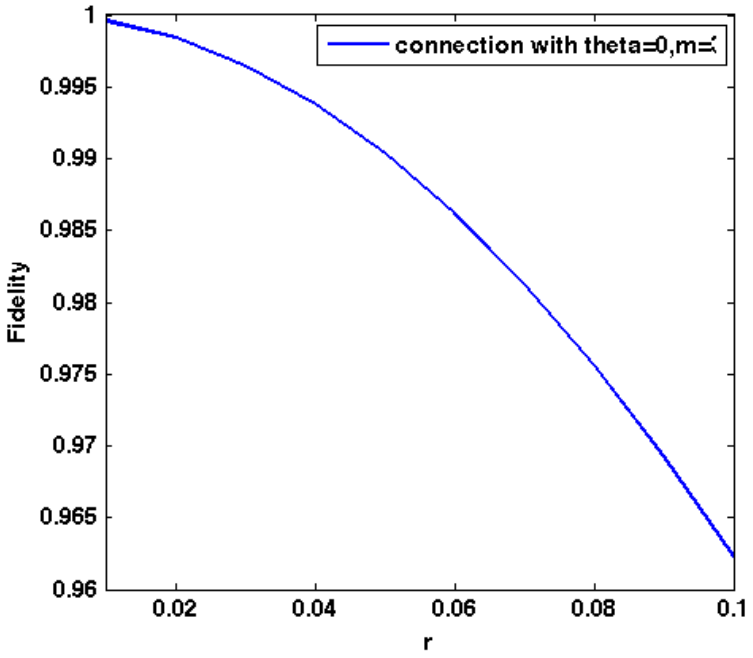

(c) r dependence of the fidelity

Figure 5.8: How the fidelity depends on the parameters r, θ and Δ. The fidelity is taken with the state in eq. (5.32). In figure b) $\vec{\Delta}$ is represented as the rate of the generation of the one-mode states in units of the source repetition rate.

5.3 Entanglement swapping

The final step of the altered quantum repeater protocol is the entanglement swapping, which is of crucial importance if entanglement is be distributed over a large distance. The method of Ref. [13] based on homodyne detection is used to do entanglement swapping. The swap procedure is seen in figure 5.9.

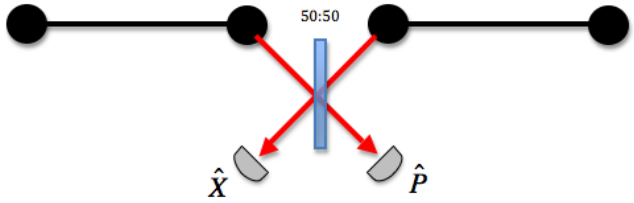

Figure 5.9: Setup of the swap procedure. The black dots are quantum memories containing the two-mode states. Two of the modes are combined on a balanced beam splitter and the $\hat{X}$ and $\hat{P}$ quadratures are measured. A successful swap is conditioned on the $\hat{X}$ measurement being close to zero.

If m is large and the outcome of the $\hat{X}$ measurement is close to zero the state (5.32) is swapped into a state well approximated by

$$\hat{S}_a(2)\hat{S}_b(2)\left|\gamma(\theta_p,\alpha)\right\rangle = \frac{1}{M_\alpha^+(\theta_p)}\left(\left|-\alpha\right\rangle_a\left|\alpha\right\rangle_b e^{i\theta_p} + \left|\alpha\right\rangle_a\left|-\alpha\right\rangle_b e^{-i\theta_p}\right) \tag{5.48}$$

where the phase θ_p depends on the $\hat{P}$ measurement. This is because for large m the state (5.32) looks like a locally squeezed two-mode cat state. The swap behavior of a two-mode cat state is shown in section 4.3 and the local squeeze operators do not influence the outcome of the swap[7] The probability of an $\hat{X}$ measurement close to zero is roughly $\frac{1}{2}$. Note that this implies that for large m, near-deterministic swapping can be obtained using the procedure described in Ref. [13].
It is not clear what happens when the state (5.32) is swapped for small m. This is studied in some detail.

The state prior to the swap is considered to be

$$\left|\Psi_m\right\rangle_{aa'}\left|\Psi_m\right\rangle_{bb'} = \frac{1}{2}(\left|0_m\right\rangle_a\left|1_m\right\rangle_{a'} + \left|1_m\right\rangle_a\left|0_m\right\rangle_{a'})(\left|0_m\right\rangle_b\left|1_m\right\rangle_{b'} + \left|1_m\right\rangle_b\left|0_m\right\rangle_{b'}) \tag{5.49}$$

[7]To obtain state (5.48) the x and p modes should be interchanged in eq. (4.17) since the output modes where the $\hat{X}$ and $\hat{P}$ quadratures are measured are interchanged.

The modes a' and b are connected on a 50:50 beam splitter. Let x, x' denote mode a, a' and y, y'denote mode b, b'. This brings the state to the form

$$|\Psi_m\rangle_{aa'} |\Psi_m\rangle_{bb'} \rightarrow$$
$$\left\{ \sum_{s=0}^{2^m} \sum_{t=0}^{2^m} \tilde{A}_{s,t} x^{2^m-1} y'^{2^m-1} + \tilde{B}_{s,t} x^{2^m} y'^{2^m} + \tilde{C}_{s,t} x^{2^m} y'^{2^m-1} + \tilde{D}_{s,t} x^{2^m-1} y'^{2^m} \right\} \times e^{-\frac{1}{2}(x^2+y'^2)} \quad (5.50)$$

where

$$\tilde{A}_{s,t} = \binom{2^m}{s}\binom{2^m}{t} 2^{-2^m} (-1)^t x'^{s+t} y^{2^{m+1}-s-t} e^{-\frac{1}{2}(x'^2+y^2)} \quad (5.51)$$

$$\tilde{B}_{s,t} = \frac{(2^m-s)}{2^m}\frac{(2^m-t)}{2^m}\binom{2^m}{s}\binom{2^m}{t} 2^{-2^m+1} (-1)^{t+1} x'^{s+t} y^{2^{m+1}-2-s-t} e^{-\frac{1}{2}(x'^2+y^2)} \quad (5.52)$$

$$\tilde{C}_{s,t} = \frac{(2^m-s)}{2^m}\binom{2^m}{s}\binom{2^m}{t} 2^{-2^m+1/2} (-1)^t x'^{s+t} y^{2^{m+1}-1-s-t} e^{-\frac{1}{2}(x'^2+y^2)} \quad (5.53)$$

$$\tilde{D}_{s,t} = \frac{(2^m-t)}{2^m}\binom{2^m}{s}\binom{2^m}{t} 2^{-2^m+1/2} (-1)^{t+1} x'^{s+t} y^{2^{m+1}-1-s-t} e^{-\frac{1}{2}(x'^2+y^2)} \quad (5.54)$$

The $\hat{X}$ quadrature of the mode described by x' and the P quadrature of the mode described by y is measured. This produces the unnormalized state

$$\Phi(x, y') = \frac{A}{\Gamma(2^m - 1/2)} x^{2^m-1} y'^{2^m-1} + \frac{B}{\Gamma(2^m + 1/2)} x^{2^m} y'^{2^m} + \left(C x^{2^m} y'^{2^m-1} + D x^{2^m-1} y'^{2^m}\right) \left[\Gamma(2^m - 1/2)\Gamma(2^m - 1/2)\right]^{-1/2}. \quad (5.55)$$

The normalized state can be written as

$$|\Phi_m\rangle_{ab'} = \frac{1}{N} \left(A |0_m\rangle_a |0_m\rangle_{b'} + B |1_m\rangle_a |1_m\rangle_{b'} + C |1_m\rangle_a |0_m\rangle_{b'} + D |0_m\rangle_a |1_m\rangle_{b'}\right) \quad (5.56)$$

where

$$A = \sum_{(s,t)=0}^{2^m} \binom{2^m}{s}\binom{2^m}{t} 2^{-2^m} (-1)^t H_{s,t} \Gamma(2^m - 1/2) \quad (5.57)$$

$$B = \sum_{(s,t)=0}^{2^m} \frac{(2^m-s)}{2^m}\frac{(2^m-t)}{2^m}\binom{2^m}{s}\binom{2^m}{t} 2^{-2^m+1} (-1)^{t+1} F_{s,t} \Gamma(2^m + 1/2) \quad (5.58)$$

$$C = \sum_{(s,t)=0}^{2^m} \frac{(2^m-s)}{2^m}\binom{2^m}{s}\binom{2^m}{t} 2^{-2^m+1/2} (-1)^t G_{s,t} [\Gamma(2^m - 1/2)\Gamma(2^m - 1/2)]^{\frac{1}{2}} \quad (5.59)$$

$$D = \sum_{(s,t)=0}^{2^m} \frac{(2^m-t)}{2^m}\binom{2^m}{s}\binom{2^m}{t} 2^{-2^m+1/2} (-1)^{t+1} G_{s,t} [\Gamma(2^m - 1/2)\Gamma(2^m - 1/2)]^{\frac{1}{2}} \quad (5.60)$$

$$N = \left(|A|^2 + |B|^2 + |C|^2 + |D|^2\right)^{-1/2} \quad (5.61)$$

The matrix elements $F_{s,t}$, $H_{s,t}$ and $G_{s,t}$ depend on the measurement of the $\hat{X}$ and $\hat{P}$ quadrature. The expression for these can be seen in Appendix B.2.

5.3.1 Entanglement investigations

The measure of the entanglement in the state (5.56) is the entropy of the reduced density matrix for system b'. In the basis of $\{|1_m\rangle_{b'}, |0_m\rangle_{b'}\}$ the reduced density matrix of system b' is

$$\rho_{b'} = \begin{pmatrix} |A|^2 + |D|^2 & AC^* + DB^* \\ CA^* + BD^* & |C|^2 + |B|^2 \end{pmatrix}.$$

The entropy is $S(\rho) = -\mathrm{Tr}[\rho \log(\rho)]$. The entropy as a function of the outcome of the $\hat{P}$ measurement is seen in figure 5.10 for different m's and different outcomes of the $\hat{X}$ measurement. For large values of the $\hat{X}$ measurement outcome the entropy would essentially be zero since the swapped state would be a product state (see section 4.3). In figure 5.10 the outcomes of the $\hat{X}$ measurements were chosen small enough for the swap to be successful.

The entropy and hence the entanglement of the swapped state depends rather strongly on the outcome of the $\hat{P}$ measurement even at $m = 3$. However the $\hat{P}$ dependence is expected to wear off as m increases since the input states begins to look like locally squeezed two-mode cat states with large amplitudes.
Figure 5.10 also shows that the acceptance interval around zero of the $\hat{X}$ measurement ($[-\delta, \delta]$) can be increased for large m. This is due to the same concept as in the growing of the cat states where the acceptance interval $[-\Delta, \Delta]$ could be increased (see section 5.1).

To understand the entanglement behavior seen in the plots the states prior to the swapping are assumed to be of the general form

$$|\Phi\rangle_{xx',1} = a_1 |0_m\rangle_x |0_m\rangle_{x'} + b_1 |1_m\rangle_x |1_m\rangle_{x'} + c_1 |1_m\rangle_x |0_m\rangle_{x'} + e_1 |0_m\rangle_x |1_m\rangle_{x'}. \quad (5.62)$$

Consequently the product state before the 50:50 beam splitter is

$$\begin{aligned} &|\Phi\rangle_{xx',1} |\Phi\rangle_{yy',2} = \\ &\Big[a_1a_2 |0_m\rangle_{x'} |0_m\rangle_y + a_1c_2 |0_m\rangle_{x'} |1_m\rangle_y + e_1a_2 |1_m\rangle_{x'} |0_m\rangle_y + e_1c_2 |1_m\rangle_{x'} |1_m\rangle_y\Big] |0_m\rangle_x |0_m\rangle_{y'} \\ &\Big[b_1b_2 |1_m\rangle_{x'} |1_m\rangle_y + b_1e_2 |1_m\rangle_{x'} |0_m\rangle_y + c_1b_2 |0_m\rangle_{x'} |1_m\rangle_y + c_1e_2 |0_m\rangle_{x'} |0_m\rangle_y\Big] |1_m\rangle_x |1_m\rangle_{y'} \\ &\Big[a_1b_2 |0_m\rangle_{x'} |1_m\rangle_y + a_1e_2 |0_m\rangle_{x'} |0_m\rangle_y + e_1b_2 |1_m\rangle_{x'} |1_m\rangle_y + e_1e_2 |1_m\rangle_{x'} |0_m\rangle_y\Big] |0_m\rangle_x |1_m\rangle_{y'} \\ &\Big[b_1a_2 |1_m\rangle_{x'} |0_m\rangle_y + b_1c_2 |1_m\rangle_{x'} |1_m\rangle_y + c_1a_2 |0_m\rangle_{x'} |0_m\rangle_y + c_1c_2 |0_m\rangle_{x'} |1_m\rangle_y\Big] |1_m\rangle_x |0_m\rangle_{y'} \end{aligned} \quad (5.63)$$

In section 5.2 it was shown that

$$|1_m\rangle_q \approx \hat{S}(2) \frac{1}{\sqrt{N^+_{\mu_m}}} (|\mu_m\rangle_q + |-\mu_m\rangle_q), \qquad |0_m\rangle_q \approx \hat{S}(2) \frac{1}{\sqrt{N^-_{\tilde{\mu}_m}}} (|\tilde{\mu}_m\rangle_q - |-\tilde{\mu}_m\rangle_q) \quad (5.64)$$

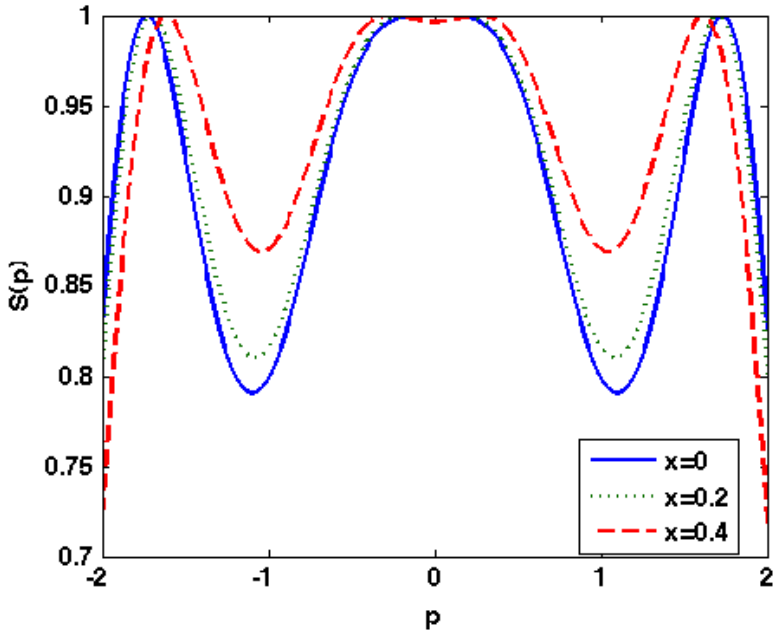

(a) The entropy for $m = 1$ iteration

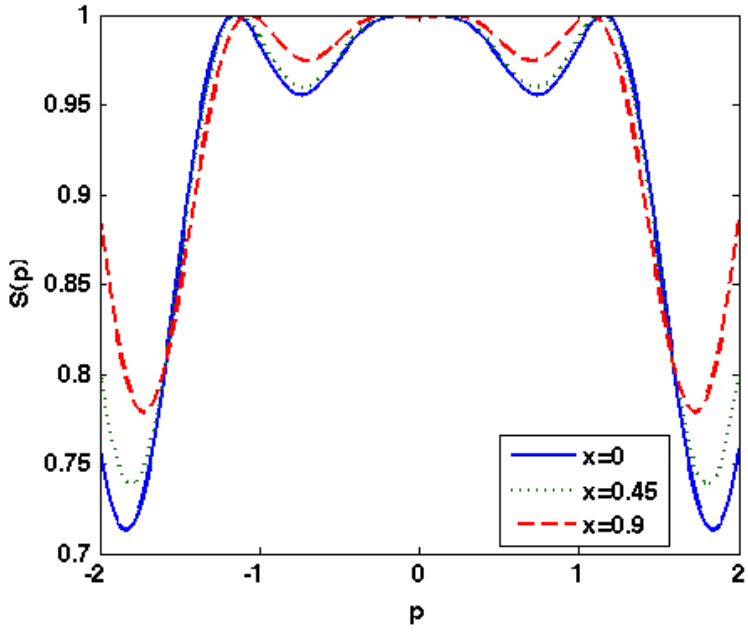

(b) The entropy for $m = 2$ iteration

Figure 5.10

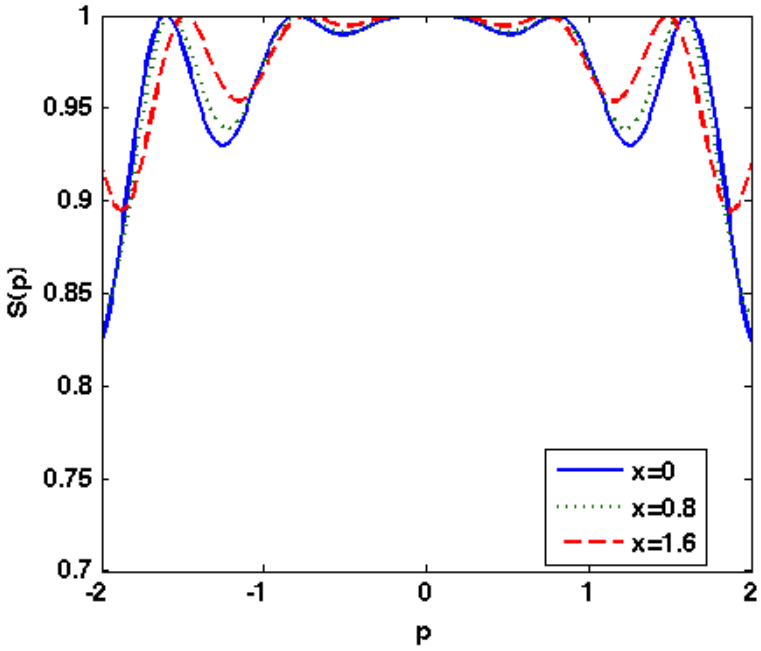

(c) The entropy for $m = 3$ iteration

Figure 5.10: The entropy $S(p)$ for different outcomes of the $\hat{X}$ measurements and different values of m. The dependence on the $\hat{P}$ measurement is quite strong even for $m = 3$.

Using these approximations and assuming that $\langle 2\tilde{\mu}_m|\ \mu_m - \tilde{\mu}_m\rangle \approx 0$, $N^+_{\mu_m} \approx N^-_{\tilde{\mu}_m}$ [8] the unnormalized state after the beam splitter with an outcome of the $\hat{X}$ measurement close to zero is

$$|\Phi\rangle_{xy'} = \mathbb{A}\,|0_m\rangle_x\,|0_m\rangle_{y'} + \mathbb{B}\,|1_m\rangle_x\,|1_m\rangle_{y'} + \mathbb{C}\,|1_m\rangle_x\,|0_m\rangle_{y'} + \mathbb{D}\,|0_m\rangle_x\,|1_m\rangle_{y'} \tag{5.65}$$

Where

$$\begin{aligned}
\mathbb{A} &= 2e_1c_2\cos(\sqrt{2}\mu_m p') - 2a_1a_2\cos(\sqrt{2}\tilde{\mu}_m p') + e^{-\frac{1}{2}(\mu_m-\tilde{\mu}_m)^2} \times \\
&\Big\{(a_1c_2 + e_1a_2)\left[e^{-\sqrt{2}x(\mu_m-\tilde{\mu}_m)} - e^{\sqrt{2}x(\mu_m-\tilde{\mu}_m)}\right]\cos(\frac{1}{\sqrt{2}}(\mu_m+\tilde{\mu}_m)p') \\
&+\mathbb{I}(e_1a_2 - a_1c_2)\left[e^{-\sqrt{2}x(\mu_m-\tilde{\mu}_m)} + e^{\sqrt{2}x(\mu_m-\tilde{\mu}_m)}\right]\sin(\frac{1}{\sqrt{2}}(\mu_m+\tilde{\mu}_m)p')\Big\} \qquad (5.66)\\
\mathbb{B} &= 2b_1b_2\cos(\sqrt{2}\mu_m p') - 2c_1e_2\cos(\sqrt{2}\tilde{\mu}_m p') + e^{-\frac{1}{2}(\mu_m-\tilde{\mu}_m)^2} \times \\
&\Big\{(b_1e_2 + c_1b_2)\left[e^{-\sqrt{2}x(\mu_m-\tilde{\mu}_m)} - e^{\sqrt{2}x(\mu_m-\tilde{\mu}_m)}\right]\cos(\frac{1}{\sqrt{2}}(\mu_m+\tilde{\mu}_m)p') \\
&+\mathbb{I}(b_1e_2 - c_1b_2)\left[e^{-\sqrt{2}x(\mu_m-\tilde{\mu}_m)} + e^{\sqrt{2}x(\mu_m-\tilde{\mu}_m)}\right]\sin(\frac{1}{\sqrt{2}}(\mu_m+\tilde{\mu}_m)p')\Big\} \qquad (5.67)\\
\mathbb{C} &= 2b_1c_2\cos(\sqrt{2}\mu_m p') - 2c_1a_2\cos(\sqrt{2}\tilde{\mu}_m p') + e^{-\frac{1}{2}(\mu_m-\tilde{\mu}_m)^2} \times \\
&\Big\{(b_1a_2 + c_1c_2)\left[e^{-\sqrt{2}x(\mu_m-\tilde{\mu}_m)} - e^{\sqrt{2}x(\mu_m-\tilde{\mu}_m)}\right]\cos(\frac{1}{\sqrt{2}}(\mu_m+\tilde{\mu}_m)p') \\
&+\mathbb{I}(b_1a_2 - c_1c_2)\left[e^{-\sqrt{2}x(\mu_m-\tilde{\mu}_m)} + e^{\sqrt{2}x(\mu_m-\tilde{\mu}_m)}\right]\sin(\frac{1}{\sqrt{2}}(\mu_m+\tilde{\mu}_m)p')\Big\} \qquad (5.68)\\
\mathbb{D} &= 2e_1b_2\cos(\sqrt{2}\mu_m p') - 2a_1e_2\cos(\sqrt{2}\tilde{\mu}_m p') + e^{-\frac{1}{2}(\mu_m-\tilde{\mu}_m)^2} \times \\
&\Big\{(a_1b_2 + e_1e_2)\left[e^{-\sqrt{2}x(\mu_m-\tilde{\mu}_m)} - e^{\sqrt{2}x(\mu_m-\tilde{\mu}_m)}\right]\cos(\frac{1}{\sqrt{2}}(\mu_m+\tilde{\mu}_m)p') \\
&+\mathbb{I}(e_1e_2 - a_1b_2)\left[e^{-\sqrt{2}x(\mu_m-\tilde{\mu}_m)} + e^{\sqrt{2}x(\mu_m-\tilde{\mu}_m)}\right]\sin(\frac{1}{\sqrt{2}}(\mu_m+\tilde{\mu}_m)p')\Big\} \qquad (5.69)
\end{aligned}$$

In the first swap $a_1 = a_2 = b_1 = b_2 = 0$ and $c_1 = e_1 = c_2 = e_2 = 1$. This means that it is the difference between μ_m and $\tilde{\mu}_m$ that determines the entanglement of the swapped states. For subsequent swapping the measurement outcome in the previous swaps also influence the entanglement.

For large m, $\mu_m \approx \tilde{\mu}_m \approx 2^{m/2}$ and the coefficients $\mathbb{A}, \mathbb{B}, \mathbb{C}$ and $\mathbb{D}$ reduce to

$$\begin{aligned}
\mathbb{A} &= (e_1c_2 - a_1a_2)\cos(2^{(m+1)/2}p') + \mathbb{I}(e_1a_2 - a_1c_2)\sin(2^{(m+1)/2}p') &(5.70)\\
\mathbb{B} &= (b_1b_2 - c_1e_2)\cos(2^{(m+1)/2}p') + \mathbb{I}(b_1e_2 - c_1b_2)\sin(2^{(m+1)/2}p') &(5.71)\\
\mathbb{C} &= (b_1c_2 - c_1a_2)\cos(2^{(m+1)/2}p') + \mathbb{I}(b_1a_2 - c_1c_2)\sin(2^{(m+1)/2}p') &(5.72)\\
\mathbb{D} &= (e_1b_2 - a_1e_2)\cos(2^{(m+1)/2}p') + \mathbb{I}(e_1e_2 - a_1b_2)\sin(2^{(m+1)/2}p') &(5.73)
\end{aligned}$$

[8] This is true for large m

Assuming that $b_1 = -a_1^*$ and $e_1 = c_1^*$, the unnormalized swapped state can be written as

$$|\Phi\rangle_{xy'} = A\,|0_m\rangle_x\,|0_m\rangle_{y'} - A^*\,|1_m\rangle_x\,|1_m\rangle_{y'} + C\,|1_m\rangle_x\,|0_m\rangle_{y'} + C^*\,|0_m\rangle_x\,|1_m\rangle_{y'}\,, \qquad (5.74)$$

which is a maximally entangled state. When swapping states of the type (5.32), $b_1 = -a_1^*$ and $e_1 = c_1^*$ in the first swap level. Consequently for large enough m the initial maximally entangled state in eq. (5.32) is swapped into another maximally entangled state independently of the number of swap levels performed as long as the $\hat{X}$ measurements are close to zero, which occurs with probability $\sim \frac{1}{2}$. This is because the state (5.32) looks like a locally squeezed two-mode cat state for large m. It is shown in Appendix B.3 that $\Im(A) = 0$ and $\Re(C) = 0$ when the initial states are of the form (5.32) and hence the swapped state in eq.(5.74) reduces to state (5.48).

To see how well the state (5.32) swaps it is necessary to calculate the average entropy of the output state after a number of swap levels. Assuming an $\hat{X}$ measurement of zero the average entropy of the output state in the first swap is:

$$\bar{S} = \int_{-\infty}^{\infty} \mathrm{d}p_1 S(p_1) P(p_1) \qquad (5.75)$$

where $S(p_1)$ is the entropy as a function of the outcome, p_1 of the $\hat{P}$ measurement and $P(p_1)$ is the probability density function of p_1. The mean entropy of the next swap level is

$$\bar{S} = \int_{-\infty}^{\infty} \mathrm{d}p_1 \int_{-\infty}^{\infty} \mathrm{d}p_2 \int_{-\infty}^{\infty} \mathrm{d}p_3 S(p_1, p_2, p_3) P(p_1, p_2, p_3) \qquad (5.76)$$

where p_1, p_2 are the outcomes of the $\hat{P}$ measurements in the two prior swaps and p_3 is the outcome in this swap. It would require 15 integrals to calculated the mean entropy of the fourth swap level and the calculation would take a very long time. To circumvent this problem a number of experiments with given outcomes of the $\hat{P}$ measurement are simulated for every swap level. The simulation is made by picking an outcome of the $\hat{P}$ measurement according to the probability distribution of $\hat{P}$ in every swap, which produces a set $\{p_1, p_2, \ldots, p_n\}$. Afterwards the entropy, $S_1(p_1, p_2, \ldots, p_n)$ corresponding to the set can be calculated.
This procedure is repeated a 100 times for a maximum of four swap levels and the mean entropy from the resulting 100 outcomes of $S(\vec{p})$ is calculated. All $\hat{X}$ measurements are assumed to have an outcome of zero. The method used to pick a value according to the probability distribution of $\hat{P}$ is described in Appendix B.4. The four swap levels have been simulated for $m = 1, 2$ and 3 and the result is seen in figure 5.11. The error bars in the plots are the standard deviation of the mean:

$$\sigma_{\bar{x}} = \frac{\sigma_x}{\sqrt{N}}. \qquad (5.77)$$

This is of the order of 1% in the fourth swap level with 100 simulations, which is acceptable.

Figure 5.11 shows that the mean entropy of the outcome state drops with the number of swap levels in the repeater. This is caused by the accumulation of errors in each swap level - the starting states of the second level of swapping are not maximally entangled as in the first swap level. The drop in the entropy decreases with m since the starting state begins to look like state (5.35) for large m.

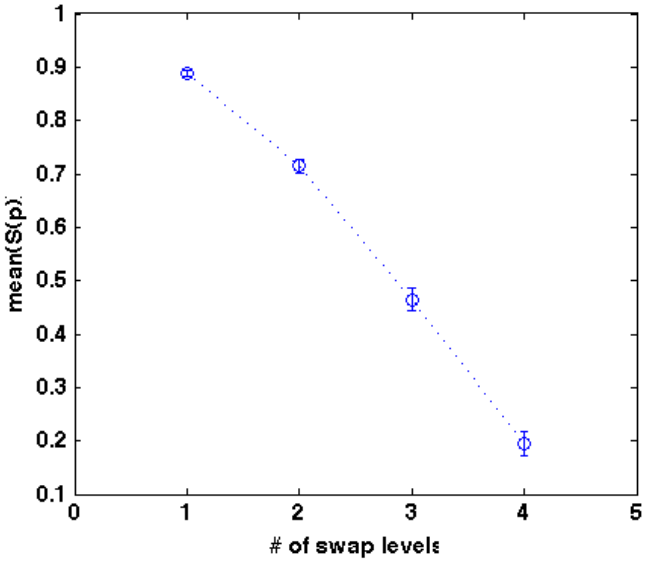

(a) $\bar{S}$ for $m = 1$ iterations

Figure 5.11

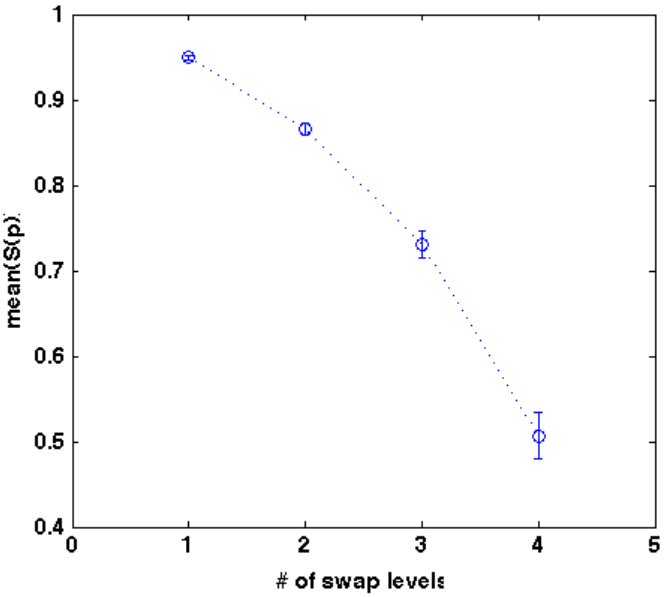

(b) $\bar{S}$ for $m = 2$ iterations

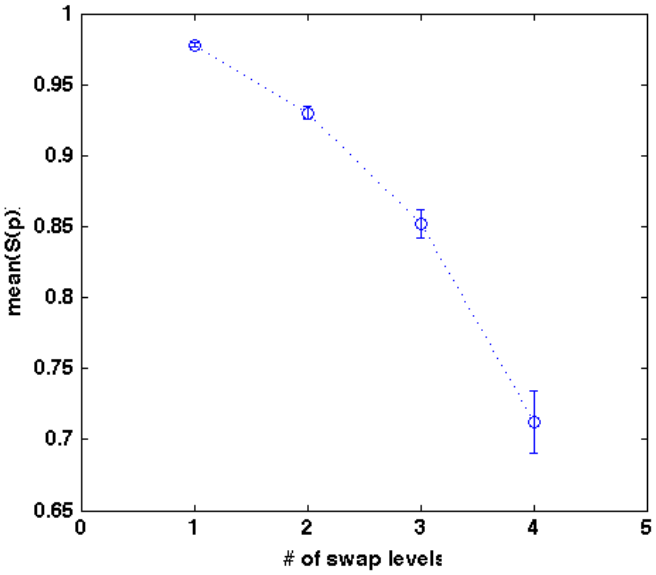

(c) $\bar{S}$ for $m = 3$ iterations

Figure 5.11: The mean entropy $\bar{S}$ for different values of m assuming that all $\hat{X}$ measurements have an outcome of zero. The plots were made by picking the outcome for the $\hat{P}$ measurement according to the related probability distribution. The simulation was repeated a 100 times to calculate the mean entropy. The error was calculated as the standard deviation of the mean

5.3.2 Swapping with Wigner functions

The growing and connection step of the repeater protocol were simulated using Wigner functions to calculate the average outcome of the steps. To investigate the performance of the repeater the entanglement swapping should be performed with the two-mode Wigner functions of the connection step. The input state of the first swap is

$$\begin{aligned} W_m(x,x',p,p')W_m(y,y',q,q') &= \sum_{(s,t,k,l)=0}^{2^{m+1}} w_{stkl}x^k x'^s p^l p'^t e^{-x^2-x'^2-p^2-p'^2} \times \\ &\quad \sum_{(s',t',k',l')=0}^{2^{m+1}} w_{s't'k'l'}y^k y'^s q^l q'^t e^{-y^2-y'^2-q^2-q'^2}. \end{aligned} \tag{5.78}$$

In the swap the modes described x', p' and y, q are connected on a balanced beam splitter. After measuring the $\hat{X}$ and $\hat{P}$ quadrature of these modes the unnormalized state in the quantum memories is

$$W_m(x,p,y',q') = \sum_{(s',t',k,l)=0}^{2^{m+1}} \tilde{w}_{s't'kl}x^k p^l y'^{s'} q'^{t'} e^{-x^2-p^2-y'^2-q'^2}. \tag{5.79}$$

The matrix elements $\tilde{w}_{s't'kl}$ are

$$\begin{aligned} \tilde{w}_{s't'kl} &= \sum_{(s,t,k',l')=0}^{2^{m+1}} w_{stkl}w_{s't'k'l'} \sum_{(i,j,u,n)=0}^{s,t,k',l'} \binom{s}{i}\binom{k'}{u}\binom{t}{j}\binom{l'}{n}(-1)^{k'-u+n}2^{-\frac{1}{2}(s+t+k'+l')} \\ &\quad \times\Lambda\left(s+k'-u-i\right)\Lambda\left(t+l'-j-n\right)x_0'^{i+u}q_0^{j+n}e^{-x_0'^2-q_0^2} \end{aligned} \tag{5.80}$$

where x_0' and q_0 are the outcomes of the $\hat{X}$ and $\hat{P}$ measurements and

$$\Lambda(\lambda) = \begin{cases} 0 & \text{if} \quad \lambda < 0, \lambda \text{ odd}, \\ \Gamma\left(\frac{1+\lambda}{2}\right) & \text{if} \quad \lambda \text{ even}. \end{cases} \tag{5.81}$$

It is not possible to make an average over the measurement outcomes because it is necessary to find the entanglement of the swapped state, which depends on the specific values of the outcomes. As a measure of entanglement the fidelity with a maximally entangled state called the *target state* is used. To obtain an expression for the target state some assumptions are made for the state (5.65) . Assuming that

$$\begin{aligned} \cos(\frac{1}{\sqrt{2}}(\mu_m+\tilde{\mu}_m)p') &= \cos(\sqrt{2}\mu_m p') = \cos(\sqrt{2}\tilde{\mu}_m p') = \cos(\theta) \\ \sin(\frac{1}{\sqrt{2}}(\mu_m+\tilde{\mu}_m)p') &= \sin(\theta) \end{aligned} \tag{5.82}$$

and that $b = -a^*$ and $e = c^*$ the unnormalized target state can be written as

$$\begin{aligned} |\Phi_{target}\rangle_{xq'} &= [\mathbb{A}\cos(\theta) + \mathbb{B}\sin(\theta)]\,|0_m\rangle_x\,|0_m\rangle_{q'} - [\mathbb{A}^*\cos(\theta) + \mathbb{B}^*\sin(\theta)]\,|1_m\rangle_x\,|1_m\rangle_{q'} \\ &+ [\mathbb{C}\cos(\theta) + \mathbb{D}\sin(\theta)]\,|1_m\rangle_x\,|0_m\rangle_{q'} + [\mathbb{C}^*\cos(\theta) + \mathbb{D}^*\sin(\theta)]\,|0_m\rangle_x\,|1_m\rangle_{q'}\,, \end{aligned} \tag{5.83}$$

which is a maximally entangled state. Since the assumption that $b = -a^*$ and $e = c^*$ is true for the first swap, this holds true for any swap within assumption (5.82). The coefficients $\mathbb{A}, \mathbb{B}, \mathbb{C}$ and $\mathbb{D}$ depend on the measurements in the previous swaps. The expression for the coefficients can be seen in Appendix B.5. θ is found by optimizing the fidelity as a function of θ. The fidelity, F of state (5.83) and the normalized version of state (5.79) can be written as:

$$F = (\mathcal{A}\cos^2(\theta) + \mathcal{B}\sin^2(\theta) + \mathcal{C}\cos(\theta)\sin(\theta))(\mathcal{D} + \mathcal{E}\cos^2(\theta))^{-1}. \tag{5.84}$$

The optimal choice of θ is found by solving $\frac{\partial F}{\partial \theta} = 0$. The expressions for the constants $\mathcal{A}, \mathcal{B}, \mathcal{C}, \mathcal{D}, \mathcal{E}$ can be seen in Appendix B.6.
The fidelity of state (5.83) and state (5.56) in the first swap is seen in figure 5.12 for different outcomes of the $\hat{X}$ measurement.
Figure 5.12 shows that the state (5.83) is a good choice of a target state since the fidelity pattern is very similar to the entropy pattern seen in figure 5.10.

In order to swap the Wigner functions measurement outcomes for the $\hat{P}$ and $\hat{X}$ measurements are simulated using the method described in Appendix B.4. Hence a set $\{(p_1, x_1), (p_2, x_2), \ldots, (p_n, x_n)\}$ is obtained for a maximum of four swap levels and the fidelity of the resulting Wigner function and the state (5.83) is calculated. The procedure is repeated a 100 times to obtain the average fidelity after each swap level. To see how the fidelity drops with the number of swap levels the starting state is the Wigner function of state (5.32). The simulations are made for $m = 1, 2, 3$ with different acceptance intervals $[-\delta, \delta]$ for the outcome of the $\hat{X}$ measurements. The plots resulting from the simulation are seen in figure 5.13.
The fidelity behaves in the same way as the entropy, which again confirms that state (5.65) is a good target state. For $m = 3$ the final fidelity after four swap levels is $\sim 90\%$ for $\delta \leq 1.8$. Figure 5.13 also shows that the acceptance interval can be increased for larger values of m as expected.

The entanglement swapping in the altered hybrid repeater is not as effective as in the original hybrid repeater since a bound of 90% on the output fidelity was assumed in the original repeater. This bound is already reached after four swap levels when swapping states of the type (5.32) in the altered repeater, which is in the limit of $\Delta \to 0$ and $r \to 0$. The fidelity will of course drop as Δ and r increase because the starting state will look less like the state (5.32)[9] and thus a lower bound of 90% cannot be assumed in the altered hybrid repeater for $m \leq 3$ when more than three swap levels are made.

[9]This will also weakly influence the probability of a successful swapping i.e. the probability that the $\hat{X}$ measurement falls in the acceptance interval.

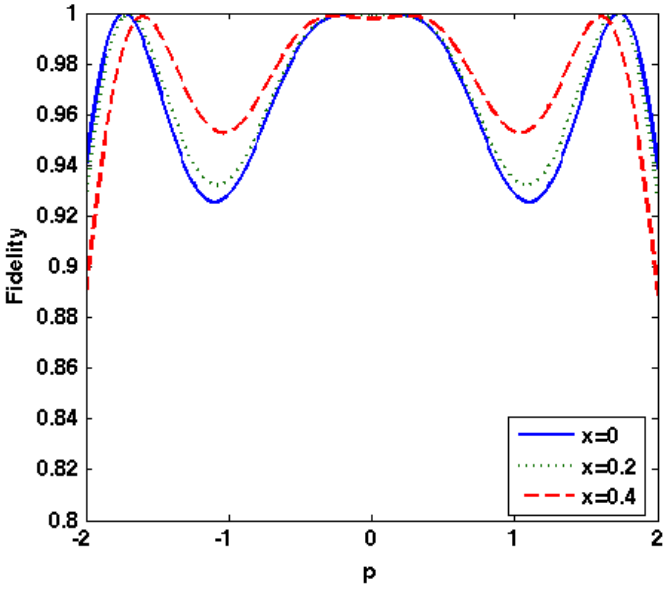

(a) Fidelity for $m = 1$ iterations

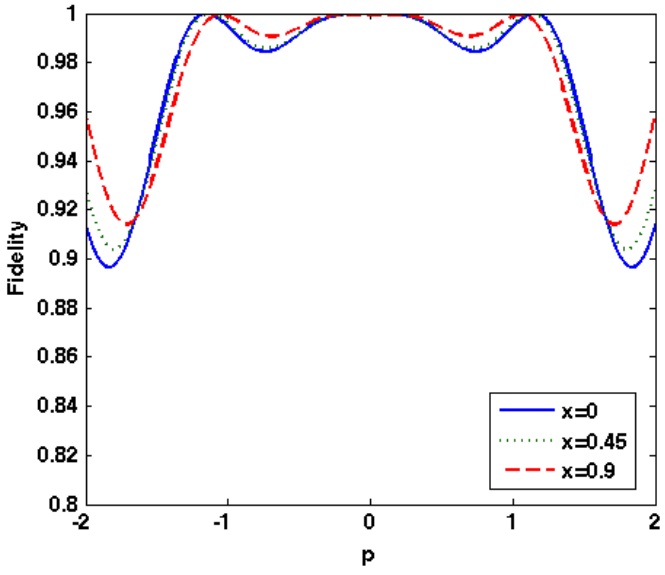

(b) Fidelity for $m = 2$ iterations

Figure 5.12

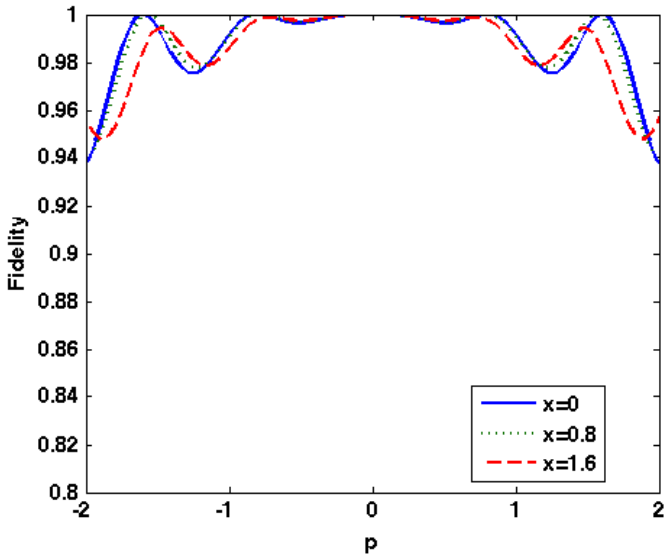

(c) Fidelity for $m = 3$ iterations

Figure 5.12: The fidelity as a function of the $\hat{P}$ measurement for different values of m and different outcomes of the $\hat{X}$ measurement. The similarity with figure 5.10 indicates that state (5.83) is a good target state.

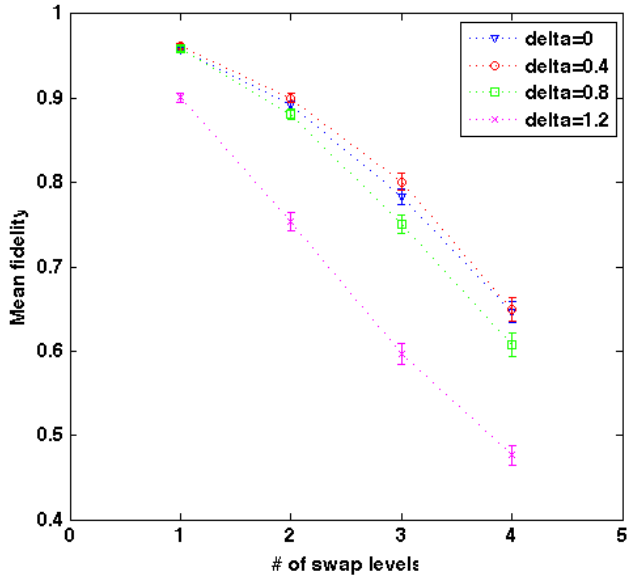

(a) Mean fidelity for $m = 1$ iterations

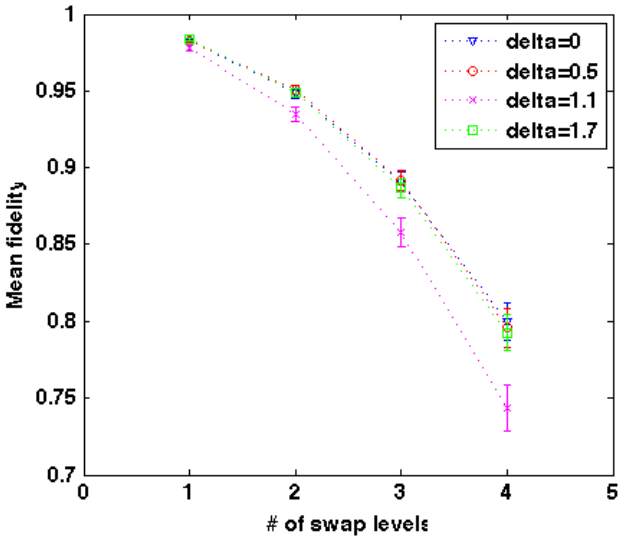

(b) Mean fidelity for $m = 2$ iterations

Figure 5.13

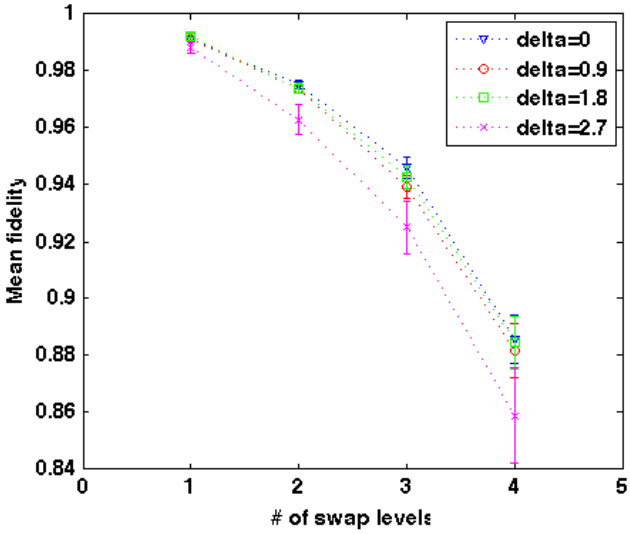

(c) Mean fidelity for $m = 3$ iterations

Figure 5.13: The mean fidelity as a function of the swap level for different values of m and different choices of acceptance intervals (δ). The plots were made by picking outcomes of the $\hat{X}$ and $\hat{P}$ measurements according to the related probability distributions. This corresponds to simulating 4 swap levels in an experiment. The simulation was repeated a 100 times and the mean fidelity was calculated. The error was calculated as the standard deviation of the mean.

Chapter 6

Performance and Final Results

6.1 Optimization

The full scheme of the altered hybrid repeater is seen in figure 6.1 and is the nested collection of all three steps - growing, connecting and entanglement swapping. To find the highest rate of entanglement distribution the performance of the repeater is optimized. The fidelity between the distributed state and the state in eq. (5.83) is used as a measure of entanglement and a lower bound of 80% for the distributed entanglement is required i.e.

$$F = |\langle \Phi_{target}| \hat{\rho}_{out} |\Phi_{target}\rangle|^2 \geq 0.8 \tag{6.1}$$

where ρ_{out} is the density operator of the distributed state and $|\Phi_{target}\rangle$ is the target state. This bound is lower than in Ref. [13] because the entanglement swapping is not as effective in the altered hybrid repeater as in the original hybrid repeater for iteration number $m \leq 3$. Do to runtime reasons the simulations are restricted to $m \leq 3$ and it is necessary to have $m \geq 4$ in order to have a lower bound of 90% in the altered repeater.
There are 5 parameters to consider in the optimization:

- $\vec{\Delta}$: Smaller acceptance intervals in the growing procedure increases the fidelity of the one-mode states with the optimal state obtained for $\vec{\Delta} = 0$ but it also decreases the rate at which the states are generated.

- m: Increasing m lowers the rate at which the one-mode states are generated but increases the fidelity of the connected two-mode states and a locally squeezed two-mode cat state. Thus the swap performance of the states are increased for large m.

- r: The parameter r determines the reflectivity of the beam splitters in the connection of the one-mode states. The entanglement of the connected states increases for $r \to 0$ but the probability of a successful connection will likewise tend to zero.

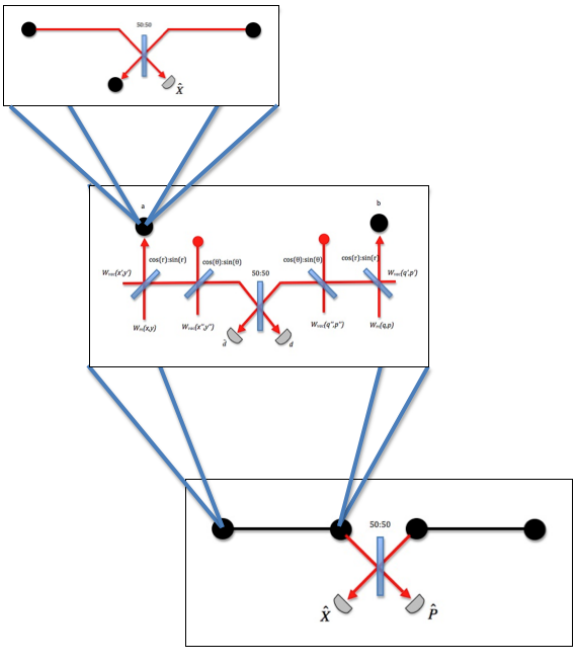

Figure 6.1: The nested collection of the altered hybrid repeater.

- δ: δ determines the probability of a successful swap and the fidelity of the output state with the target state. The fidelity seems almost independent of δ up to a certain value $\delta_{max,m}$ where it drops (see figure 5.13). The probability of a successful swap increases with δ and the optimal choice of δ is found be investigating how the increase in the success probability compensates for the drop in the fidelity.

- n: The number of swap levels (n) determines the classical communication time (L_0/c) between the stations in the elementary links and hense the loss in the fibers between the stations in the connection step.[1]

The optimization could be made by simply calculating the rate of the repeater on a grid of values for Δ, m, r, δ and n. However do to runtime reasons this grid would not be very dense for a straightforward calculation and the uncertainty in the optimal rate would be large. Instead an analytical approximation of the repeater is made to determine in what vicinity the optimal parameters lies and as a result get a denser grid around the optimal values. Furthermore a optimal choice of δ is found by investigating the mean entropy of the swapped state as a function of the outcome of the $\hat{X}$ measurement in the first swap. $\delta_{max,m}$ denotes the optimal choice of δ for iteration m. The values of $\delta_{max,m}$ and the procedure of

[1]The probability that a photon is lost in the fibers is $e^{-\frac{L_0}{2L_{att}}}$ where L_0 is the length of the elementary link and L_{att} is the attenuation length of the fibers

choosing $\delta_{max,m}$ are described in Appendix B.7.

The analytical approximation is based on the assumption that the errors in every step of the repeater simply add up to give the drop in the final fidelity. This assumption allows the output fidelity to be written as:

$$F_{out,m}(\vec{\Delta}, r, \theta, \delta, n) = 1 - g_m(\vec{\Delta}) - f_m(r, \theta) - h_m(\delta, n) \tag{6.2}$$

where $g_m(\vec{\Delta}), f_m(r, \theta)$ and $h_m(\delta, n)$ account for the errors in the first, second and third step of the repeater. The simplification: $h_m(\delta, n) \to h_m(\delta_{max,m}, n) = h_m(n)$ is made since the optimal choice of δ is $\delta = \delta_{max,m}$. Also $f_m(r, \theta) \to f_m(r)$ since the θ dependence is very weak when r is small, which will be the case in the optimization.

The rate of the repeater is determined by the probabilities of a successful growing, connection and entanglement swapping, which are denoted $P_{grow,m}(\vec{\Delta}), P_{connect,m}(r, \theta)$ and $P_{swap,m}(\delta)$. It is necessary to express the output fidelity as a function of these probabilities in order to make an optimization of the rate of the repeater. In the optimization $\delta = \delta_{max,m}$ and therefore $P_{swap,m}$ is a constant for a given number of iterations. Furthermore it is assumed that

$$P_{connect,m}(r, \theta) \approx P_{connect,m}(r)\cos(\theta)^2. \tag{6.3}$$

[2]This assumption underestimates the actual success probability of the connection step since it is only true when one photon is extracted from the input states. However it is not a grave underestimation since r is very small, which means that essentially only one photon is extracted. With this assumption the output fidelity is

$$F_{out,m,n}(R_{grow,m}, P_{connect,m}, n) = 1 - G(R_{grow,m}(\vec{\Delta})) - F(P_{connect,m}(r)) - H_{n,m} \tag{6.4}$$

where $G(R_{grow,m}(\vec{\Delta})), F(P_{connect,m}(r))$ and $H_{n,m}$ accounts for the errors in the first, second and third step of the repeater. $R_{grow,m}(\vec{\Delta})$ denotes the rate of the growing step in units of the source repetition rate (see eq. (4.15)).

The repeater was simulated numerically in Matlab to find the expressions for the functions $G(x), F(x)$ and the values of $H_{n,m}$. The simulations were made by varying one parameter at a time and plot the resulting output fidelity against the probability associated with that parameter. The resulting curve was fitted with either a polynomial or an exponential function. $\theta = 0$ and $\delta = \delta_{max,m}$ in all simulations. The procedure used to determine $H_{n,m}, G(x)$ and $F(x)$ can be described as follows:

- $H_{n,m}$: Let $\vec{\Delta} \to 0$, $r \to 0$ and vary n and m. Then $H_{n,m}$ is calculated as $1 - F_{out}$.

[2]Note that $P_{connect,m}(r) = P_{connect,m}(r, 0)$.

- $F(P_{connect,m}(r))$: Let $\vec{\Delta} \to 0$ and vary r. Plot the resulting output fidelity against $P_{connection,m}(r)$ for all combinations of m and n. The output fidelity should be corrected by adding it with $H_{n,m}$. The resulting 12 curves are fitted with a function $f(x) = ax^2 + bx + 1$ in which the fit parameters are a and b.

- $G(P_{grow,m}(\vec{\Delta}))$: Let $r \to 0$ and vary $\vec{\Delta}$. Correct the output fidelity by adding it with $H_{n,m}$ and plot it against $P_{grow,m}(\vec{\Delta})$ for all combinations of m and n. The resulting 12 plots are all fitted with a function $f(x) = 1 + ce^{bx}$ in which the fit parameters are c and b.

The result of the simulations can be seen in Appendix C.1. The simulations showed that the output fidelity can be written as:

$$\begin{aligned} F_{out,m,n}(R_{grow,m}, P_{connect,m}) &= 1 - a_{n,m}P_{connect,m}(r)^2 - b_{n,m}P_{connect,m}(r) \\ &\quad -c_{n,m}e^{d_{n,m}R_{grow,m}(\vec{\Delta})} - H_{n,m} \end{aligned} \tag{6.5}$$

where $a_{n,m} \leq 0$, $b_{n,m} \geq 0$, $c_{n,m} \geq 0$,$d_{n,m} \geq 0$ and $H_{n,m} \geq 0$.
The fact that $a_{m,n} \leq 0$ confirms that expression (6.5) is only a valid approximation for $P_{connection,m} \ll 1$. The validity of the approximation (6.5) was studied by running simulations of the repeater for different values of $m, \vec{\Delta}, r, \theta$ and n. The output fidelities were compared with the results obtained by using expression (6.5). In the simulations differences $\leq 10\%$ for the output fidelity were seen for $P_{connection,m} \ll 1$ and therefore approximation (6.5) should only be used to give a first guess of the optimal values of the success probabilities. Furthermore approximation (6.5) resulted in higher output fidelities than obtained in the simulations.

The approximation (6.5) is used to optimize the rate of the repeater but additional assumptions are necessary. Perfect one-mode quantum memories where the quantum signal can be stored without losses are assumed. This assumption is common in quantum repeater schemes and is also made in Ref. [13]. Furthermore the classical communication time L_0/c is assumed to be the time it takes to make one connection attempt in step two of the repeater. The length of the elementary links will be ~ 100 km, which corresponds to a classical communication time of ~ 0.3 ms. The local processes in the connection step take less than 1 μs and hence the assumption is valid.
The time it takes to provide the initial one-photon states for the growing of cat states cannot be neglected. Since it is a local process this time is assumed to be $t_{local} = 1$ μs and thus the average time needed to grow a cat state is

$$t_{cat} = \frac{t_{local}}{R_{growth,m}(\vec{\Delta})} \tag{6.6}$$

In a sense the entanglement swapping is a non-local process because after a swap attempt a signal needs to be transmitted to the two stations telling whether the swap was successful

or not. Therefore the average time needed to perform a swap at the n'th swap level given entanglement in two neighboring links at level $n-1$ is

$$t_{swap} = \frac{2^{n-1}L_0}{c} \cdot \frac{1}{P_{swap}(\delta_{max,m})} \tag{6.7}$$

since the time of the local operations in the swap is negligible.
With the preceding assumptions the rate of the repeater is

$$\begin{aligned}
\frac{1}{r_0} &= \frac{t_{local}}{R_{growth,m}(\vec{\Delta})} \cdot \frac{1}{P_{connect,m}(r,\theta)} \cdot \frac{3}{2} + \frac{L_0}{c} \cdot \frac{1}{P_{connect,m}(r,\theta)} && (6.8)\\
\frac{1}{r_1} &= \frac{1}{r_0} \cdot \frac{3}{2} \cdot \frac{1}{P_{swap}(\delta_{max,m})} + \frac{L_0}{c} \cdot \frac{1}{P_{swap}(\delta_{max,m})} && (6.9)\\
\frac{1}{r_2} &= \frac{1}{r_1} \cdot \frac{3}{2} \cdot \frac{1}{P_{swap}(\delta_{max,m})} + \frac{2L_0}{c} \cdot \frac{1}{P_{swap}(\delta_{max,m})} && (6.10)\\
&\vdots \\
\frac{1}{r_n} &= \frac{1}{r_{n-1}} \cdot \frac{3}{2} \cdot \frac{1}{P_{swap}(\delta_{max,m})} + \frac{2^{n-1}L_0}{c} \cdot \frac{1}{P_{swap}(\delta_{max,m})} && (6.11)
\end{aligned}$$

where n is the number of swap levels in the repeater. The assumption of eq.(3.21) gives the factors of $\frac{3}{2}$'s.

The rate should be optimized under the constraint that $F_{out} \geq 80\%$, which is possible using the method of Lagrange multipliers. The approximation (6.5) is used to define the functions

$$T_{m,n} = r_n - \Lambda \cdot (F_{out,m,n}(R_{grow,m}, P_{connect,m}) - 0.8)\,. \tag{6.12}$$

and solve the equations

$$\begin{aligned}
\frac{\partial T_{m,n}}{\partial P_{connect,m}(r)} &= 0\\
\frac{\partial T_{m,n}}{\partial R_{grow,m}(\vec{\Delta})} &= 0\\
\frac{\partial T_{m,n}}{\partial \Lambda} &= 0 && (6.13)
\end{aligned}$$

The solution $\left\{R^*_{grow,m}, P^*_{connect,m}, \Lambda^*\right\}$ are the optimal values of the connection success probability and the rate of the growing procedure within assumption (6.5)[3]. For a given distance d the optimization is made for all combinations of m and n. The optimal number of iterations (m) and the optimal number of swap levels (n) are found by comparing the

[3]Note that $P_{connect,m}(r,\theta) = P_{connect,m}(r)\cos^2(\theta)$ in the expression for r_n

rates for the different combinations of m and n. An attenuation length (L_{att}) of 20 km is assumed and accordingly $\cos^2(\theta) = e^{-L_0/40\text{km}}$. The result of the optimization is seen in table 6.1.

In order to find the optimal rate of the repeater table 6.1 is used to make a grid of

d/km	m	n	$R^*_{grow,m}(\vec{\Delta})$	$P^*_{connect,m}(r)\cos^2(\theta)$
100	1	0	0.205	0.221
200	2	1	0.0673	0.115
300	2	2	0.0586	0.0500
400	3	2	0.0143	0.0505
500	3	3	0.0133	0.0211
600	3	3	0.0128	0.0214
700	3	3	0.0124	0.0216
800	3	3	0.0120	0.0218
900	3	3	0.0116	0.0219
1000	3	3	0.0113	0.0221
1200	3	3	0.0110	0.0223
1400	3	4	0.00798	0.00668
1600	3	4	0.00773	0.00676
1800	3	4	0.00751	0.00683
2000	3	4	0.00731	0.00690

Table 6.1: Result of the optimization using the approximation (6.5) and the method of Lagrange multipliers.

values for $\vec{\Delta}, m, r$ and n on which to simulate the repeater. The number of iterations m and the number of swap levels n are set to the values in table 6.1 since the uncertainty of these is small[4]. Furthermore the values for $\delta_{max,m}$ found in Appendix B.7 are used for the acceptance intervals in the entanglement swapping. $R_{grow,m}(\vec{\Delta})$ spans the interval $\left[\frac{1}{2}R^*_{grow,m}(\vec{\Delta}), \frac{3}{2}R^*_{grow,m}(\vec{\Delta})\right]$ in 10 equally spaced steps and likewise $P_{connect,m}(r,\theta)$ spans the interval $\left[\frac{1}{2}P^*_{connect,m}(r)\cos^2(\theta), \frac{3}{2}P^*_{connect,m}(r)\cos^2(\theta)\right]$ in 10 equally spaced steps. To get an average output fidelity for each point 100 swap procedures are simulated for each of the 100 grid points. The result is a grid of 100 points from which the optimal rate subject to the bound $F_{out} \geq 80\%$ is found. If the optimal point consists of one of the outer points in the original intervals of $R_{grow,m}(\vec{\Delta})$ and $P_{connect,m}(r,\theta)$ a new simulation with different intervals is made.
The assumptions in the simulations are: $L_{att} = 20\text{km}$, $t_{local} = 1\mu\text{s}$, SPD detector efficiencies of 50% (not number resolving) and that a connection attempt takes the time L_0/c.

[4]The rate-difference for different combinations of m and n was large

Furthermore perfect quantum memories and sources of perfect one-photon states are assumed. The result of the simulation is shown in table 6.2 and the resulting figure 6.2.

d/km	m	n	$R_{grow,m}(\vec{\Delta})$	$P_{connect,m}(r,\theta)$	rate (pairs pr second)
100	1	0	0.15	0.011	32
200	2	1	0.075	0.0051	4.4
300	2	2	0.075	0.0045	1.5
400	3	2	0.014	0.0024	0.55
500	3	3	0.012	0.0023	0.26
600	3	3	0.012	0.0017	0.17
700	3	3	0.011	0.0012	0.11
800	3	3	0.011	0.00091	0.071
900	3	3	0.011	0.00067	0.048
1000	3	3	0.011	0.00049	0.033
1200	3	3	0.0085	0.00025	0.014
1400	3	4	0.0030	0.00044	0.0067
1600	3	4	0.0030	0.00032	0.0047
1800	3	4	0.0030	0.00023	0.0033
2000	3	4	0.0030	0.00017	0.0023

Table 6.2: Result of the optimization of the altered repeater. The rate is measured in entangled pairs pr. second. A lower bound of 80% with state (5.83) was assumed

Table 6.2 shows that the repeater has a rate of ~ 2 pairs/minute at a distance of 1000 km with a lower bound of 80% on the fidelity. This is 20 times higher than the rate of the original hybrid repeater scheme by Jonathan B. Brask et al., which was 0.1 pairs/minute at a distance of 1000km. Nonetheless a lower bound of 90% on the fidelity was assumed in Ref. [13] and furthermore figure 6.2 shows that the fractional difference of the rate of the altered repeater and the original repeater decreases with the distance[5]. This is because the states in the altered repeater do not swap as good as the states in the original repeater. Consequently the altered repeater do not perform significantly better than the original repeater except at small distances (< 500 km).

[5]The rate of the altered repeater is 33 times higher than the rate of the original repeater at a distance of 100km, 20 times higher at a distance of 1000 km and 13 times higher at a distance of 2000km

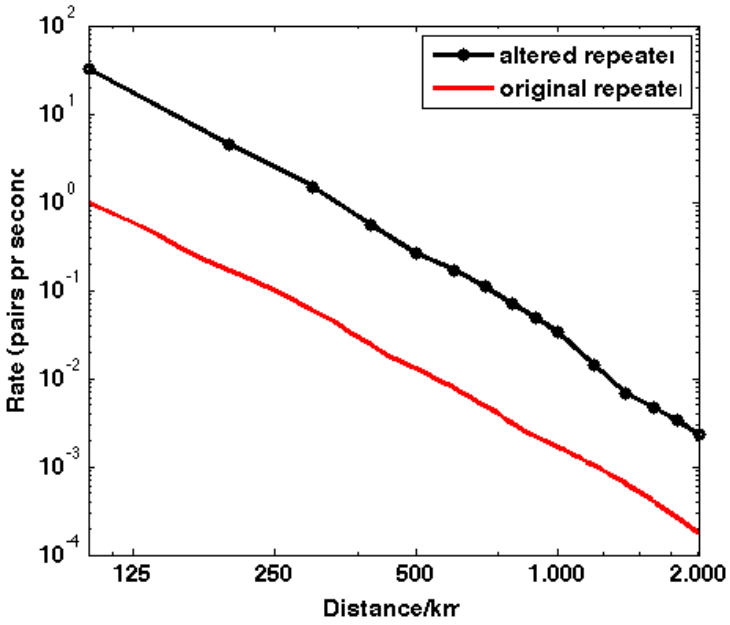

Figure 6.2: The optimal rate of the altered hybrid repeater and the original repeater vs. the distance/km. The rate is measured in pairs pr. second. A lower bound of 80% with state (5.83) was assumed in the altered repeater. The data needed to plot the rate of the original repeater was provided by Jonathan B. Brask.

6.2 Two-photon errors

So far perfect one-photon states have been assumed as input states for step one in the altered repeater scheme. However this is not assumed in Ref. [13] in which the optimization includes two-photon contributions. The rate at which the input states can be provided is determined by the percentage contribution of two-photon errors (p). In the altered repeater $t_{local} = 1$ μs, which is optimistic when perfect one-photon states are assumed i.e. for vanishing p. Thus it is necessary to allow for two-photon errors in the repeater and study how this affects the rate.

The perturbative approach of Ref.[26] is used to include two-photon errors in the altered repeater. The input states of the repeater are

$$W(x,p) = (1-p)W_1(x,p) + pW_2(x,p) \tag{6.14}$$

where W_1 is a one photon state and W_2 is a two-photon state. The product state at the beginning of the repeater is

$$W^N = ((1-p)W_1 + pW_2)^N = \sum_{i=0}^{N} \binom{N}{i} ((1-p)W_1)^i (pW_2)^{N-i} \tag{6.15}$$

where $N = 2^{m+n+1}$, m is the number of iterations in the growing step and n is the number of swap levels. Assuming that $p \ll 1$ all terms with $p^{i>1}$ are neglected. Thus the input state of the repeater is

$$(1-Np)W_1^N + NpW_1^{N-1}W_2. \tag{6.16}$$

Eq. (6.16) describes the situation where either all input states are one-photon states ($(1-Np)W_1^N$) or where exactly one of the input states is a two-photon state ($NpW_1^{N-1}W_2$). The output fidelity of the repeater is calculated as:

$$F(p,m,n,\vec{\Delta},r) = (1-f_2Np)F_1(m,n,\vec{\Delta},r) + f_2NpF_2(m,n,\vec{\Delta},r) \tag{6.17}$$

where F_1 is the output fidelity with perfect one-photon states and F_2 is the output fidelity where one of the input states is a two-photon state. The factor of N takes care of the fact that the two-photon state could be any of the 2^{m+n+1} input states and the factor f_2 takes into account that the probability of a two-photon state being accepted is different from the probability of a one-photon state being accepted. f_2 is determined numerically from simulating the growing step of the repeater since the probability of a successful connection and swapping is more or less the same with or without a two-photon error.

$F_2(m,n,\vec{\Delta},r)$ is calculated with the same grid used for the optimization of $F_1(m,n,\vec{\Delta},r)$ except that only grid points for which $F_1(m,n,\vec{\Delta},r) \geq 80\%$ are considered. The runtime

of the simulation is increased since a simulation with a two-photon input state and m iterations corresponds to a simulation of $m+1$ iterations with one-photon inputs in terms of the number of calculations. Therefore the simulations are restricted to distances $\leq$1000km. From the simulations the largest value of p for which the bound

$$(1 - f_2 Np)F_1(m, n, \vec{\Delta}, r) + f_2 NpF_2(m, n, \vec{\Delta}, r) \geq 80\% \tag{6.18}$$

is still satisfied is determined for each grid point individually.
It is necessary for the rate of the repeater to depend on p when two-photon components are included. Assuming sources of two-mode squeezed vacuum states to produce the one-photon states as in Ref.[13], the probability of producing a one-photon state, p_1 and a two-photon state, p_2 is

$$p_1 = \frac{\tanh^2 r}{\cosh^2 r}, \qquad p_2 = \frac{\tanh^4 r}{4\cosh^2 r} \tag{6.19}$$

where r is the squeezing parameter and it is assumed that $\theta = 0$ (see eq.(4.3)). For weak squeezing ($r \ll 1$) $p_2 \approx \frac{1}{4}p_1^2$ and the percentage contribution of two-photon states, p is

$$p = \frac{1}{1 + \frac{p_1}{p_2}} \approx \frac{1}{1 + \frac{4}{p_1}} \approx \frac{p_1}{4}. \tag{6.20}$$

When using sources of two-mode squeezed vacuum states it is possible to produce photons for the repeater in a deterministic way. A detector is placed to measure one of the output modes from the source and the other output mode is kept if the detector 'clicks'. A click means that the other mode contains at least one photon[6]. The average time it takes to generate one input state for the repeater including two-photon errors and assuming sources of two-mode squeezed vacuum states is

$$t_{input} = \frac{t_{source}}{4p\eta_{detector}} \tag{6.21}$$

where $\eta_{detector}$ is the probability of the detector to measure a photon. The rate of the whole repeater is obtained by letting

$$t_{local} \to \left(\frac{3}{2}\right) \frac{t_{source}}{4p\eta_{detector}} \tag{6.22}$$

in eq. (6.8) - (6.11). Photodetectors with efficiencies of 50% were assumed in the preceding simulations and therefore $\eta_{detector} = 50\%$. t_{source} is varied in order to determine how the rate of the altered repeater depends on the source repetition rate. For each distance d and each value of t_{source} the optimal rate is found from the grid points. The result of the calculation is seen in figure 6.3.

[6]The possibility of *dark counts* where the detector clicks without any photon hitting it is neglected

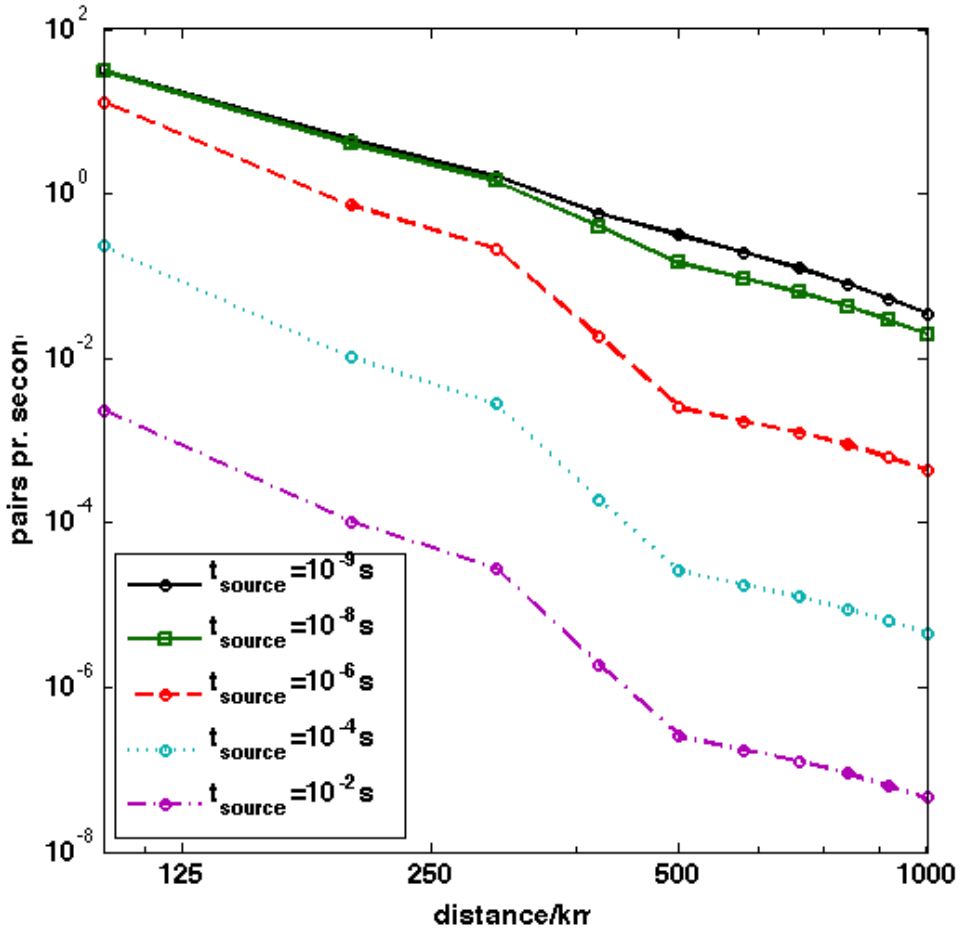

Figure 6.3: The optimal rate vs. the distance for different values of t_{source}. The rate obtained when assuming perfect one-photon input states is reached for $t_{source} \sim 10^{-9}$ s. The rate for $t_{source} \geq 10^{-8}$ s and distances $>$ 300km could be improved by including the two-photon contribution in the Lagrange-optimization instead of using the grid where perfect one-photon input states were assumed.

The rate obtained when assuming perfect one-photon input states is reached when $t_{source} \sim 10^{-9}$ s, which corresponds to a source repetition rate of GHz. This is a high repetition rate when the signal needs to be stored in quantum memories[7].
The procedure used to include two-photon errors in the repeater effectively amounts to a perturbative treatment of p. As a small test of eq.(6.17) the repeater was simulated for the gridpoints where $m = 2$ and $n = 1$ using states of the form (6.14) as input states. The resulting output fidelities deviated with $\leq 5\%$ from the results using eq.(6.17). Furthermore eq.(6.17) resulted in higher output fidelities than the simulations.
It is desirable to include the two-photon error in the Lagrange-optimization as well, which would result in a grid for each value of p. Looking at figure 6.3 it seems that the rate could be improved for distances > 300km and $t_{source} \geq 10^{-8}$ s. However, it requires numerous simulations of the repeater to do the Lagrange optimization including two-photon errors, which is time consuming.

[7] A high source repetition rate also means a broad energy bandwidth of the photons which is hard to read into e.g. a quantum memory based on an atomic ensemble.

Chapter 7

Conclusion and Outlook

7.1 Conclusion

The main subject of this thesis was the hybrid quantum repeater protocol suggested by Jonathan B. Brask et al. in Ref. [13]. This repeater protocol consists of three steps described in chapter 4. The first step is to create entanglement in the elementary links in form of bell-like states. I the next step approximately squeezed two-mode cat states are grown from the bell-like states. The final step of the protocol is entanglement swapping, which is performed using balanced beam splitters and homodyne detection.

The objective of this thesis was to improve the original hybrid repeater protocol by Jonathan B. Brask et al. Two ways of improving the protocol was studied, which resulted in an altered repeater protocol. The first of these was to optimize the method used to grow the approximately squeezed cat states. The method was studied using single-photon states as input states, which produced approximately squeezed one-mode cat states. The optimization was made by allowing for different acceptance intervals in every iteration of the growing procedure. The optimal choices of acceptance intervals was found by implementing the growing procedure in the program *Matlab* and making a numerical simulation of the growing step. Wigner functions were used in the simulation in order to get the average outcome of the growing procedure. The average success probability and the average output fidelity with a squeezed one-mode cat state was calculated on a grid of different values for $\Delta_1, \Delta_2 \ldots \Delta_m$ where Δ_m determines the acceptance interval of iteration m. The simulation was performed for a maximum of three iterations under the assumption that $\Delta_{m+1} > \Delta_m$.
The optimization showed that the rate of growing approximately squeezed cat states was improved by allowing for different acceptance intervals in each iteration. However the improvement was not significantly high for output fidelities $> 90\%$. For an output fidelity of 90% the rate of growing in units of the source repetition rate was raised from 0.1378 to

0.1423 for two iterations and from 0.03791 to 0.04104 for three iterations. Perfect one-mode quantum memories were assumed in the simulation.

The other idea to improve the original scheme was to interchange step one and two. In this way it is not necessary to reestablish entanglement in the elementary links every time a growing procedure fails. The method suggested by N. Sanguard et al. in Ref. [14] to connect one-mode cat states into two-mode cat states was used. The squeezing of the one-mode cat states made it necessary to use another target state for the connection than the two-mode cat states of Ref. [14]. The new target state was a maximally entangled state described in a basis of $\{|1_m\rangle, |0_m\rangle\}$ where the subscript m refers to the number of iterations in the growing procedure. $|1_m\rangle$ and $|0_m\rangle$ are superpositions of even and odd Fock states respectively. For $m \geq 5$ the target state is a locally squeezed two-mode cat state. A numerical simulation of the connection step was made in *Matlab* in which photon losses and imperfect photo-detectors were included. The average time needed to establish entanglement using the approximately squeezed cat states as input states was shown to be comparable to the time of entanglement creation in Ref.[14].

In section 5.3 the swapping procedure of Ref. [13] was applied to the connected two-mode states of the altered repeater. The swapping procedure was simulated in *Matlab* using Wigner functions to describe the states. The measurement outcomes for the $\hat{X}$ and $\hat{P}$ measurements in the swapping procedure were simulated by picking values according to the corresponding probability distributions of the outcomes. The target state of the repeater after a number of swap levels was a maximally entangled state described in the basis of $\{|1_m\rangle, |0_m\rangle\}$. For $m \geq 5$ this target state is essentially a locally squeezed two-mode cat state and thus near-deterministic swapping can be obtained using the method described in Ref.[13] for large m. The result of the simulation was that the two-mode states of the altered repeater do not swap as good as the connected states in Ref.[13].

The final step of the thesis was to assemble the three steps of growing cat states, connecting them and entanglement swapping into an altered hybrid repeater protocol. The performance of the repeater depended on a number of parameters belonging to each of the three steps. An analytical approximation of how the final fidelity with the target state depended on these parameters was made in order to find the optimal rate at which the repeater could distribute entanglement. The approximation was based on numerical simulations of the repeater in Matlab and was used to find a first guess of the optimal choice of each parameter at a given distance. Afterwards the repeater was simulated numerically on a grid around each point in order to find the optimal rate of the repeater. When calculating the rate of the repeater perfect one-mode quantum memories, an attenuation length of 20km in the fibers and a time of L_0/c to do a connection attempt was assumed[1]. Fur-

[1] L_0 is the length of an elementary link and c is the speed of light

thermore a source of perfect one-photon states were assumed. The time needed to produce the one-photon states was 1μs and the lower bound on the final fidelity was 80%.
The result of the optimization was that the altered hybrid repeater had a rate of ~ 2 pairs/minute at a distance of 1000km with a lower bound of 80% on the fidelity with the maximally entangled target state. The original hybrid repeater by Jonathan B. Brask et al. had a rate of 0.1 pairs/minute at a distance of 1000 km with a lower bound of 90% on the fidelity with a maximally entangled target state. Furthermore the fractional difference of the rate of the altered repeater and the original repeater decreased with the distance because the states in the altered repeater did not swap as good as the states in the original repeater. It was not possible to set a lower bound of 90% on the fidelity in the altered repeater scheme because the simulation was restricted to $m \leq 3$.

Two-photon errors were included in the repeater in a perturbative way and sources of two-mode squeezed vacuum states were imagined to generate the input states of the repeater. This made it possible to study how the rate of the altered repeater depended on the source repetition rate. It was shown that a source repetition rate around 1 GHz was required to obtain a rate comparable to to the rate where perfect one-photon states were assumed as input states. A repetition rate of 1 GHz is high because the signals need to be stored in quantum memories.

7.2 Outlook

The initial hope was that the altered hybrid repeater would perform significantly better than the original hybrid repeater of Ref. [13]. The rate of the altered repeater turned out to be higher than the rate of the original repeater but with a lower bound of 80% on the output fidelity with a maximally entangled state compared to a bound of 90% in Ref. [13]. A lower bound of 90% in the altered repeater requires simulations with $m > 3$, which would decrease the rate at which the cat states are grown. However, this does not influence the time-consuming connection step and the swap performance of the two-mode states would be increased. Hence it is possible that the rate of the altered repeater with a bound of 90% would be comparable to the rate obtained in Ref. [13] and perhaps higher. The programs that I have written in *Matlab* to simulate the repeater can be used directly to simulate the whole repeater for $m > 3$ but the simulation will be time consuming, which is the reason that I have not done this.

It would also be interesting to include the two-photon error in the Lagrange-optimization since it seems that the grid used for the two-photon simulation could be chosen more wisely. The plots in figure 6.3 indicate that a higher rate could be obtained for distances > 300km and $t_{source} \geq 10^{-8}$ s if another grid was chosen. I have written the programs necessary to simulate the repeater with two-photon errors in *Matlab* and the only obsta-

cle is that the simulations are time-consuming. The programs are described in Appendix D

Another approach to improve the altered hybrid repeater would be to remove the squeezing of the approximate cat states before the connection. The connected states swap 'poorly' for small m because of the squeezing in the one-mode input states, which makes the connected states deviate from two-mode cat states. The squeezing produced when growing the cat states are $\sim$ 3dB,[2] which is accessible experimentally and therefore could be removed [30, 31, 32]. To remove the squeezing in the $\hat{X}$ quadrature the state would have to be equally "squeezed" in the $\hat{P}$ quadrature. It is hard to squeeze the state in a quantum memory and it might be necessary to read out the state, squeeze it and read it in again. This would lower the rate of the repeater along with the possibility of errors in the process.

The Achilles heel of the altered repeater scheme is the swapping operation, which could be improved by letting $m > 3$ or by removing the squeezing in the one-mode states. However perfect quantum memories allowing a signal to be stored and retrieved without any losses were also assumed in the repeater. This is not a very realistic assumption though it is common to assume highly efficient quantum memories in quantum repeater literature [13, 14, 29, 34, 35]. The quantum memories realized experimentally are far from being 100% effective [33] and thus an effective way of dealing with the errors introduced by inefficient quantum memories is necessary. One solution is to make an entanglement purification protocol for the repeaters. Entanglement purification is the process where 'copies' of the distributed pair are used to increase the entanglement. By local operations the 'copies' are manipulated to produce a more entangled pair [36, 37, 38]. This means that the initial entanglement of the distributed pairs do not need to be as high because the final entanglement can be enhanced by the purification protocol.
Such purifications protocols exists for various type of states but to my knowledge it does not exist for the cat states used in the hybrid repeaters. Developing an entanglement purification protocol for cat states would be an interesting challenge.

Another approach to the problem of inefficient quantum memories is to use multimode quantum memories. In the optimization quantum memories capable of storing one mode each were assumed while multimode memories can store a number of modes. Multimode memories could be used in both *parallelization* and *multiplexing* schemes where parallel channels are used to distribute entanglement. Especially multiplexed schemes have shown to be robust to memory inefficiencies [39]

A side from the preceding suggestions to improve the repeater scheme there are some other areas of the altered repeater to consider. The possibility of *dark counts* was neglected in the simulations. It was assumed in both the generation of the one-photon states and in

[2] See Ref. [13]

the connection step that the photodetectors did not click if nothing hit them. However, the photodetectors realized experimentally have the possibility of *dark counts* where the detector clicks without any photon hitting it. This would be a serious error in the repeater since it allows for vacuum components in the input states and decreases the performance of the connection step. Thus including dark counts in the simulation would decrease the rate of the repeater.
Finally the local operations in the altered repeater made use of beam splitters and homodyne detection. Losses connected with these operations were neglected but could also be included in the simulation.

Appendix A

Teleportation

The general scheme of entanglement assisted teleportation is shown in this appendix. The appendix is based on material form the course "Quantum Information Theory" at NBI, Copenhagen.

First a set of tools is defined:

Tool 1 *Let $|\Omega\rangle$ be a maximally entangled state in the Hilbert space $\mathbb{H} = \mathbb{C}^d \otimes \mathbb{C}^d$. There exits a orthonormal basis $\{|1\rangle, \ldots, |d\rangle\}$ such that*

$$|\Omega\rangle = \frac{1}{\sqrt{d}} \sum_{i=1}^{d} |i\rangle \otimes |i\rangle \tag{A.1}$$

This is the Schmidt decomposition of $|\Omega\rangle$

Tool 2 *Let U be a $d \times d$ matrix. Then*

$$(U \otimes \mathbb{I}) |\Omega\rangle = (\mathbb{I} \otimes U^T) |\Omega\rangle \tag{A.2}$$

proof:

$$\begin{aligned} \langle k,l| U \otimes \mathbb{I} |\Omega\rangle &\stackrel{?}{=} \langle k,l| \mathbb{I} \otimes U^T |\Omega\rangle \\ \frac{1}{\sqrt{d}} \sum_{i=1}^{d} \langle k| U |i\rangle \cdot \langle l| i\rangle &\stackrel{?}{=} \frac{1}{\sqrt{d}} \sum_{i=1}^{d} \langle l| U^T |i\rangle \cdot \langle k| i\rangle \\ \frac{1}{\sqrt{d}} \langle k| U |l\rangle &= \frac{1}{\sqrt{d}} \langle l| U^T |k\rangle \end{aligned} \tag{A.3}$$

Figure A.1: Alice and Bob shares a maximally entangled state $|\Omega\rangle_{A_2B}$ symbolized with the connected black dots. Furthermore Alice has a unknown state $|\Psi\rangle_{A_1}$ that she wishes to teleport to Bob

Tool 3 *Let* $|\Psi\rangle_A \in \mathbb{C}^d$ *be a state in system* A *and* $|\Omega\rangle_{AB} \in \mathbb{C}^d \otimes \mathbb{C}^d$ *be a maximally entangled state of the bipartite system* AB*. Then*

$$(\langle\Psi|_A \otimes \mathbb{I}_b)\,|\Omega\rangle_{AB} = \frac{1}{\sqrt{d}}\,|\Psi^*\rangle_B \tag{A.4}$$

proof: Let $|\Psi\rangle = \sum_{j=1}^{d} C_j\,|j\rangle$*. Then:*

$$\begin{aligned}(\langle\Psi|_A \otimes \mathbb{I}_b)\,|\Omega\rangle_{AB} &= \frac{1}{\sqrt{d}}\sum_{i,j=1}^{d} C_j^*\,(\langle j|_A \otimes \mathbb{I}_B)\,(|i\rangle_A \otimes |i\rangle_B)\\ &= \frac{1}{\sqrt{d}}\sum_{i=1}^{d} C_i^*\,|i\rangle_B\\ &= \frac{1}{\sqrt{d}}\,|\Psi^*\rangle_B\end{aligned} \tag{A.5}$$

Tool 4 *There exist unitaries* $\{U_i\}_{i=1\ldots d^2}$ *such that:*

$$|\Omega_i\rangle = (\mathbb{I} \otimes U_i)\,|\Omega\rangle \tag{A.6}$$

is a orthonormal basis in $\mathbb{C}^d \otimes \mathbb{C}^d$*. For d=2:*

$$\begin{aligned}\{U_i\} &= \{\mathbb{I}, \sigma_x, \sigma_y, \sigma_z\} and\\ \{|\Omega_i\rangle\} &= \left\{\left|\Psi^+\right\rangle, \left|\Psi^-\right\rangle, \left|\Phi^+\right\rangle, \left|\Phi^-\right\rangle\right\}\end{aligned} \tag{A.7}$$

With these tools in place the teleportation scheme can be shown. The setup is seen in figure A.1 The initial state is

$$|\Psi\rangle_{A_1} \otimes |\Omega\rangle_{A_2B} \in \mathbb{C}^d \otimes \mathbb{C}^d \otimes \mathbb{C}^d \tag{A.8}$$

where $|\Psi\rangle_{A_1}$ is the unknown state that Alice wants to teleport to Bob. Now alice performs a joint measurement of the von Neumann type on system A_1 and A_2 and gets outcome i. Consequently the system is:

$$\left(|\Omega_i\rangle\langle\Omega_i|_{A_1A_2} \otimes \mathbb{I}_B\right)\left(|\Psi\rangle_{A_1} \otimes |\Omega\rangle_{A_2B}\right) \tag{A.9}$$

Using *tool 4* Bob's system is:

$$\begin{aligned}
\left(\langle\Omega|_{A_1A_2}\left(\mathbb{I}_{A_1} \otimes U^\dagger_{i,A_2}\right) \otimes \mathbb{I}_B\right)\left(|\Psi\rangle_{A_1A_2} \otimes |\Omega\rangle_{A_2B}\right) &= \text{(use } \textit{tool 2}\text{)} \\
\left(\langle\Omega|_{A_1A_2} \otimes \mathbb{I}_B\right)|\Psi\rangle_{A_1} \otimes \left(U^\dagger_{i,A_2} \otimes \mathbb{I}_B\right)|\Omega\rangle_{A_2B} &= \text{(use } \textit{tool 3)} \\
\frac{1}{\sqrt{d}}\left(\langle\Psi^*|_{A_2} \otimes \mathbb{I}_B\right)\left(\mathbb{I}_{A_2} \otimes U^*_{i,B}\right)|\Omega\rangle_{A_2B} &= \\
\frac{1}{d}U^*_{i,B}|\Psi\rangle_B &
\end{aligned} \tag{A.10}$$

If Bob are told the measurement outcome from Alice he can apply U_i^T to get $|\Psi\rangle_B$. Thus the state $|\Psi\rangle$ has been teleportet to Bob.

Appendix B

Supplement to Chapter 5

B.1 Matrix element w_{stkl}

The Matrix element w_{stkl} is

$$\begin{aligned} w_{stkl} &= \frac{2}{\pi^4} \sum_{\{i,i',j,j'\}=0}^{2^{m+1}} \sum_{\{s',t',k',l'\}=0}^{\{i-s,j-t,i'-k,j'-l\}} \sum_{\{s'',t'',k'',l''\}=0}^{\{s',t',k',l'\}} \\ &\quad \tilde{w}_{ij}\tilde{w}_{i'j'}\mu^{ij}_{sts't'}\mu^{i'j'}_{klk'l'}\gamma^{k's'}_{k''s''}\gamma^{t'l'}_{t''l''} \\ &\quad \times(\underbrace{\eta^{k''s''}\eta^{t''l''}}_{\text{a}} - \underbrace{2\kappa^{k''s''}\kappa^{t''l''}}_{\text{b}}) \end{aligned} \tag{B.1}$$

Term a describes the situation where there is no click in detector $\tilde{d}$ and anything can happen at detector d while term b describes the situation where no detector fires. The combination $a - b$ is the situation where detector d fires and detector $\tilde{d}$ do not.

$\tilde{w}$ are the matrix elements of the one-mode input states being connected. The expressions for η,γ and κ are

$$\mu^{i,j}_{sts't'} = \begin{cases} \binom{i}{s}\binom{j}{t}\binom{i-s}{s'}\binom{j-t}{t'}\cos(r)^{s+t}\sin(r)^{i+j-s-t}\cos(\theta)^{s'+t'}\sin(\theta)^{i+j-s-t-s'-t'} & \\ \times\Lambda(\infty, i-s-s')\Lambda(\infty, j-t-t') & \text{if} \quad i>s, j>t \\ 0 & \text{if} \quad s>i, t>j \end{cases}$$

$$\gamma^{k's'}_{s''k''} = 2^{-\frac{1}{2}(2k'+2s'-k''-s''+1)}\binom{s'}{s''}\binom{k'}{k''}(-1)^{s'-s''}\Lambda(\infty, k'-s'-k''-s'')$$

$$\eta^{s''k''} = \Lambda(\infty, k''+s'')$$

$$\kappa^{s''k''} = 2^{-\frac{1}{2}(k''+s''+1)}\Lambda(\infty, k''+s'')$$

where

$$\Lambda(\varepsilon,\lambda)=\begin{cases}0 & \text{if} \quad \lambda<0,\lambda \text{ odd},\\ \int_{-\varepsilon}^{\varepsilon} x^{\lambda}e^{-x^2}\mathrm{dx} & \text{if} \quad \lambda \text{ even}.\end{cases} \tag{B.2}$$

B.2 Matrix elements $F_{s,t}, G_{s,t}$ and $H_{s,t}$

The expressions of the matrix elements $F_{s,t}, G_{s,t}$ and $H_{s,t}$ seen in eq.(5.57) -eq.(5.60) are:

$$F_{s,t} = 2^{-\frac{1}{2}(s+t)}x^{s+t}e^{-\frac{1}{2}x^2}\begin{cases}\sqrt{2}\Gamma\left(2^m-\frac{1}{2}(s+t+1)\right){}_1F_1\left(2^m-\frac{1}{2}(s+t+1),\frac{1}{2},-\frac{p^2}{2}\right) & \text{if} \quad s+t=\text{even},\\ -2ip\Gamma\left(2^m-\frac{1}{2}(s+t)\right){}_1F_1\left(2^m-\frac{1}{2}(s+t),\frac{3}{2},-\frac{p^2}{2}\right) & \text{if} \quad s+t=\text{odd}.\end{cases}$$

$$G_{s,t} = 2^{-\frac{1}{2}(s+t)}x^{s+t}e^{-\frac{1}{2}x^2}\begin{cases}-2ip\Gamma\left(2^m-\frac{1}{2}(s+t-1)\right){}_1F_1\left(2^m-\frac{1}{2}(s+t-1),\frac{3}{2},-\frac{p^2}{2}\right) & \text{if} \quad s+t=\text{even},\\ \sqrt{2}\Gamma\left(2^m-\frac{1}{2}(s+t)\right){}_1F_1\left(2^m-\frac{1}{2}(s+t),\frac{1}{2},-\frac{p^2}{2}\right) & \text{if} \quad s+t=\text{odd}.\end{cases}$$

$$H_{s,t} = 2^{-\frac{1}{2}(s+t)}x^{s+t}e^{-\frac{1}{2}x^2}\begin{cases}\sqrt{2}\Gamma\left(2^m-\frac{1}{2}(s+t-1)\right){}_1F_1\left(2^m-\frac{1}{2}(s+t-1),\frac{1}{2},-\frac{p^2}{2}\right) & \text{if} \quad s+t=\text{even},\\ -2ip\Gamma\left(2^m-\frac{1}{2}(s+t-2)\right){}_1F_1\left(2^m-\frac{1}{2}(s+t-2),\frac{3}{2},-\frac{p^2}{2}\right) & \text{if} \quad s+t=\text{odd}.\end{cases}$$

where x and p are the outcomes of the $\hat{X}$ and $\hat{P}$ measurements.
${}_1F_1$ are the *confluent hypergeometric function* defined as:

$${}_1F_1=\sum_{n=0}^{\infty}\frac{(a)_n z^n}{(b)_n n!} \tag{B.3}$$

where $(a)_n = a(a+1)(a+2)\ldots(a+n-1)$

B.3 Coefficients A and C

The explicit expressions for the coefficients A and C in eq.(5.74) are:

$$\begin{aligned}A &= [\Re(c_1)\Re(c_2)+\Im(c_1)\Im(c_2)-\Re(a_1)\Re(a_2)+\Im(a_1)\Im(a_2)]\cos(2^{(m+1)/2}p')\\ &\quad -[\Re(c_1)\Im(a_2)-\Re(a_2)\Im(c_1)-\Re(a_1)\Im(c_2)-\Re(c_2)\Im(a_1)]\sin(2^{(m+1)/2}p')\\ &\quad +\mathbb{I}[\Re(c_1)\Im(c_2)-\Re(c_2)\Im(c_1)-\Re(a_1)\Im(a_2)-\Re(a_2)\Im(a_1)]\cos(2^{(m+1)/2}p')\\ &\quad +\mathbb{I}[\Re(c_1)\Re(a_2)+\Im(c_1)\Im(a_2)-\Re(a_1)\Re(c_2)+\Im(a_1)\Im(c_2)]\sin(2^{(m+1)/2}p') \qquad \text{(B.4)}\\ C &= [\Im(c_1)\Im(a_2)-\Re(a_1)\Re(c_2)-\Im(a_1)\Im(c_2)-\Re(c_1)\Re(a_2)]\cos(2^{(m+1)/2}p')\\ &\quad -[\Re(a_2)\Im(a_1)-\Re(c_2)\Im(c_1)-\Re(c_1)\Im(c_2)-\Re(a_1)\Im(a_2)]\sin(2^{(m+1)/2}p')\\ &\quad +\mathbb{I}[\Re(c_2)\Im(a_1)-\Re(a_1)\Im(c_2)-\Re(a_2)\Im(c_1)-\Re(c_1)\Im(a_2)]\cos(2^{(m+1)/2}p')\\ &\quad +\mathbb{I}[\Im(c_1)\Im(c_2)-\Re(a_1)\Re(a_2)-\Re(c_1)\Re(c_2)-\Im(a_1)\Im(a_2)]\sin(2^{(m+1)/2}p') \qquad \text{(B.5)}\end{aligned}$$

When states of the type (5.32) are swapped, $a_1=a_2=0$ and $c_1=c_2=1$ in the first swap level. In that case $\Im(A)=0$ and that $\Re(C)=0$ in this swap level and hence in all later swap levels.

B.4 Simulating measurement outcomes

The *cumulative distribution functions* (CDF) of the outcome of the $\hat{X}$ and $\hat{P}$ measurements are used to pick the outcomes according to the probability distributions. The definition of the cumulative distribution function is:

Definition 1 *Let $f(x)$ be probability density function of a real valued variable x. The cumulative distribution function, $F(x)$ is*

$$F(x) = \int_{-\infty}^{x} f(t)\mathrm{d}t \tag{B.6}$$

The cumulative distribution function can be used to find the probability that the variable x lies in some interval $]a; b]$:

$$P(a < x \leq b) = F(b) - F(a) \tag{B.7}$$

Where $P(a < x \leq b)$ is the probability that x lies in the interval $]a; b]$.

The procedure of picking measurement outcomes is:

- Use the build-in random number generator in Matlab to pick a number, $c \in [0; 1]$.
- Solve the equation $CDF(x) = c$, where $CDF(x)$ is the cumulative distribution function corresponding to the relevant quadrature operator.
- The solution x^* is the measurement outcome picked according to the probability distribution.

B.5 Coefficients $\mathbb{A}, \mathbb{B}, \mathbb{C}$ and $\mathbb{D}$

The expressions of the coefficients $\mathbb{A}, \mathbb{B}, \mathbb{C}$ and $\mathbb{D}$ in eq. (5.83) are:

$$
\begin{aligned}
\mathbb{A} &= 2\left[\Re(c_1)\Re(c_2)+\Im(c_1)\Im(c_2)+\Im(a_1)\Im(a_2)-\Re(a_1)\Re(a_2)\right]+e^{-\frac{1}{2}(\mu_m-\tilde{\mu}_m)^2}\times \\
&\quad \Big\{\left(\Re(a_1)\Re(c_2)-\Im(a_1)\Im(c_2)+\Im(c_1)\Im(a_2)+\Re(c_1)\Re(a_2)\right)\left[e^{-\sqrt{2}x(\mu_m-\tilde{\mu}_m)}-e^{\sqrt{2}x(\mu_m-\tilde{\mu}_m)}\right] \\
&\quad +i\left[\Re(a_1)\Im(c_2)+\Re(c_2)\Im(a_1)+\Re(c_1)\Im(a_2)-\Re(a_2)\Im(c_1)\right]\left[e^{-\sqrt{2}x(\mu_m-\tilde{\mu}_m)}-e^{\sqrt{2}x(\mu_m-\tilde{\mu}_m)}\right]\Big\} \\
&\quad +2i\left[\Re(c_1)\Im(c_2)-\Re(c_2)\Im(c_1)-\Re(a_1)\Im(a_2)-\Re(a_2)\Im(a_1)\right] \qquad \text{(B.8)} \\
\mathbb{B} &= \Big\{-\left[\Re(c_1)\Im(a_2)-\Re(a_2)\Im(c_1)-\Re(a_1)\Im(c_2)-\Re(c_2)\Im(a_1)\right] \\
&\quad +i\left[\Re(c_1)\Re(a_2)-\Re(a_1)\Re(c_2)+\Im(c_1)\Im(a_2)+\Im(a_1)\Im(c_2)\right]\Big\} \\
&\quad \times\left[e^{-\sqrt{2}x(\mu_m-\tilde{\mu}_m)}+e^{\sqrt{2}x(\mu_m-\tilde{\mu}_m)}\right]e^{-\frac{1}{2}(\mu_m-\tilde{\mu}_m)^2} \qquad \text{(B.9)} \\
\mathbb{C} &= 2\left[\Im(c_1)\Im(a_2)-\Re(a_1)\Re(c_2)-\Im(a_1)\Im(c_2)-\Re(c_1)\Re(a_2)\right]+e^{-\frac{1}{2}(\mu_m-\tilde{\mu}_m)^2}\times \\
&\quad \Big\{\left(\Re(c_1)\Re(c_2)-\Im(a_1)\Im(a_2)-\Im(c_1)\Im(c_2)-\Re(a_1)\Re(a_2)\right)\left[e^{-\sqrt{2}x(\mu_m-\tilde{\mu}_m)}-e^{\sqrt{2}x(\mu_m-\tilde{\mu}_m)}\right] \\
&\quad +i\left[\Re(a_2)\Im(a_1)+\Re(c_2)\Im(c_1)+\Re(c_1)\Im(c_2)-\Re(a_1)\Im(a_2)\right]\left[e^{-\sqrt{2}x(\mu_m-\tilde{\mu}_m)}-e^{\sqrt{2}x(\mu_m-\tilde{\mu}_m)}\right]\Big\} \\
&\quad +2i\left[\Re(c_2)\Im(a_1)-\Re(a_1)\Im(c_2)-\Re(a_2)\Im(c_1)-\Re(c_1)\Im(a_2)\right] \qquad \text{(B.10)} \\
\mathbb{D} &= \Big\{-\left[\Re(a_2)\Im(a_1)-\Re(c_2)\Im(c_1)-\Re(c_1)\Im(c_2)-\Re(a_1)\Im(a_2)\right] \\
&\quad +i\left[\Im(c_1)\Im(c_2)-\Re(c_1)\Re(c_2)-\Re(a_1)\Re(a_2)-\Im(a_1)\Im(a_2)\right]\Big\} \\
&\quad \times\left[e^{-\sqrt{2}x(\mu_m-\tilde{\mu}_m)}+e^{\sqrt{2}x(\mu_m-\tilde{\mu}_m)}\right]e^{-\frac{1}{2}(\mu_m-\tilde{\mu}_m)^2} \qquad \text{(B.11)}
\end{aligned}
$$

B.6 Coefficients $\mathcal{A}, \mathcal{B}, \mathcal{C}, \mathcal{D}$ and $\mathcal{E}$

The expressions of the coefficients $\mathcal{A}, \mathcal{B}, \mathcal{C}, \mathcal{D}$ and $\mathcal{E}$ in eq.(5.84) are:

$$\begin{aligned}
\mathcal{A} &= |\mathbb{A}|^2 (F_{0000} + F_{1111}) - (\mathbb{A}^*)^2 F_{1100} + \mathbb{A}^*\mathbb{C}(F_{1000} - F_{1101)} + \mathbb{A}^*\mathbb{C}^*(F_{0100} - F_{1110}) \\
&\quad -\mathbb{A}^2 F_{0011} - \mathbb{A}\mathbb{C}(F_{0001} - F_{1011}) + \mathbb{A}\mathbb{C}^*(F_{0010} - F_{0111}) + |\mathbb{C}|^2 (F_{1010} + F_{0101}) \\
&\quad +(\mathbb{C}^*)^2 F_{0110} + \mathbb{C}^2 F_{1001} \qquad \text{(B.12)} \\
\mathcal{B} &= |\mathbb{B}|^2 (F_{0000} + F_{1111}) - (\mathbb{B}^*)^2 F_{1100} + \mathbb{B}^*\mathbb{D}(F_{1000} - F_{1101)} + \mathbb{B}^*\mathbb{D}^*(F_{0100} - F_{1110}) \\
&\quad -\mathbb{B}^2 F_{0011} - \mathbb{B}\mathbb{D}(F_{0001} - F_{1011}) + \mathbb{B}\mathbb{D}^*(F_{0010} - F_{0111}) + |\mathbb{D}|^2 (F_{1010} + F_{0101}) \\
&\quad +(\mathbb{D}^*)^2 F_{0110} + \mathbb{D}^2 F_{1001} \qquad \text{(B.13)} \\
\mathcal{C} &= (\mathbb{A}^*\mathbb{B} + \mathbb{B}^*\mathbb{A})(F_{0000} + F_{1111}) - 2\mathbb{A}^*\mathbb{B}^* F_{1100} + (\mathbb{A}^*\mathbb{D} + \mathbb{B}^*\mathbb{C})(F_{1000} - F_{1101}) \\
&\quad +(\mathbb{A}^*\mathbb{D}^* + \mathbb{B}^*\mathbb{C}^*)(F_{0100} - f_{1110}) - 2\mathbb{A}\mathbb{B} F_{0011} + (\mathbb{A}\mathbb{D} + \mathbb{B}\mathbb{C})(F_{0001} - F_{1011}) \\
&\quad +(\mathbb{A}\mathbb{D}^* + \mathbb{B}\mathbb{C}^*)(F_{0010} - F_{0111}) + (\mathbb{C}^*\mathbb{D} + \mathbb{D}^*\mathbb{C})(F_{1010} + F_{0101}) + 2\mathbb{C}^*\mathbb{D}^* F_{0110} \\
&\quad 2\mathbb{C}\mathbb{D} F_{1001} \qquad \text{(B.14)} \\
\mathcal{D} &= 2(|\mathbb{B}|^2 + |\mathbb{D}|^2) \qquad \text{(B.15)} \\
\mathcal{E} &= 2(|\mathbb{B}|^2 + |\mathbb{D}|^2 + |\mathbb{A}|^2 + |\mathbb{C}|^2) \qquad \text{(B.16)}
\end{aligned}$$

where

$$\begin{aligned}
F_{0000} &= \int_{-\infty}^{\infty} \mathrm{d}x \int_{-\infty}^{\infty} \mathrm{d}y \int_{-\infty}^{\infty} \mathrm{d}p \int_{-\infty}^{\infty} \mathrm{d}q \int_{-\infty}^{\infty} \mathrm{d}k \int_{-\infty}^{\infty} \mathrm{d}l \\
&\quad \langle x + \frac{1}{2}l | \langle y + \frac{1}{2}k | \, |0_m, 0_m\rangle \, \langle 0_m, 0_m| \, |y - \frac{1}{2}k\rangle | x - \frac{1}{2}l\rangle \\
&\quad \times e^{-iql} e^{-ipk} W(x, p, y, q) \qquad \text{(B.17)}
\end{aligned}$$

The Wigner function $W(x, p, y, q)$ is the Wigner function in eq.(5.79).

B.7 Choice of $\delta_{max,m}$

The optimal choice of δ is found by calculating the average entropy in the first swap level for a given outcome of the $\hat{X}$ measurement . The initial states are assumed to be of the form in eq.(5.32) and the average entropy, $\bar{S}$ is calculated by numerically evaluating the integral

$$\bar{S} = \int_{-\infty}^{\infty} \mathrm{d}p S(p_1) P(p_1) \qquad \text{(B.18)}$$

p_1 is the outcome of the $\hat{P}$ measurement, $S(p_1)$ is the entropy of the swapped state and $P(p_1)$ is the probability density function of the outcome p_1. The average entropy as a function of the $\hat{X}$ measurement is seen in figure B.1

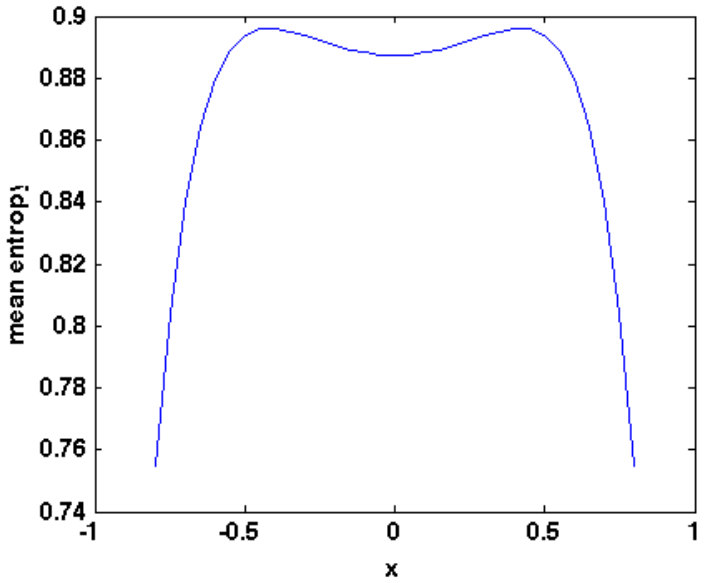

(a) The mean entropy as a function of the outcome of the $\hat{X}$ measurement for $m = 1$

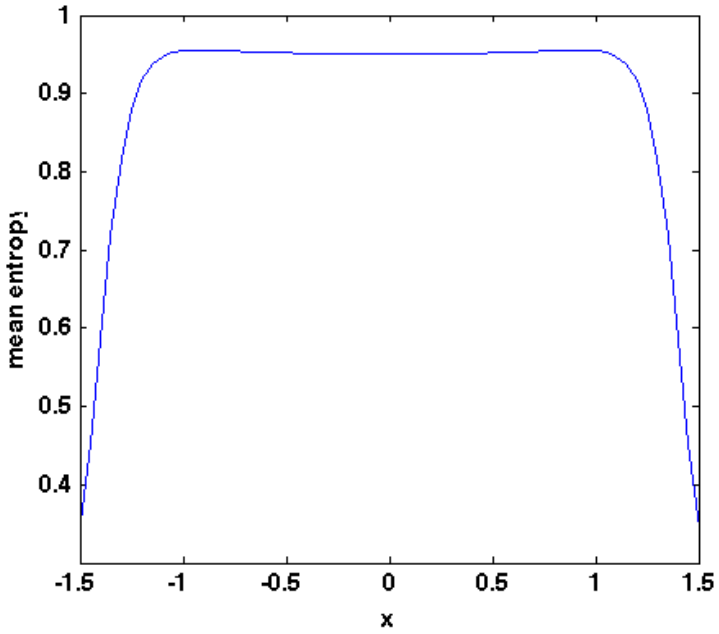

(b) The mean entropy as a function of the outcome of the $\hat{X}$ measurement for $m = 2$

Figure B.1

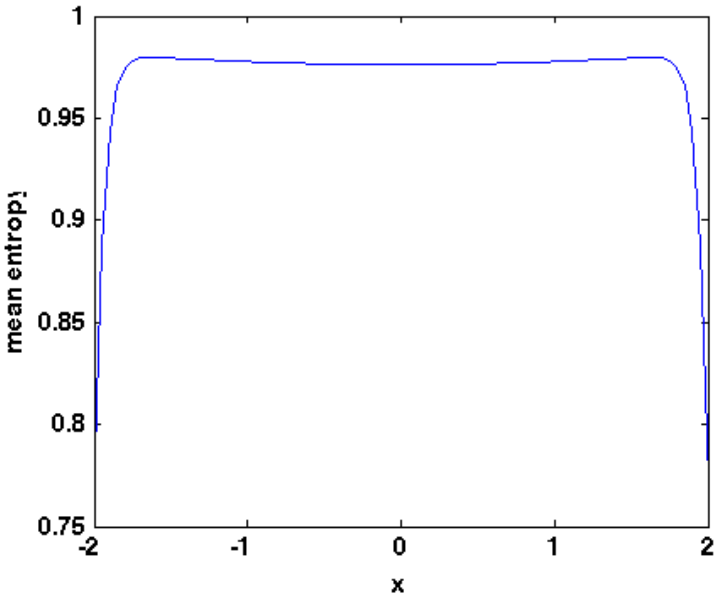

(c) The mean entropy as a function of the outcome of the $\hat{X}$ measurement for $m = 2$

Figure B.1: The mean entropy as a function of the outcome of the $\hat{X}$ measurement for $m = 1, 2$ and 3. From these plots the value of $\delta_{max,m}$ is found.

Figure B.1 shows that the average entropy actually increases a bit until a maximal value of the $\hat{X}$ measurement outcome, $\left|\hat{X}_{max,m}\right|$ is reached. The values of $\left|\hat{X}_{max,m}\right|$ are

$$\begin{aligned}\left|\hat{X}_{max,1}\right| &= 0.4 \\ \left|\hat{X}_{max,2}\right| &= 1.0 \\ \left|\hat{X}_{max,3}\right| &= 1.7\end{aligned} \tag{B.19}$$

Choosing $\delta_{max,m} = \left|\hat{X}_{max,m}\right|$ gives success probabilities of ~ 0.28 for $m = 1$, ~ 0.46 for $m = 2$ and ~ 0.50 for $m = 3$. Since the upper limit of the success probability is $\frac{1}{2}$ the optimal choice of δ clearly is $\delta_{max,m} = 1.7$ for $m = 3$.
Furthermore $\delta_{max,m} = 0.5$ for $m = 1$ and $\delta_{max,m} = 1.1$ for $m = 2$ was chosen, which correspond to success probabilities of ~ 0.30 and ~ 0.47. This was checked by simulating the repeater numerically with $\delta > \delta_{max,m}$ for $m = 1$ and $m = 2$. The simulations confirmed that $\delta_{max,m} = 0.5$ for $m = 1$ and $\delta_{max,m} = 1.1$ for $m = 2$ since the increase in the success probability was not large enough to compensate for the drop in the output fidelity.

Appendix C

Supplement to Chapter 6

C.1 Analytical approximation

The simulation showed that the output fidelity could be written as:

$$\begin{aligned} F_{out,m,n}(P_{grow,m}, P_{connect,m}) &= 1 - a_{n,m}P_{connect,m}(r)^2 - b_{n,m}P_{connect,m}(r) \\ &\quad -c_{n,m}e^{d_{n,m}P_{grow,m}(\vec{\Delta})} - H_{n,m} \end{aligned} \tag{C.1}$$

The numerical matrices of the constants $a_{n,m}, b_{n,m}, c_{n,m}, d_{n,m}$ and $H_{n,m}$ are seen in eq.(C.2)-(C.6)

$$\mathbf{a} = \begin{pmatrix} 0 & 0 & 0 \\ 0 & 0 & 0 \\ -2.19 & -5.39 & -6.81 \\ -9.75 & -14.6 & -20.1 \\ -15.6 & -26.1 & -39.9 \end{pmatrix} \tag{C.2}$$

$$\mathbf{b} = \begin{pmatrix} 0.90 & 0.91 & 0.95 \\ 1.40 & 1.53 & 1.65 \\ 2.25 & 3.08 & 3.40 \\ 3.69 & 4.92 & 5.83 \\ 4.26 & 6.46 & 8.54 \end{pmatrix} \tag{C.3}$$

$$\mathbf{c} = \begin{pmatrix} 0.0063 & 1.0 & 4.7 \\ 0.223 & 1.50 & 5.08 \\ 0.460 & 2.59 & 6.26 \\ 1.56 & 3.73 & 8.77 \\ 2.02 & 6.68 & 16.1 \end{pmatrix} \cdot 10^{-3} \tag{C.4}$$

$$\mathbf{d} = \begin{pmatrix} 15.0 & 24.2 & 92.0 \\ 13.1 & 23.1 & 93.8 \\ 12.3 & 21.6 & 94.5 \\ 10.2 & 21.0 & 92.6 \\ 9.47 & 19.0 & 83.8 \end{pmatrix} \tag{C.5}$$

$$\mathbf{H} = \begin{pmatrix} 0 & 0 & 0 \\ 0.039 & 0.017 & 0.009 \\ 0.111 & 0.052 & 0.021 \\ 0.215 & 0.111 & 0.056 \\ 0.350 & 0.192 & 0.113 \end{pmatrix} \tag{C.6}$$

Eq. (C.6) shows that the state's swap performance increases for large values of m and eq. (C.2)-(C.5) shows that the fidelity drops as a function of r and $\vec{\Delta}$. Hence the approximation of the output fidelity behaves as expected The fact that $a_{n,m} \leq 0$ shows that the approximation is valid when $P_{connect,m}(r) \ll 1$.

Appendix D

Matlab programs

The program used for the simulation of the repeater was *Matlab R2009b* developed by Mathworks. Additional analytical calculations was made in the program *Mathematica* by Wolfram. The main m-files and functions used in the simulations are listed in this appendix. The notebooks produced in Mathematica are not listed since they contain only minor analytical calculations.
The code with comments is posted on the web under headlines that correspond to the ones listed below. It can be found at http://fys.ku.dk/snappy. The code is not printed since the amount of code is considerable.

Generation of cat states

***precat.m*:** This m-file calculates a number of matrices used in the calculations of the growing of cat states. The matrices are all independent of the choice of acceptance interval and are calculated separately from the rest of the growing step. "*precat.m*" should be executed before any of the other m-files in the folder.

***grid.m*:** This m-file calulates the rate in units of the source repetition rate of a growing procedure of m iterations as well as the fidelity with either a squeezed one-mode cat state or the state in eq. (4.12). Which state to calculate the fidelity with and the number of iterations should be specified in the m-file. When executing "*grid.m*" it calculates the fidelity and rate on a specified grid of values for $\vec{\Delta}$. *grid* assumes perfect one-photon states as input states

***Optim3e1.m*:** This function calculates the Wigner function of the output state after one iteration. The function needs the acceptance interval as input. The function can be used to calculations with both pure one-photon inputs and with one two-photon component.

***Optim3e2.m*:** This function calculates the Wigner function of the output state after two iterations. The function needs the acceptance intervals as input. The function can

be used to calculations with both pure one-photon inputs and with one two-photon component.

***Optim3e3.m*:** This function calculates the Wigner function of the output state after three iterations. The function needs the acceptance intervals as input. The function can be used to calculations with both pure one-photon inputs and with one two-photon component.

Connection of cat states

***connection.m*:** This m-file calculates the Wigner function of the two-mode state that results from connecting two of the one-mode states produced in step one of the altered repeater scheme. The Wigner function of the one-mode states should be put in a cell named "Set" which is loaded into the workspace before running "*connection.m*". In "*connection.m*" the length of the elementary links, the reflectivity of the beam splitters and the number of iterations performed in the growing step should be specified. "*connection.m*" also calculates the fidelity with state (5.30) and the probability of a successful connection.

Swapping optimal

***precalc.m*:** This m-file calculates matrices used to simulate the swap levels. The matrices are all independent of the choice of acceptance interval and the outcome of the $\hat{X}$ and $\hat{P}$ measurements. "*precalc.m*" should be executed before any of the other m-files in this folder.

***xprobability1-4.m*:** These are the probability density functions for the $\hat{X}$ quadrature in swap level 1-4 using the state (5.30) as starting state. The functions use the outcomes of the previous $\hat{X}$ and $\hat{P}$ measurements as inputs as well as the outcome of the $\hat{X}$ measurement in the relevant swap level. The number of iterations in the growing step should be specified in the functions

***probability1-4.m*:** These are the probability density functions for the $\hat{P}$ quadrature in swap level 1-4 using the state (5.30) as starting state. The functions use the outcome of the previous $\hat{X}$ and $\hat{P}$ measurements as inputs as well as the outcome of the $\hat{X}$ and $\hat{P}$ measurement in the relevant swap level.The number of iterations in the growing step should be specified in the functions

***entanglement1-4.m*:** These functions calculates the entropy of the output state after swap level 1-4. They use the outcome of the previous $\hat{X}$ and $\hat{P}$ measurements as inputs as well as the outcome of the $\hat{X}$ and $\hat{P}$ measurement in the relevant swap level. The number of iterations in the growing step should be specified in the functions

Swapping

***precalc.m*:** This m-file calculates matrices used to simulate the entanglement swapping. The matrices are independent of the acceptance interval and the measurement outcomes for the $\hat{X}$ and $\hat{P}$ measurements. "*precalc.m*" should be executed before any of the other m - files in the folder.

***gridswap1-4.m*:** These m-files simulate swap level 1-4 using the two-mode Wigner functions from the connection step as input states. The two-mode Wigner functions resulting from pure one-photon states should be put in a cell named "Setcon" and the Wigner functions with a two-photon error should be put in a cell named "Setcon2". Both cells should be loaded into the workspace before executing the m-files. The acceptance interval, the number of simulations and the number of iterations in the growing step should be specified in each m-file. The m-files makes use of the functions *"swapw1.m","swapw2.m", "swappf1.m","swappf2.m", "Mus1.m","Mus2.m","CDFp1.m"* and *"CDFx1.m"*

***swapw1-2.m*:** Used to calculate the Wigner function after a swap. The functions needs the Wigner functions for the two states that are swapped and the outcome of the $\hat{X}$ and $\hat{P}$ measurments as inputs. The number of iterations in the growing step should be specified before executing the functions.

***swappf1-2.m*:** These functions calculates the fidelity with the target state in eq.(5.83) and the coefficients of this state in a given swap. The functions needs the Wigner function of the state after the swap, the coefficients from the previous target states and the outcome of the $\hat{X}$ measurement as inputs. The number of iterations in the growing step should also be specified.

***Mus1-2.m*:** Calculates matrices used in the functions *"CDFx1.m"* and *"CDFp1.m"*. The Wigner function of the two states that are swapped are given as input states. The number of iterations in the growing step should be specified.

***CDFx1.m*:** This calculates the cumulative distribution function of the $\hat{X}$ quadrature in a swap. The number of iterations in the growing step should be specified.

***CDFp1.m*:** This calculates the cumulative distribution function of the $\hat{P}$ quadrature in a swap. The number of iterations in the growing step and the outcome of the $\hat{X}$ measurement in the swap should be specified.

***probx1.m*:** This is the probability density function of the $\hat{X}$ quadrature in a given swap. It is used to normalize after the measurement of $\hat{X}$.

A part from these functions and m-files the function *tprod* developed by Jason Farquhar has been used. This function makes it possible to perform tensor products in Matlab. The code for this function is available at: http://www.mathworks.com/matlabcentral/fileexchange/16275

Extensively use of the tensor toolbox developed by Scandia National Laboratories has also been made. The toolbox is available at: http://csmr.ca.sandia.gov/ tgkolda/TensorToolbox/.

Bibliography

[1] J.F. Sherson et al: *"Quantum teleportation between light and matter"*, Nature 443, 557-560 (2006)

[2] Charles H. Bennett et al: *"Teleporting an Unknown Quantum State via Dual Classical and Einstein-Podolsky-Rosen Channels"*, Phys. Rev. Lett. 70 (1993)

[3] C. Kurtsiefer et al: *"Quantum cryptography: A step towards global key distribution"*, Nature 419, 450 (2002)

[4] A. K. Ekert: *"Quantum cryptography based on Bell's theorem"*, Phys. Rev. Lett. 67, 661 (1991)

[5] J. I. Cirac and P. Zoller: *"A scalable quantum computer with ions in an array of microtraps"*, Nature 404, 579-581 (2000)

[6] D. Dieks: *"Communication by EPR devices"*, Physics Letters A 92, 271 (1982)

[7] W. K. Wootters and W.H. Zurek: *"A single quantum cannot be cloned"*, Nature 299, 802 (1982)

[8] H. J. Briegel et al: *"Quantum Repeaters: The Role of Imperfect Local Operations in Quantum Communication"*, Phys. Rev. Lett. 81, 5932-5935 (1998)

[9] L. M. Duan et al: *"Long-distance quantum communication with atomic ensembles and linear optics"*, Nature 414, 413-418 (2001)

[10] T.X. Mueller et al:*"Graphene photodetetors for high-speed optical communications"*, Nature Photonics 4, 297-301 (2010)

[11] J. Bae et al:*"Si nanowire metal-insulator-semiconductor photodetectors as efficient light harvesters"*, Nanotechnology 21, 095502 (2010)

[12] K. Ishikura Ando et al:*"Highly Efficient Blue-Ultraviolet Photodetectors Based on II-VI Wide-Bandgap Compound Semiconductores"*,physica status solidi 229, 1065-1071 (2002)

[13] Jonathan B. Brask et al: *"A Hybrid Long-Distance Entanglement Distribution Protocol"*, Phys. Rev. Lett. 105,160501 (2010)

[14] N. Sangouard et al: *"Quantum repeaters with entangled coherent states"*, J. Opt. Soc. Am. B27, A137-A145 (2010)

[15] Christopher C. Gerry and Peter L. Knight: *"Introductory Quantum Optics"*, Cambridge University Press, 2008 (third printing)

[16] J. C. Garrison and R. Y. Chiao: *"Quantum optics"*, Oxford University Press, 2008

[17] A. M. Fox: *"Quantum optics"*, Oxford University Press, 2006

[18] M.A. Nielsen and I. L. Chuang: *"Quantum computation and quantum information"*, Cambridge University Press, 2000

[19] Roman Schnabel: *"Gravitational wave detectors: Squeezing up the sensitivity"*,Nature Physics 4, 440-441 (2008)

[20] Ryszard Horodecki et al: *"Quantum entanglement"*, Rev. Mod. Phys.81, 865-942 (2009)

[21] E. Schrödinger: *"Die gegenwrtige Situation in der Quantummechanik"*, Naturewissenschaften 23, 807 (1935)

[22] J. A. Wheeler and W. H. Zurek: *"Quantum Theory and Measurement"*, Princeton University Press, 1983

[23] J. F. Clauser: *"Proposed Experiment to Test Local Hidden-Variable Theories"*, Phys. Rev. Lett. 23, 880-884 (1969)

[24] M. Kroutvar et al: *"Optically programmable electron spin memory using semiconductor quantum dots"*, Nature 423,81-84 (2004)

[25] C. A. Muschik et al: *"Efficient quantum memory and entanglement between light and an atomic ensemble using magnetic fields"*, Phys. Rev. A 73, 062329 (2006)

[26] Jonathan B. Brask: *Long-distance distribution of discrete and continuous variable entanglement with atomic ensembles"*, Theoretical Quantum Optics Group, Niels Bohr Institute, Ph.d thesis

[27] Ling-An Wu et al: *"Generation of Squeezed States by Parametric Down Conversion"*, Phys. Rev. Lett. 57, 2520-2523 (1986)

[28] J. B. Brask and A. S. Sørensen: *"Memory imperfections in atomic-ensemble-based quantum repeaters"*, Phys. Rev. A. 78, (2008)

[29] N. Sangouard et al: *"Quantum repeaters based on atomic ensembles and linear optics"*, Rev. Mod. Phys; 83,33 (2011)

[30] R. Dong et al: *"Experimental evidence for Raman-induced limits to efficient squeezing in optical fibers"*, Optics Letters 33, 116-118 (2008)

[31] M. Mehmet et al: *"Observation of squeezed states with strong photon-number oscillations"*, Phys. Rev. A 81, 013814 (2010)

[32] Y. Takeno et al: *"Observation of -9 dB quadrature squeezing with improvement of phase stability in homodyne measurement"*, Optics Express 15, 4321-4327 (2007)

[33] Morgan P. Hedges et al: *"Efficient quantum memory for light"*, Nature 465, 1052-1056 (2010)

[34] L. Jiang et al: *"Fast and robust approach to long-distance quantum communication with atomic ensembles"*, Phys. Rev. A 76, 012301 (2007)

[35] L. M. Duan et al: *"Long-distance quantum communication with atomic ensembles and linear optics"*, Nature 414, 413-418 (2001)

[36] D. Deutsch et al: *"Quantum Privacy Amplification and the Security of Quantum Cryptography over Noisy Channels"*, Phys. Rev. Lett. 77, 2818-2821 (1996)

[37] C.H. Bennett et al: *"Purification of Noisy Entanglement and Faithful Teleportation via Noisy Channels"*, Phys. Rev. Lett. 78, 2031 (1997)

[38] Jian-Wei Pan et al: *"Experimental entanglement purification of arbitrary unknown states"*, Nature 423, 417-422 (2003)

[39] O. A. Collins et al: *"Multiplexed Memory-Insensitive Quantum Repeaters"*, Phys. Rev. Lett. 98, 060502 (2007)